ANALYSIS OF INTERNAL EXPLOSION AND STRUCTURAL RESPONSE TO BLAST LOADING

A THESIS SUBMITTED TO
THE GRADUATE SCHOOL OF NATURAL AND APPLIED SCIENCES
OF
MIDDLE EAST TECHNICAL UNIVERSITY

BY

UĞUR CAN TURCAN

IN PARTIAL FULFILLMENT OF THE REQUIREMENTS
FOR
THE DEGREE OF MASTER OF SCIENCE
IN
MECHANICAL ENGINEERING

DECEMBER 2012

Approval of the thesis:

ANALYSIS OF INTERNAL EXPLOSION AND STRUCTURAL RESPONSE TO BLAST LOADING

submitted by **UĞUR CAN TURCAN** in partial fulfillment of the requirements for the degree of **Master of Science in Mechanical Engineering Department, Middle East Technical University** by,

Prof. Dr. Canan Özgen _____
Dean, Graduate School of **Natural and Applied Sciences**

Prof. Dr. Suha Oral _____
Head of Department, **Mechanical Engineering**

Prof. Dr. Abdullah Ulaş
Supervisor, **Mechanical Engineering Dept., METU** _____

Dr. Nadir Serin
Co-Supervisor, **TÜBİTAK SAGE** _____

Examining Committee Members

Prof. Dr. Hüseyin Vural _____
Mechanical Engineering Dept., METU

Prof. Dr. Abdullah Ulaş _____
Mechanical Engineering Dept., METU

Prof. Dr. Levend Parnas _____
Mechanical Engineering Dept., METU

Assist. Prof. Dr. Cüneyt Sert _____
Mechanical Engineering Dept., METU

Dr. Nadir Serin _____
TÜBİTAK SAGE

Date: 12.12.2012

I hereby declare that all information in this document has been obtained and presented in accordance with academic rules and ethical conduct. I also declare that, as required by these rules and conduct, I have fully cited and referenced all material and results that are not original to this work.

Name, Last Name : Uğur Can Turcan

Signature :

ABSTRACT

ANALYSIS OF INTERNAL EXPLOSION AND STRUCTURAL RESPONSE TO BLAST LOADING

Turcan, Uğur Can
M.Sc., Department of Mechanical Engineering
Supervisor : Prof. Dr. Abdullah Ulaş
Co-Supervisor: Dr. Nadir Serin

December 2012, 129 pages

In this thesis, blast overpressure due to internal explosion and dynamic response to this loading of the structure is analyzed. Firstly, theoretical backgrounds of computational procedures are presented. The basic principles of the hydrocodes and semi empirical methods are explained in detail.

In the analysis of blast overpressure, partially vented structures are examined. Three different venting areas and three different charge weights are employed in the study. Peak pressure, time and impulse parameters are investigated in detail. Remapping and scaling laws are employed in order to reduce the computational cost. Experiments are carried out with similar conditions where pressure histories are recorded. Results from a semi empirical program and a commercial hydrocode are compared with the experimental data.

After investigating the accuracy of blast calculation methods, dynamic response to blast loading is reviewed. For this purpose, two methods are used: The fully coupled method in hydrocode and the hybrid method - uniquely coupled semi empirical program and hydrocode. In the fully coupled method, hydrocode solves both blast

and response; whilst in the hybrid method, hydrocode is used as the structural solver and semi empirical program is employed for the blast calculation. A deformable test setup is used to observe the response. Results from computational methods are compared with the experimental data.

Finally, it can be concluded that semi empirical program and hydrocode are applicable to blast overpressure problems with partial venting. In addition, the methods introduced in dynamic response section can be used as preliminary analysis tools in the prediction of structural response to blast loading. Also, it is shown that the hybrid method is much faster than the fully coupled method in hydrocode.

Keywords: Blast Loading, Internal Explosion, C4, Structural Response, Hydrocode, Scaling Law, Experiments on Vented Structure

ÖZ

KAPALI HACİMLERDE OLUŞAN PATLAMALARIN VE DARBE BASINCI YÜKLERİ ALTINDAKİ YAPILARIN DAVRANIŞLARININ ÇÖZÜMLENMESİ

Turcan, Uğur Can
Yüksek Lisans, Makina Mühendisliği Bölümü
Tez Yöneticisi : Prof. Dr. Abdullah Ulaş
Ortak Tez Yöneticisi: Dr. Nadir Serin

Aralık 2012, 129 sayfa

Bu tezde, kapalı hacimlerde meydana gelen patlama sonucu oluşan basınç dağılımı ve yapının gösterdiği dinamik davranışlar incelenmiştir. Öncelikli olarak, hesaplama yöntemlerinin teorik altyapısı sunulmuş; hidrokodların ve yarı deneysel yöntemlerin dayandığı temel prensipler açıklanmıştır.

Basınç darbesi incelemeleri aşamasında, bir yüzeyinde açık alan bulunan küpler kullanılmıştır. İnceleme kapsamında üç farklı açık küp tipi ve üç farklı patlayıcı ağırlığı kullanılmıştır. Tepe basıncı, zaman ve darbe parametreleri detaylı incelenmiştir. Hesaplama süresini kısaltabilmek amacıyla yeniden eşleştirme yöntemi (*Ing. Remapping*) ve ölçeklendirme kuralı kullanılmıştır. Modellenen kurgulara benzer şekilde deneyler yapılmış ve zamana bağlı basınç verileri elde edilmiştir. Yarı deneysel program ve hidrokod kullanılarak yapılan hesaplama sonuçları deney verileri ile karşılaştırılmıştır.

Basınç darbesi hesaplama yöntemleri üzerinde çalışıldıktan sonra patlamayla oluşan basınç darbesi sonucu yapıda görülen dinamik tepkiler incelenmiştir. Bu amaçla, iki çözüm yöntemi kullanılmıştır: Sadece hidrokod kullanılarak yapılan çözüm ve hidrokod ile yarı deneysel programlarının birleştirilmesi ile yapılan çözüm.

İlk yöntemde, tüm çözümleme hidrokod yetenekleri dahilinde sahip olduğu etkileşim algoritması kullanılarak gerçekleştirilmiştir. İkinci yöntemde; yarı deneysel programının basınç darbesini çözdüğü, hidrokodun ise yapısal hesapları yaptığı hibrit yaklaşım benimsenmiştir. Dinamik tepkilerin gözlemlenebilmesi amacıyla şekli bozulabilen bir test düzeneği kullanılmıştır. Her iki yöntemle bulunan sonuçlar deney verileri ile karşılaştırılmıştır.

Hidrokod ve yarı deneysel programlarının kısmen açık yüzeyi bulunan kapalı alanlarda meydana gelen patlamaların çözümlenmesi için kullanılabilir olduğu belirlenmiştir. Ayrıca, yapıların basınç darbesine karşı gösterdiği dinamik tepkinin öngörülebilmesi amacıyla önerilen yöntemlerin, ön hesaplamalar için kullanılabileceği değerlendirilebilir. Ek olarak, hibrit yöntemin sadece hidrokod kullanılarak yapılan hesaplamalardan çok daha hızlı olduğu sonucuna ulaşılmıştır.

Anahtar Kelimeler: Basıç Darbesi, Kapalı Hacim Patlamaları, C4, Yapısal Davranış, Hidrokod, Basınç Darbesi Hesaplama Yöntemleri, Ölçeklendirme Kuralı, Deneysel Çalışma

To My Family

ACKNOWLEDGEMENTS

I would like to express my sincere gratitude to my supervisors Prof. Dr. Abdullah Ulaş and Dr. Nadir Serin for their supervisions, patience, encouragements and guidance throughout this study.

I am grateful to all my friends, my superiors and colleagues in TUBİTAK SAGE for their support, patience and valuable comments. I would like to express special thanks to Tahir Turgut for valuable suggestions and comments. In addition, I would like to thank to the members of the Laboratory Services Division for their effort during the tests.

I would like to thank my dearest friends Yordam Kocatepe, Ömer Arslan Göral, Can Kılıçturgay and Egemen Çakır who have always boosted me with their positive energy, moral support and sincere understanding.

I would also like to express special thanks to Didem Örs for her endless love and encouragement.

Finally, my deepest thanks go to my family who gave me the support and love, which made this thesis possible.

TABLE OF CONTENTS

LIST OF TABLES

TABLES

LIST OF FIGURES

FIGURES

NOMENCLATURE

1D	One dimensional
3D	Three dimensional
C4	Composition 4
EOS	Equation of State
JWL	Jones-Wilkins-Lee
SDOF	Single Degree of Freedom
TNT	Trinitrotoluene

Symbols

A	Yield strength of the material
B	Strain hardening constant
b	Empirical constant (JWL)
c_0	Empirical constants (SHOCK)
C	Strain rate constant (Johnson-Cook)
C_1	Empirical constant (JWL)
C_2	Empirical constant (JWL)
E	Total energy
f	Body force
m	Thermal softening exponent
M	Mean
n	Strain hardening coefficient
p	Overpressure
p_0	Peak overpressure
p_{shift}	Pressure shift
p_{SO}	Incident (side on) Pressure

R	True distance
r_1	Empirical constant (JWL)
r_2	Empirical constant (JWL)
s	Empirical constant (SHOCK)
T	Temperature
T_{melt}	Melting temperature
T_{room}	Room temperature
t	Time
t_a	Arrival time
t_0	Positive blast pressure duration
U	Shock velocity
u_p	Particle velocity
V	Velocity
v	Specific volume
x	Displacement
W	Charge weight
w	Empirical constant (JWL)
Z	Scaled distance
β	Decay constant
γ	Ideal gas constant
γ_0	Ratio of heat capacities
ϵ	Strain
$\dot{\epsilon}$	Strain rate
$\dot{\varepsilon}$	Strain tensor
$\dot{\varepsilon_0}$	Reference strain rate
ρ	Density
σ	Stress

CHAPTER 1

INTRODUCTION AND LITERATURE SURVEY

1.1. An Introduction to Blast Loading

1.1.1. Blast Wave

The detonation of a high explosive is a chemical reaction that produces gases which are at a very high pressure and temperature. The violent expansion of these gases transfers energy to the surrounding medium causing it to be compressed in front of the disturbance. Regardless of the source, the properties of air as a compressible gas will cause the disturbance front to steepen as it passes through the air until it exhibits nearly discontinuous increase in pressure, density and temperature. The resulting shock front is called blast wave and moves supersonically (Figure 1.1).

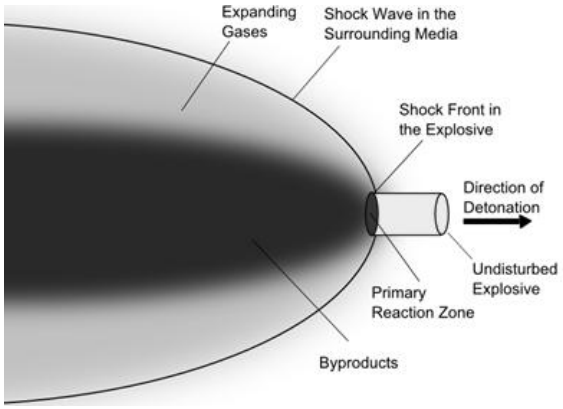

Figure 1.1. Blast Wave

In other words, the expanding gases push the surrounding medium out of the volume it occupies so rapidly that it forms a blast wave front. Thus, a blast wave is simply high compressed, fast-moving air.

The blast wave is characterized by an instantaneous rise in pressure at the wave front to the peak overpressure followed by an exponential decay. As shown in Figure 1.2, the decay is followed by the negative phase before the pressure return to normal atmospheric conditions.

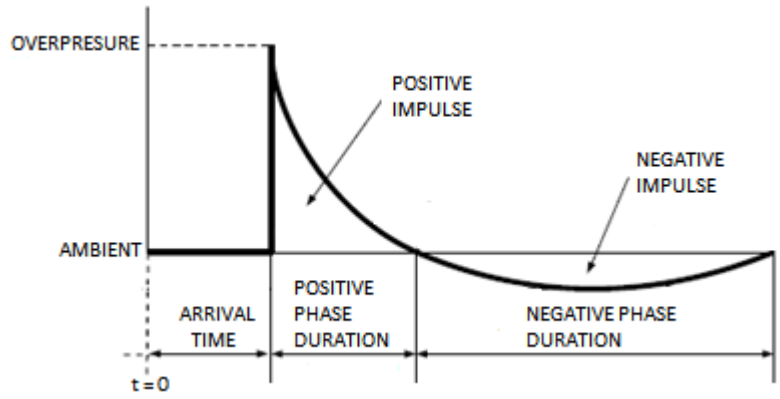

Figure 1.2. Ideal Blast Pressure History

Ideal incident (side-on) pressure profile is observed at any point away from the detonation in free field. However, if the blast wave impinges on a rigid surface, a reflected (face-on) pressure is instantly developed on the surface. In Figure 1.3, the rapid increase in pressure to a higher value can be seen [1].

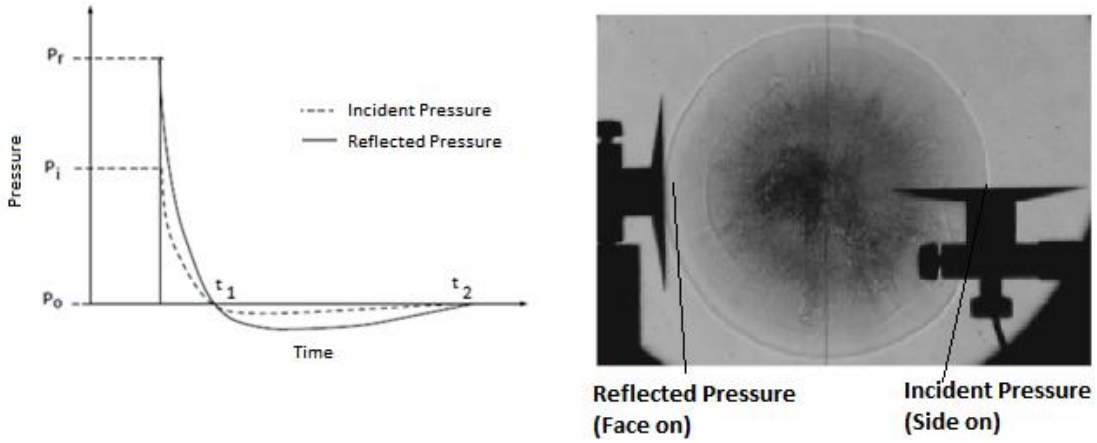

Figure 1.3. Reflected Pressure [1]

Reflection phenomenon becomes crucially important especially for the internal explosion because of its destructive effects on the structures. In the reflection process, the air molecules comprising the blast wave at the wave front are brought to rest and hence undergo a momentum change with the surface. The layer of air molecules behind those is the next to be affected. The momentum of the second layer applies an extra compressive effect on the first layer. This process continues for succeeding layers and the net result on the surface is called the reflected pressure. Reflected pressure is the combination of the incident pressure and the dynamic pressure of the blast associated with the velocity of the air molecules. However, algebraic sum of the incident pressure and the dynamic pressure components will not yield to reflected pressure due to the momentum change of the air and its increased compression. It is also named as the blast loading on the structure since it represents the total pressure applied on the regarding surface.

1.1.2. Internal Explosion

Structures in which the detonation of a high explosive may occur are referred as either ‘unvented’ structures or ‘vented’ structures (Figure 1.4).

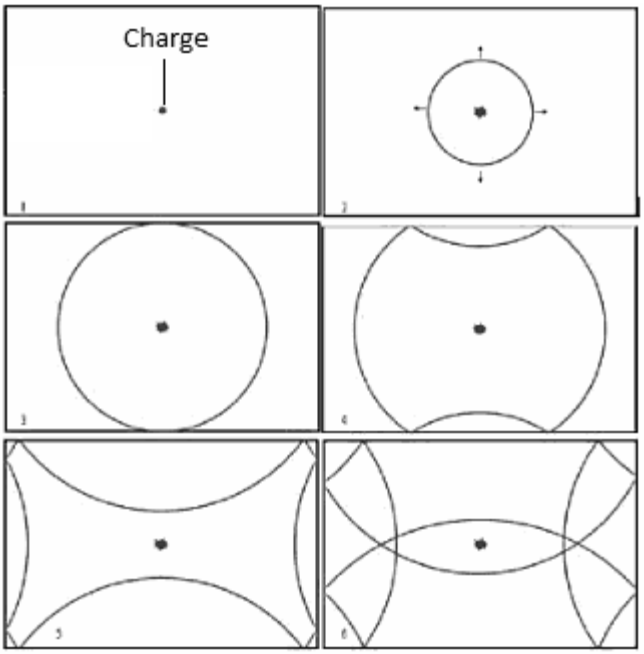

Figure 1.4. Internal Explosion [2]

Although they both experience the same loading phases, every phase has a different effect depending on the venting area. The loading inside a structure can be divided into three phases:

I. Reflected blast pressure
II. Re-reflection
III. Gas pressure loading

The difference due to venting area is observed in the gas pressure loading and re-reflection phases. Pressure relief inside the unvented structure occurs relatively slow compared to the vented structures. Both structures eventually are stabilized in atmospheric conditions, but the pressure inside the unvented structure decays slower. In addition, the number of re-reflection waves is relatively higher due to the containment. On the other hand, reflected blast pressure would be identical.

In this work, vented and partially vented structures are investigated.

1.2. Literature Survey

Until recent years, methods on prediction of blast wave and its effects on structures were primarily depended on experimental data. These methods are called “empirical methods” and generally limited by the extent of database. Although extrapolation is possible, the accuracy of the methods decrease as the problem diverges from the experimental ones.

Semi empirical methods are developed to overcome the restriction of the empirical methods. They are essentially based on simplified physical models of the problem with extensive experimental data integration. By doing so, these methods assure a wider range in problem definition with quite accurate solutions.

As the computers evolve, numerical methods find more and more users in blast calculations. Computer codes are based on governing equations that draw the most basic laws of physics: conservation of mass, momentum and energy. In addition, material behavior is depicted by constitutive equations [3], [4].

Another aspect of the blast loading is the dynamic response of the structures. Similarly, there are empirical and computational methods for this problem. First, there were theoretical methods supported by experimental studies. They were restricted and only applicable to certain problems. Likewise, computer evolution led to codes that are capable of solving almost every structural behavior under blast loading [5].

1.2.1. Blast Calculations

The structural effects of blast make it critical for examination. However, experimental investigations are too expensive and difficult for this purpose. Large scale tests may cost millions. Therefore, one should have almost infinite funding while working in full scale. In order to overcome this difficulty, computational methods and small scale experimentation are evolved. In this section; literature studies about various methods for blast calculation, scaling and experimental verifications are presented.

1.2.1.1. Empirical and Semi Empirical Methods

Empirical methods and procedures are generally presented in technical design manuals and reports. Most widely used ones are TM 5-1300 and CONWEP. TM 5-1300 includes charts, figures and formulas whereas CONWEP is a computerized methodology.

TM 5-1300 - Structures to Resist the Effects of Accidental Explosions is the manual used by both military and civilian engineers [**6**]. It is approved for public release and the distribution is unlimited. The primary objective of this manual is to establish design procedures against any mass detonation. In addition, it contains analysis and design procedures for blast loading. The blast curves demonstrated on the manual give pressure, impulse and time information for a range of experiments. Using those graphs, any parameter for a limited problem can be calculated. A simplified step by step method can be used to determine the blast wave parameters using the manual:

- Determine the charge geometry and weight as TNT equivalent
- Determine the distance from detonation center to any desired point within the limitations of the graphs
- Read the blast wave parameters from the related graphs

The second empirical method is the CONWEP. It is a computer program that uses a compilation of data from many explosive tests with a charge weight from 1 kg to 400000 kg. Curve fitting techniques are applied to represent the data mathematically. The resulting equations are called Kingery-Bulmash equations. Those equations are high order polynomial equations which uses the same methodology with TM 5-1300. Initially, TNT equivalent of the charge weight and the distance to detonation center are determined, and then they are used as an input to the equations to calculate blast parameters.

Semi empirical methods unite empirical and analytical approaches by merging simplified blast physics and vast amount of experimental data. Some examples to this methodology can be given as HULL, SHARC, CTH, SHOCK, BLASTIN, BLASTX [7]. They are generally fast running semi empirical computer codes used to predict internal and external blast effects from explosions inside or near structures. The first two codes were the SHARC and the HULL. SHARC had evidential

advantages over HULL and was chosen for further development. Unfortunately, SHARC could not be validated despite several attempts. It predicted pressures significantly higher than test results by factors of 2 to 5. SHOCK is a computer program that enables the calculation of the blast pressure and impulse on all or part of a rectangular surface. It was developed from theoretical procedures, empirical blast data and the results of response tests on slabs. After some time, BLASTX is developed in a collective work by the US and Republic of Korea. It is generally used to make pre-test predictions for gauge ranging during the test planning process. Compared to the other codes, analytical background of BLASTX is profoundly solid. Model is developed to include smaller time steps for handling rapid mass and energy flows in the process [8]. It is a fast running semi empirical code that is created by merging simplified blast physics and vast amount of experimental data.

In the scope of this work, BLASTX is employed. Detailed background information is presented in the following sections.

1.2.1.2. Numerical Codes

Numerical codes can be divided into two main categories: Individually developed codes and commercial codes.

- **Individually Developed Codes**

Benselama et al. developed a three dimensional Eulerian solver to calculate blast parameters [9]. The code solves general formulation of conservative Euler equations for compressible fluids using slip conditions for far walls and non-reflective boundaries for far field. Numerically, it uses an unstructured finite-volume cell-centered approach using the classical upwind scheme and a two-stage explicit discretization in time, yielding second-order accuracy in both space and time. The comparison between the results of the program and the experimental data shows good agreement in a rigid and closed box problem.

A particle based approach is presented by Olovsson et al [10]. The detonation products are modeled as a set of discrete particles following Maxwell's original kinetic molecular theory. Although the number of molecules are greatly reduced compared to real gases, the total molecular mass and molecular velocity are the

same. Blast loading on structures is computed as the momentum transfer due to impact and rebound of particles. The method is significantly faster than continuum based approaches and it seems to be in a good agreement with other Eulerian solvers and experimental data.

Computational fluid dynamics code Air3d is modified by Rose to be able to solve blast problems [11]. It is an explicit, finite volume formulation which solves three dimensional forms of Euler equations on a regular Cartesian grid. Equally spaced, square and cubic elements are used. The numerical method is validated by comparison with experiment and a commercial hydrocode AUTODYN.

Van den Berg compiled four different codes into single computer program called BLAST [12]. Each individual code has been specially tailored to a specific application. The program is capable of solving: Blast from pressure vessel rupture, blast from explosive evaporation of superheated liquids, fuel-air blast and high-explosive blast. Although BLAST seems to show good agreement with some of the experiments in the literature, it is still under development.

CFX-5.6 computational fluid dynamics code is developed by Rigas and Sklavounos [13]. It solves Navier-Stokes equations in their conservation form and obtains results by employing Backward Euler transient numerical scheme. Computed blast pressures are generally overestimated compared to experimental data with reasonable error margins.

- **Commercial Codes**

There are two major commercial codes specifically designed for non-linear dynamic problems: AUTODYN and LS-DYNA. They are capable of computing blast and explosion events as well as impact and penetration. AUTODYN uses finite difference, finite volume, finite element and meshless methods depending on the solution technique. It is an explicit numerical analysis code where conservation equations are coupled with material descriptions. Similarly, LS-DYNA is a general purpose finite element code that is developed to solve highly nonlinear transient problems. It employs explicit time integration, contains over 100 constitutive models.

AUTODYN and LS-DYNA are generally referred as “hydrocodes”. Although they function in the same way, both programs have their strength in different areas. For example, LS-DYNA is widely used in crash applications, whilst AUTODYN is generally preferred for detonation problems. In addition; with LS-DYNA all parameters of a run must be specified, while AUTODYN has defaults for most values. In the scope of this study, AUTODYN is selected considering its advantages.

In literature, several analysis using those commercial codes have been carried out. Some of the example studies using AUTODYN are briefly described.

One of the initial works using AUTODYN is a parametric study performed by Chapman et al [14]. The effort is mostly concentrated on the simulation of blast wave interactions with structures. A parametric study is carried out including an investigation of the effect of grid size. The results are compared with simple geometry experimental data. In conclusion, it is stated that AUTODYN is a suitable tool for blast loading.

Although some attempts have been done to perform blast calculations using hydrocodes, probably the most important guide was presented by an AUTODYN developer [15]. It is described how hydrocodes can be employed for the simulation of detonation of high explosives with such importance on modeling blast. Several case studies, including an attempt to model a street channeled explosion, are applied to AUTODYN and results showed great agreement with experimental data.

Birnbaum et al. is interested in the protection of buildings [16]. AUTODYN is used to predict blast loadings on structural components having complex geometries. The blast study of Oklahoma City Building is investigated numerically. Since there are not any pressure recordings during the bombing incident, computational results are not compared with the experimental data. However, the importance of this study is the use of hydrocodes in the aspect of structural protection.

Luccioni et al. investigate the capability of AUTODYN in solving multiple reflections of the blast load [17]. The results are compared with analytical expressions. In addition, mesh dependency of AUTODYN is investigated. After solving some generic blast problems and creating a baseline for the modeling, a case study of a real attack on a building is examined: Israel-Argentina Mutual Association in Buenos

Aires, Argentina in 1994 (Figure 1.5). An attempt is made to find the real position of the explosive charge on the street.

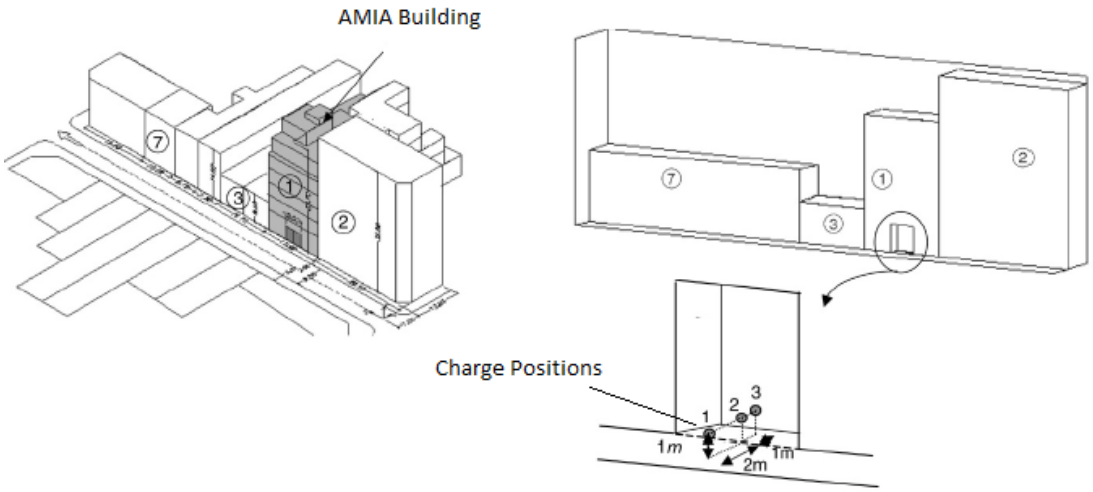

Figure 1.5. Problem Definition [17]

An effort to understand how blast loads having a certain height of burst interact with a structure is made by Trelat et al [18]. To validate the computational results, a small scale experiment is performed. Propane-oxygen stoichiometric mixtures are used as explosives. This approach was unique since it uses TNT equivalences of gaseous charge explosions. AUTODYN showed good agreement with the experimental data. In this work; small scale modeling technique in AUTODYN is also validated as a byproduct.

Another work directs the attention to protection of buildings. Zhou and Hao estimate the loading on a structure behind a protective blast barrier [19]. Numerical simulations are carried out to estimate the peak reflected pressure and the positive impulse (Figure 1.6). As a result of several simulations, a formula is derived by using a curve fitting method in order to be able to estimate blast loading at various locations behind a barrier.

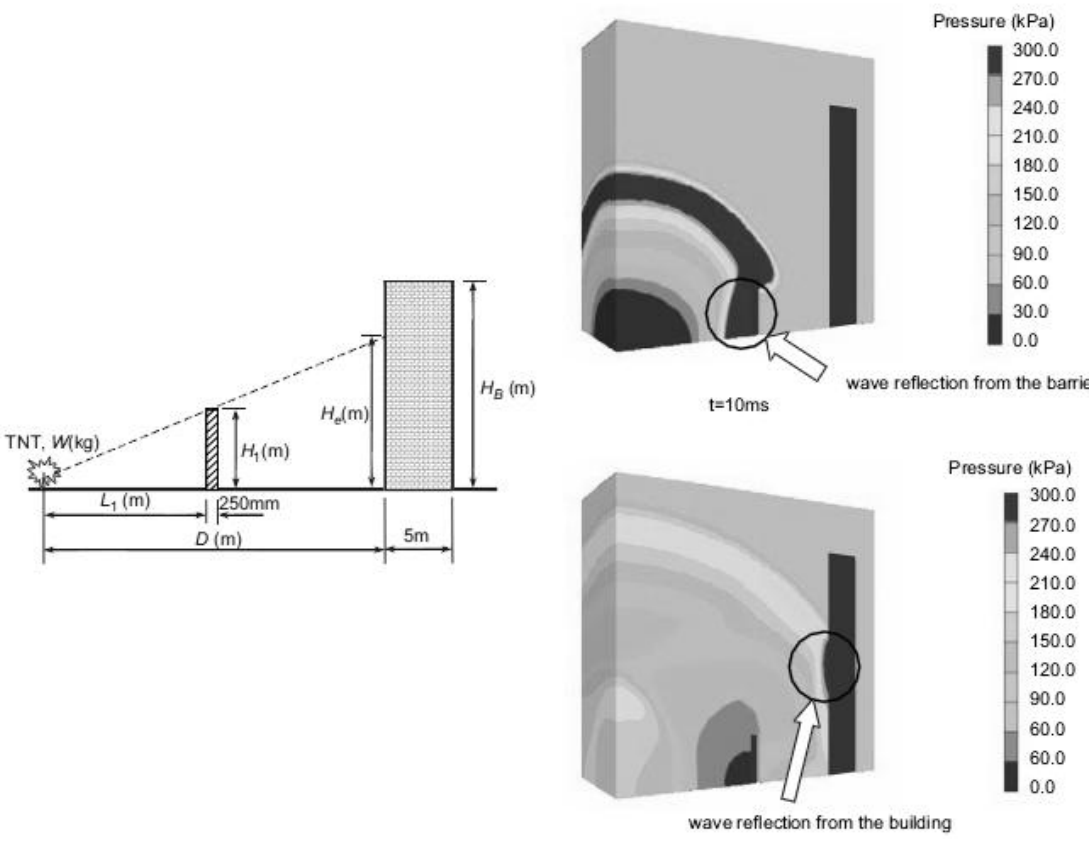

Figure 1.6. Simulation Results [19]

Zyskowski et al. use AUTODYN to predict the blast loading on structures in a confined space [20]. The effort is based on a small scale experimental setup prepared to determine the pressure on the faces of the structure. The numerical approach shows good correlation with the experimental data concluding that AUTODYN is capable of simulating explosion in confined spaces.

1.2.2. Dynamic Response Prediction to Blast Loading

Blast loading occurs due to the momentum transfer of particles impacting and rebounding from the surface of the structure. Mainly, there are two methods used in the literature.

In the first method, the detonation process and interaction of the resulting pressure loads with structure are solved by the same program. It is generally referred as “fully

coupled” method. Explosion products and fast moving air apply a certain pressure to a surface and this approach employs a coupled solution within the same computer program. AUTODYN is the most widely used hydrocode which is highly capable of performing coupled analysis.

Second method includes an integration of two separate programs. One of which calculates the blast loads using an empirical or a semi empirical approach, and the second one calculates the dynamic response to that loading. Since the coupling of two different programs is involved, this method can be named as “hybrid method”. One of the drawbacks of this methodology is that loading on the surface does not change with the deformation of structure. However, it can easily be neglected in most of the problems having a low charge-to-volume ratio or with rigid wall assumption. Also, it is substantially fast compared to the first method. Due to the empirical limitations, this method is extensively used in pre-test calculations, and explosions in underground facilities where insignificant surface deformation or large stand-off distance is observed.

Some of the important examples from both first and second method are presented below.

Nyström and Gylltoft use AUTODYN to predict the response of a concrete block to blast loading [21]. The largest midpoint deflection (Figure 1.7) is recorded and compared with Single Degree of Freedom (SDOF) analyses. Analytical and numerical results show very good agreement.

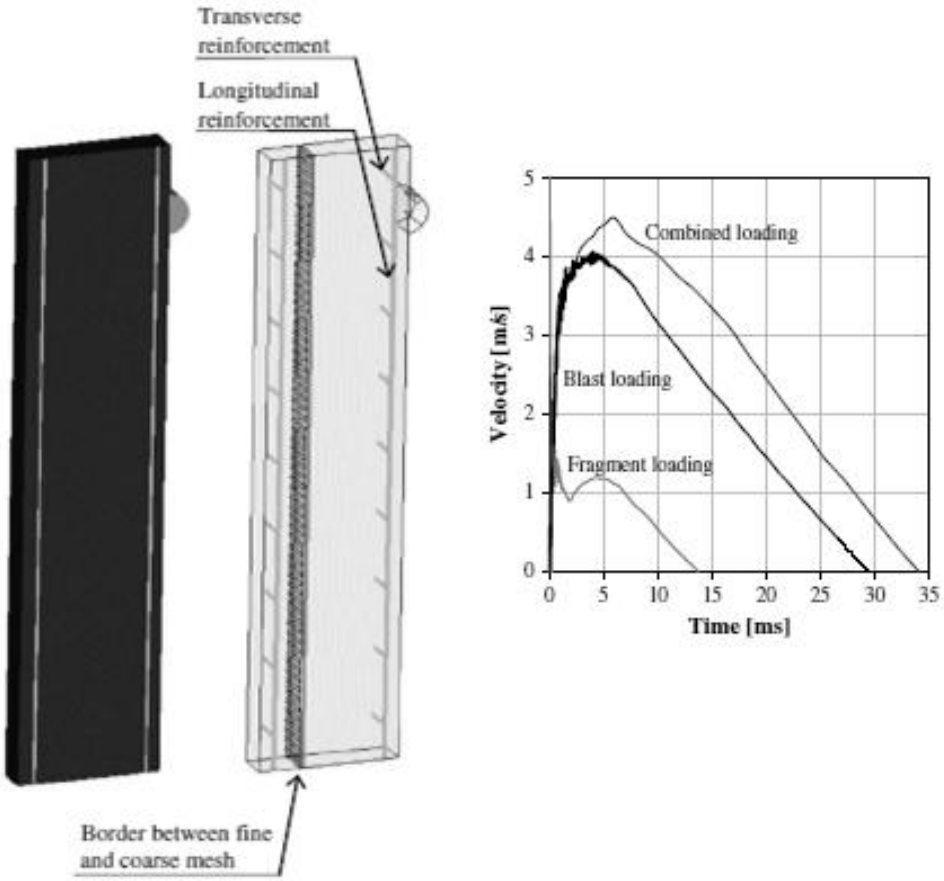

Figure 1.7. Largest Midpoint Deflection in AUTODYN [21]

Shi et al. estimate the deflection due to reflected pressure on a standalone column [22]. Although empirical data is available for very big surfaces, by employing a hydrocode, they are able to take column stiffness, geometry and diffraction around the structure into account. Based on AUTODYN simulations and small scale experimental studies (Figure 1.8), some formulae are proposed to determine the blast parameters on structural columns.

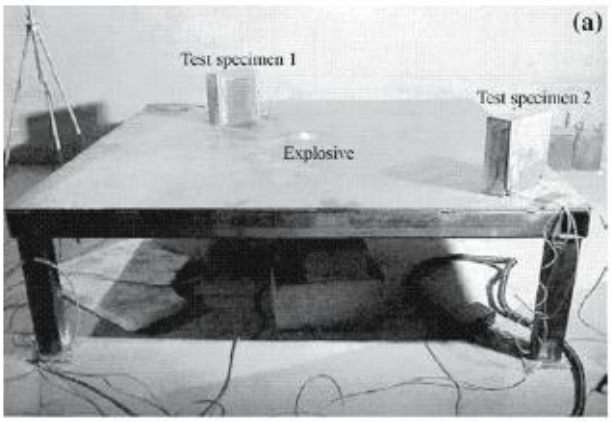

Figure 1.8. Test Setup [22]

Safari et al. investigate the dynamic response of steel and aluminum plates with different thicknesses under blast loading [23]. Experimental, theoretical and numerical results are presented for various stand-off distances and charge weights: 30 – 240 grams of spherical C4 blocks are detonated with a standoff distance 0.2 – 0.25 m (Figure 1.9). Reflected pressure, and positive impulse are recorded. Deviation of the results in maximum deflection is around 10% which can be interpreted as a good agreement.

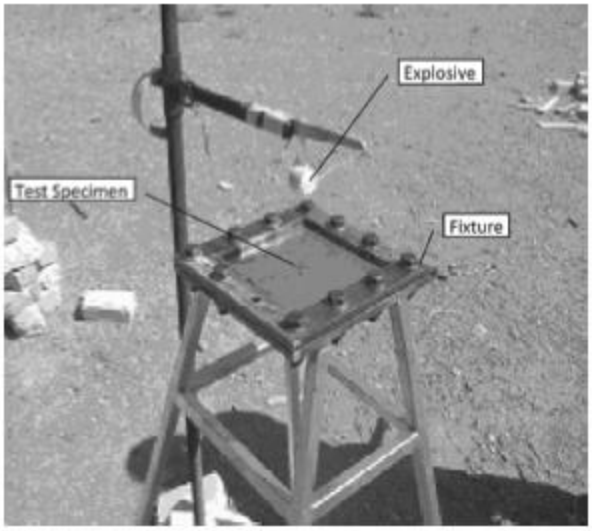

Figure 1.9. Test Setup [23]

One of the very first examples of the integration of two programs to solve dynamic response due to blast loading is performed by Randers-Pehrson and Bannister [24]. The study is started to find a fast and adequately accurate method to model problems such as vehicle response to land mines. CONWEP is implemented into DYNA3D (latter LS-DYNA) code. By doing so, empirical formulas fit to experimental blast data are used to calculate the loads on certain components. DYNA3D only computes structural response to dynamic pressure boundary condition. The method accounts for the angle of incidence of blast wave, but confinement effects are neglected. This type of coupling assures great computational cost savings.

Another unique approach is presented by Wong [25]. The effort focuses on blast load prediction using BLASTX and response analysis using LS-DYNA. A steel box structure is investigated. Inevitably, some assumptions are made during the application of blast loads as a boundary condition such as the behavior of structural elements after material yield. For comparison purposes, a simplified problem is solved with a single degree of freedom method. Nevertheless; a method is proposed with acceptable restrictions on confined space blast calculations.

1.2.3. Experimental Studies

In addition to theoretical works, several experiments are performed to understand the blast overpressure and the dynamic response to blast loading.

The first attempt to quantify the internal explosion effects is made by Weibull [26]. The work is concentrated on setting the basic rules for designing partially closed chambers for industrial and laboratory purposes (Figure 1.10).

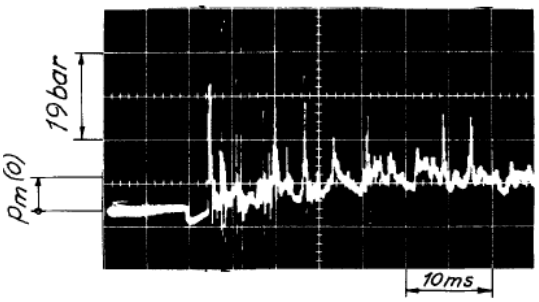

Figure 1.10. Pressure History [26]

After understanding the importance of blast load prediction in weapons facilities, much effort is put in small scale experimentation. During the planning of an explosive production plant (Pantex Plant), a 1:8 scale model of the facility is built and tested [27]. Multiple charges with different geometries are detonated inside various small scale rooms and corridors (Figure 1.11). In this work; measurements of the blast and gas pressure loads are obtained and filtered using an analog filter set to a low pass cutoff frequency of 200000 Hz. In addition, damage due to cased charge is investigated.

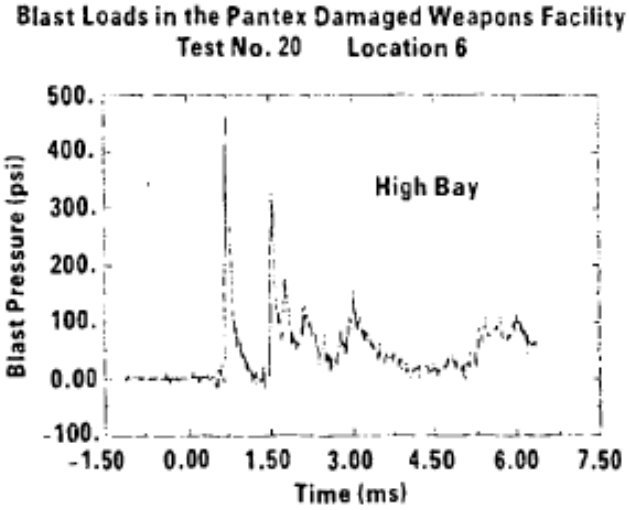

Figure 1.11. Pressure History [27]

Smith et al. demonstrated that meaningful results can be obtained using small scale setups. A series of experiments are performed using different tunnel geometries at 1:45 scale (Explosive Research and Demonstration Area at the Royal Military College of Science) and small partially vented cubicles (50 cm side length) [28]. In this work, 1-3 grams of PETN line charges and 5-10 grams of black powder charges are used. They compared the data with full scale experiments and found reasonable correlations, particularly with peak overpressure.

Aside from the explosions inside a strong structure, thin steel plate response is also investigated [29]. Steel plates with different boundary conditions (one clamped in the soil and another clamped in the four edges) are exposed to TNT detonation (0.8 – 10 kg) at several standoff distances (Figure 1.12). The blast overpressure and acceleration values on the plates are recorded. Jacinto et al. compared both numerical and experimental results on plates affected by blast loads.

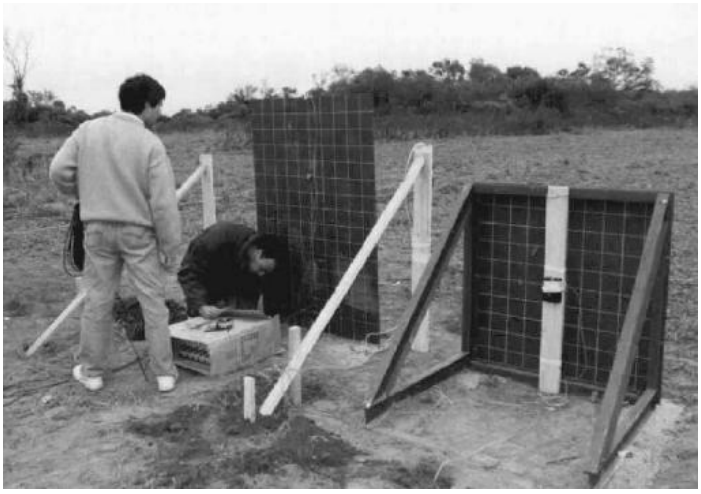

Figure 1.12. Test Setup [29]

In addition to deflection and response investigations, Boyd approaches the problem from another angle: Quantification of the response of a ship deck due to an explosion [30]. In this work, small scale experimentation is employed. A series of experiments to measure the acceleration and displacement of a square steel plate

subjected to blast loading are performed. In his results, it is proven that acceleration of metallic plates due to blast loading in a ship is extremely dangerous.

In application based studies, Edri et al. [31] and Chan and Klein [32] use experimental data to prove prediction methods applied on rectangular bunkers.

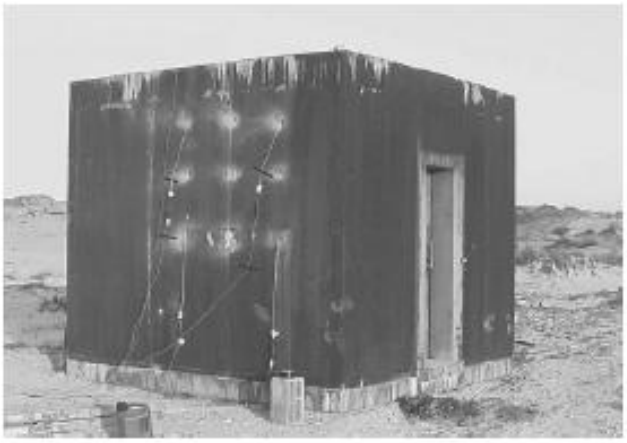

Figure 1.13. Test Setup [31]

Both studies are performed in order to understand the characteristics of an interior explosion with limited venting. Apart from the previous studies, full scale experiments are carried out and blast pressure histories are recorded from several gauge points (Figure 1.14). The effect of the charge weight on blast overpressures and pressure distribution over the walls are investigated.

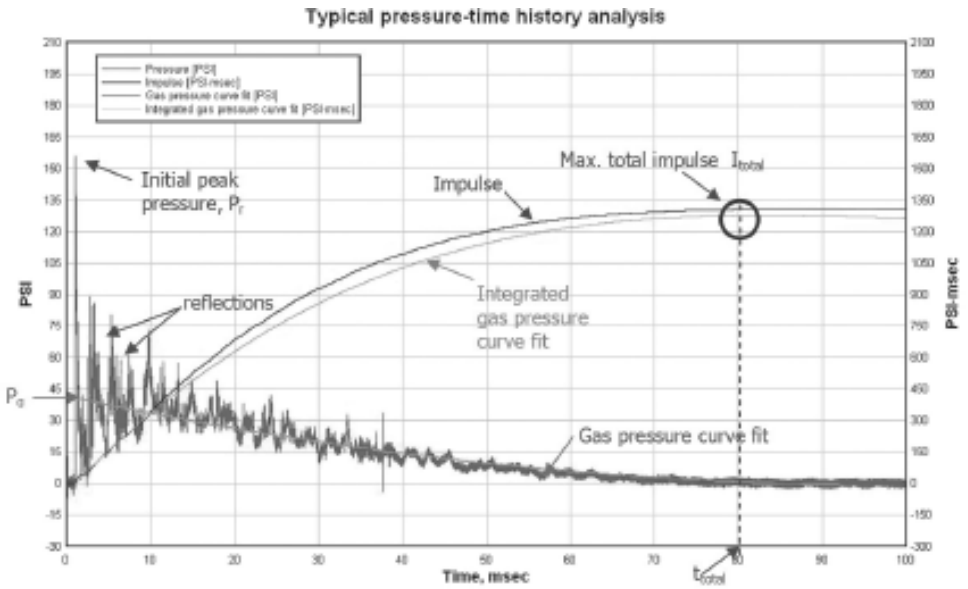

Figure 1.14. Pressure History [31]

Sometimes, authors decide to employ filtering process if the experimental data contains unrealistic peaks or oscillations. Low-pass filters provide a smoother form of a signal, removing the short-term fluctuations and peaks, and leaving the longer-term trend.

Bass et al. stated that it is essential to perform hardware antialiasing filtering for blast testing as high frequency spectral content from sensors may be large. For this purpose 20000 Hz low-pass filter is employed [33]. Similarly, Bauwens used a low-pass filter for pressure histories of hydrogen-air explosions [34]. It was concluded that the low-pass filtered results correspond to potentially damaging overpressures, while the higher frequency pressure oscillations lack sufficient impulse to cause any damage.

Loiseau directs the attention to the pressure transducers. It was stated that numerical filtering should be applied in order to get rid of oscillatory behaviour of piezoresistive pressure transducers [35].

In addition to filtering during the post process, built-in low-pass filters are also used in blast experiments. Smith and Sapko employed 40000 Hz Butterworh low-pass filter during the data acquisition phase [36].

1.3. Motivation and Objectives

Dynamic response of a structure is crucially important especially in internal explosion. Knowing the possible behavior of the structure against certain explosions becomes vital at some point. Design of important buildings is very dependent on safety parameters. In this work, the first step in understanding the possible effects of internal explosions is taken. To do so, a generic vented structure is investigated.

In the literature, there are two types of approach to this problem. First one is to use hydrocodes for the entire solution which takes a lot of computational time, and the second one is to use semi empirical programs that do not give time dependent response solution. However, those methods are either too slow or do not give enough detail about the deformation.

In order to find an alternative method, a commercial hydrocode (AUTODYN) is coupled with a semi empirical program (BLASTX). In this methodology, BLASTX solves the blast loading for a given time. Then, the output is applied as dynamic pressure boundary condition on the structural problem in AUTODYN. By doing so, the speed of empirical methods and the advantage of hydrocodes in rapid structural response solutions are integrated under certain assumptions.

To be able to create a hybrid method explained above, one should be reassured of the consistency of blast loading history calculation initially. After presenting the works from literature and explaining the theory of the programs and methods used, blast overpressure calculations are compared with the experimental results. Due to the differences in experimental and computational outputs, the energy absorption by the test setup is investigated. Next, the analysis over the dynamic response to blast loading took place. A deformable setup is constructed in order to examine the deflection. Again, computational outputs are compared with the test results.

By introducing an easy to use hybrid method, fast predictions can be made and initial steps can be taken in several hours before starting a comprehensive computer analysis.

CHAPTER 2

THEORY

In this section, theoretical backgrounds of the methods used are presented. Firstly, the foundation of the hydrocodes and the numerical applications are demonstrated. Afterwards, semi empirical method used in this work is explained in detail. A unique way of combining these two approaches is also taken into consideration. Lastly, a tolerance analysis is presented in order to show the difference in test results that should be the close within each other in theory.

2.1. Continuum Analyses and Hydrocodes

Blast loading simulations employ complex interaction problems involving multiple systems of structures and high speed gases. Hydrocodes are capable of coupling these different systems together in space and time to provide a solution. They use continuum approach which applies the principles of conservation of mass, momentum and energy. In this chapter, theoretical information about a commercial code AUTODYN and its blast calculation capabilities are provided. AUTODYN is used as the “hydrocode” to perform numerical calculations throughout the thesis.

2.1.1. Continuum Approach

In continuum approach, there is an important assumption. The material completely covers the space it occupies without any voids. Under this condition, it can be said that an infinitesimally small portion of a material shows the very same properties of the entire media. On the other hand, the assumption addresses a contradiction with

the inherent discontinuity of the material. It is known that all the materials are made of molecules or atoms which are departed from each other with a certain distance. Fortunately, if the problem is not investigated under molecular level, continuum approach is highly accurate [37].

Continuum approach employs conservation of mass, momentum and energy, and constitutive relations to consider the material properties. All the equations are solved as a coupled set of highly nonlinear differential equations. Since the exact analytical solutions of the equation set is only available for incompressible flows, numerical solution is a must. The use of hydrocodes in blast calculations emerges specifically from that need.

2.1.2. Hydrocodes

In literature, there are two alternative descriptions for the continuum mechanics: Eulerian approach and Lagrangian approach. Eulerian approach relies on material flowing through the solution space, whereas Lagrangian approach describes a mesh which represents only the geometry filled with problem considered. Collins made an analogy to depict the differences between the methods:

“One decides to add some dye to the water to monitor the flow of particles. If the observer follows the path of the dyed particles in the water, the Lagrangian description applies; if the observer remains at a certain point along the river bank and notes which particles pass with time, the Eulerian description applies.” [37].

The difference between Eulerian and Lagrangian method is the solution technique of the same conservation equations. Both methods discretize the time and space of the defined problem but they employ different spatial discretization technique. The description of the problem geometry varies due to this difference. Simply put, Lagrangian method is material based and solve discrete sections which moves with material, conversely; Eulerian method is spatially based and solve discrete sections which remain fixed in space (Figure 2.1).

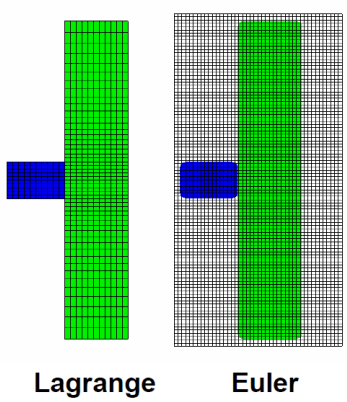

Figure 2.1. Discretization Differences of Eulerian and Lagrangian Approach [38]

It cannot be said which method is better since each one has its strengths in various areas. Eulerian approach uses advection of materials through the mesh as they flow or deform which provides the best solution for the fluid flow and extreme deformation of solids. On the other hand, Lagrange approach use meshes that are imbedded in material and move and distort with the material which provides the most efficient and accurate method for computing structural response.

Both methods are employed in blast calculations. Blast wave is calculated within Euler approach and structural response is predicted by Lagrangian approach. This is achieved by coupling both approaches that allows the interaction of Euler and Lagrange regions. Coupling is performed in both space and time. Boundaries of Lagrange parts act as flow constraints within the Euler meshes where consequently Euler meshes exert forces on the boundaries of Lagrange parts (Figure 2.2).

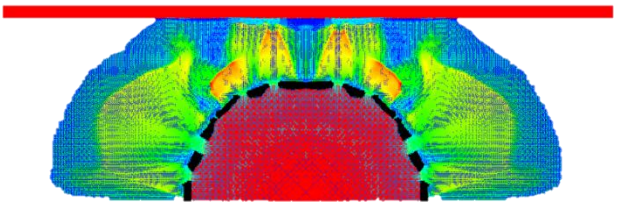

Figure 2.2. Euler – Lagrange Interaction [38]

2.1.2.1. Eulerian Approach

Eulerian approach relies on material flowing through the solution space. In this method, the whole solution space is defined by the numerical mesh which stays fixed in space. Therefore, mesh distortion is not possible. Material is transported from cell to cell. In other words; mass, momentum and energy flow across cell boundaries. Since the volume is fixed, change in the mass is calculated from the change in density. The computational cycle of Eulerian approach in AUTODYN is summarized in the below (Figure 2.3).

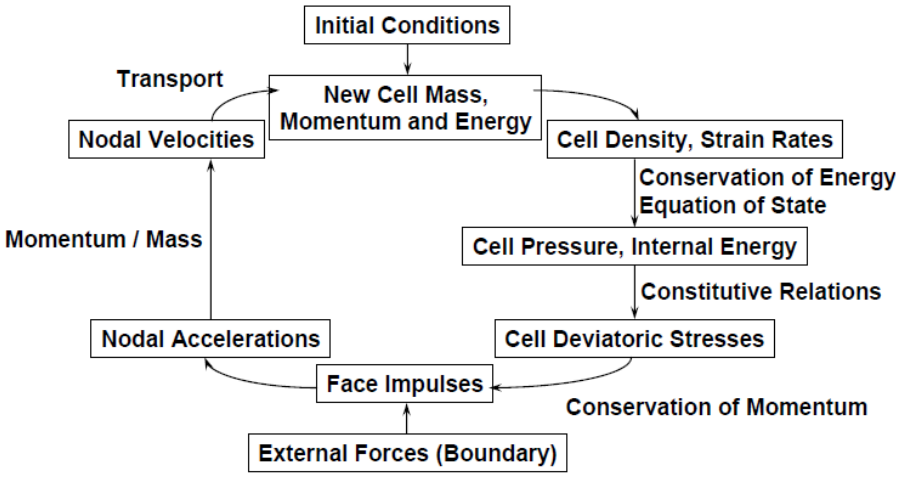

Figure 2.3. Eulerian Computational Cycle [38]

There are two types of boundary conditions used in this work for the Eulerian approach: Rigid wall and outflow. In rigid wall boundary condition, the velocity of the flow is set to zero and generally used to mimic non-deformable structures. Outflow boundary condition assumes zero pressure, density and internal energy, resulting an outflow for the preferential material.

The advantages of Eulerian approach can be listed as zero mesh distortion and ability of solving large deformations. But then, more computations per cycle is needed and it is less flexible for strength modeling.

2.1.2.2. Lagrangian Approach

Lagrangian approach describes a mesh which represents only the geometry filled with the problem considered. Since the mesh move with the material, it is generally used for structural modeling. Computational cycle of Lagrangian approach is as follows: At the start of the solution, the nodal velocities are integrated to get the new nodal positions. After that, new cell density and cell strain rates are calculated using the new nodal positions. Consequently, new stresses can be obtained from the strains. The computational cycle of Lagrangian approach in AUTODYN is summarized in the below (Figure 2.4).

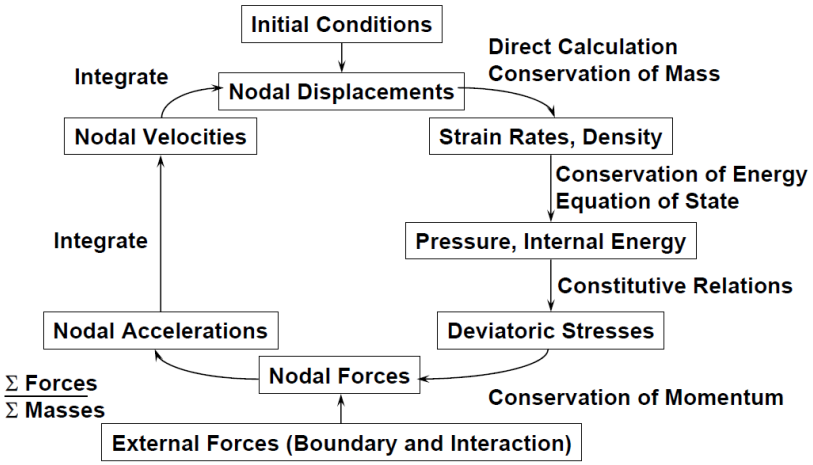

Figure 2.4. Lagrangian Computational Cycle [38]

There are two types of boundary conditions used in this work for the Lagrangian approach: Stress and General Velocity. In Stress boundary condition, one can apply any pressure data to a specific part as a function of time. In addition, zero general velocity (3D – X, Y, Z) is used for fixed boundary conditions.

The advantages of Lagrangian approach can be listed as fewer computations per cycle, more clear definition of material interfaces and boundaries, simpler code and good time history information. However, small timesteps may occur due to element distortion and special techniques are required for impacting and sliding interfaces.

2.1.2.3. Euler – Lagrange Interaction

As stated earlier both Eulerian parts and Lagrangian parts are used in this work. During the analysis of blast overpressure, Eulerian medium is considered only. However, throughout the dynamic response analysis both methods are coupled using “full” coupling. In the process of interaction, Lagrangian interface may “cut” through the fixed Eulerian mesh in an arbitrary manner. The Eulerian cells intersected by the Lagrangian interface define a stress profile for the Lagrangian boundary vertices. In return, the Lagrangian interface defines a geometric constraint to the flow of material in the Eulerian mesh. AUTODYN recognizes that the Eulerian cells adjacent to a Lagrangian boundary may be partially covered by the Lagrangian part and their volumes and face areas may be continually changing [39]. Constant information transfer between the boundaries helps calculating the dynamic response to blast loading without disregarding the structural deformation.

2.1.2.4. Governing Equations

Hydrocodes solve identical set of equations derived from continuum approach. Conservation of mass, momentum and energy provide 5 equations in total:

- Conservation of Mass :

$$\frac{\partial \rho}{\partial t} + \frac{\partial (\rho V_i)}{\partial x_i} = 0 \qquad \textbf{(2.1)}$$

- Conservation of Momentum

$$\frac{\partial V_i}{\partial t} + V_j \frac{\partial V_i}{\partial x_j} = f_i + \frac{1}{\rho} \frac{\partial \sigma_{ij}}{\partial x_j} \qquad \textbf{(2.2)}$$

- Conservation of Energy

$$\frac{\partial e}{\partial t} + V_i \frac{\partial E}{\partial x_i} = f_i V_i + \frac{1}{\rho} \frac{\partial \sigma_{ij} V_i}{\partial x_j} \qquad \textbf{(2.3)}$$

- Constitutive Model (Stress - strain relation)

$$\sigma_{ij} = g(\epsilon_{ij,}\dot{\epsilon}_{ij}, e) \quad \textbf{(2.4)}$$

- Equation of State : (Pressure- density and internal energy relation)

$$P = (E, \rho) \quad \textbf{(2.5)}$$

where V is the velocity, ρ is density, E is the total energy, f is the body force, x is the displacement, σ is the stress, ϵ is the strain, $\dot{\epsilon}$ is the strain rate and t is time.

There are 15 unknowns involved in these equations. In the continuum approach, 5 unknowns are calculated from conservation equations (1 from conservation of mass, 3 from conservation of momentum and 1 from conservation of energy). The remaining 10 unknowns are obtained using constitutive relations (9 equations) and equation of state (1 equation). The constitutive relations associate the deviatoric stresses to the strains, strain rates and internal energy where deviatoric tensor defines the resistance of the material to shear distortion. The equation of state relates the pressure to density and internal energy of the material where the pressure is the hydrostatic pressure.

Many constitutive relations and equation of states can be found in literature for a certain material. Generally speaking, each model shows good agreement for a specific problem. This is why they should be chosen carefully and compliant to the problem considered. Due to the rapid blast loading, high strain rates in the structure and rapid expansion in the detonation center are expected. For this purposes, Johnson Cook strength model as constitutive relations and Shock model as an equation of state are chosen for the structure. In the meantime, Jones-Wilkins-Lee (JWL) form of equation of state is used for the high explosive modeling. No strength relation is considered since hydrodynamic calculation is regarded only for the detonation modeling.

2.1.2.4.1. Constitutive Relations

A strength model is a set of constitutive relations that simulates the connection between stress, strain and internal energy. Although there are several models in the literature, general approach is always the same. All strength models initially

calculate an elastic stress state based on Hooke's Law. From this three dimensional stress state, an equivalent scalar stress, the Von-Mises stress is calculated. Then, it is compared to the materials yield stress to determine whether plastic flow has taken place. For the purposes of this work, Johnson-Cook strength model is selected due to its capabilities in high strain rates. It is capable of considering the effects of strain hardening, strain-rate hardening and thermal softening including melting. In Johnson-Cook model, yield stress is given by

$$\sigma_{ij} = \left[A + B\varepsilon_{ij}{}^{n}\right]\left[1 + C ln\dot{\varepsilon_{ij}}^{*}\right][1 - (T^{*})^{m}] \quad \textbf{(2.6)}$$

$$T^{*} = \frac{(T - T_{room})}{(T_{melt} - T_{room})} \quad \textbf{(2.7)}$$

$$\dot{\varepsilon}^{*} = \frac{\dot{\varepsilon}}{\dot{\varepsilon_{0}}} \quad , \quad \dot{\varepsilon_{0}} = 1.0\ s^{-1} \quad \textbf{(2.8)}$$

where A is the yield strength of the material, B is strain hardening constant, n is the strain hardening coefficient, C is strain rate constant and m is the thermal softening exponent obtained from Split Hopkinson Bar test. In addition, T is the temperature and T_{room} & T_{melt} are the room temperature and the melting temperature of the metal respectively. In the last equation, $\dot{\varepsilon}$ represents the strain tensor whereas and $\dot{\varepsilon_{0}}$ is the reference strain rate.

2.1.2.4.2. Equation of State

Equation of state (EOS) describes the relation between the pressure, density and internal energy. In practice, compressibility effects and thermodynamic processes are defined by those variables. There are several kinds of EOS defined in AUTODYN. In this work, Shock, JWL and Ideal Gas equations are used.

The propagation of shock waves can be modeled accurately with Shock EOS which is suitable for the modeling the structures affected by blast loads. An empirical relation between shock velocity and particle velocity is defined as:

$$U = c_0 + su_p \quad \textbf{(2.9)}$$

where U is the shock velocity, u_p is the particle velocity, c_0 and s are the empirical constants.

In hydrodynamic calculations of high explosives, very rapid release of energy is observed where time interval is shrunk almost to zero. Detonation wave propagates through the unreacted material at very high velocity, liberating energy and transforming the explosive into detonation products. JWL EOS is specially constructed to model this kind of rapid expansion. It is an empirical formula derived from fitting numerical models to physical experiments.

$$p = A\left(1 - \frac{w}{r_1 v}\right)e^{-r_1 v} + B\left(1 - \frac{w}{r_1 v}\right)e^{-r_2 v} + \frac{we}{v} \quad \textbf{(2.10)}$$

where A, B r_1, r_2, and w are the empirical constants. In addition, v is the specific volume and p represents the pressure.

In this study, detonation points are defined. Starting from that point at t=0, the detonation wave is assumed to travel at the prescribed detonation velocity.

The last equation of state used in this work is the ideal gas equation. When particles' kinetic energy exceed intermolecular work, the empty space between molecules becomes more important than the size of the molecules. This kind of behavior is expressed as ideal gas. Many gases such as air can be assumed as ideal gas within reasonable tolerances. In the ideal gas equation, the pressure shift is used to define small initial pressures in a model.

$$p = (\gamma - 1)\rho e + p_{shift} \quad \textbf{(2.11)}$$

where γ is the ideal gas constant, ρ is the density, p_{shift} is the pressure shift, e is the specific internal energy.

2.1.3. Numerical Aspects of Hydrocodes in Blast Calculations

Using the approaches, definitions and relations mentioned above, a model for any blast calculation can be constructed. However, one should also consider numerical

restrictions and reduction of computational costs. To do so; mesh sensitivity of AUTODYN is investigated, a technique to speed up the computation called “remapping” is deeply analyzed, and scaling law is adapted into the hydrocode to shrink the modeling space.

2.1.3.1. Mesh Sensitivity

Aside from the main purposes of their work Sklavounos and Rigas [13], Luccioni et al. [17] and Zhou and Hao [19] also showed that decreasing the mesh size in order to improve the solution estimation was not possible after some point due to both hardware and software capacities. To obtain mature dependability, accuracy and reliability in this work whilst maintaining a reasonable computational cost, sensitivity analysis is carried out.

In order to investigate the effect of mesh size in AUTODYN, a simple one dimensional (wedge) solution domain is originated. In each model, 50 mm radius Composition 4 (C4) high explosive is detonated in 500 mm air filled wedge domain (Figure 2.5).

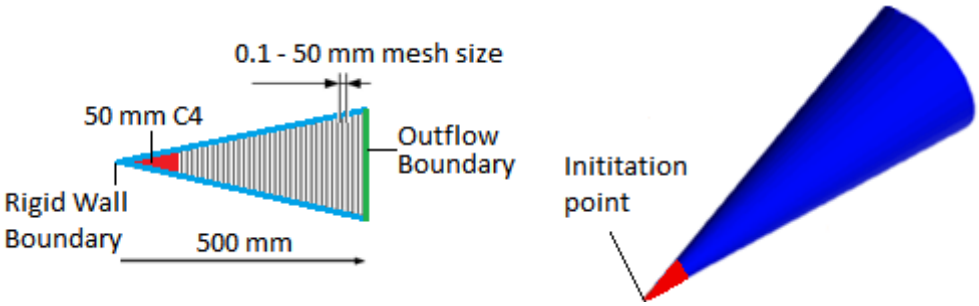

Figure 2.5. Mesh Sensitivity Problem Definition

The opposite side of the detonation point is treated as outflow boundary to prevent shock any reflection. The remaining edges are assumed as rigid wall since the problem is defined as one dimensional.

Various models are created using different mesh sizes to find the convergence of numerical results in AUTODYN. 10 models are built using 0.1 – 50 mm mesh size (Table 2.1).

Table 2.1. Mesh Sensitivity Models

Cell Size [mm]	Number of Elements
0.1	5000
0.25	2000
0.5	1000
1	500
2.5	200
5	100
6.25	80
12.5	40
25	20
50	10

Air and C4 material models are obtained from AUTODYN's default library. Air is modeled using "ideal gas" equation and C4 is modeled using JWL equation (Table 2.2)

Table 2.2. Material Modeling – Air, C4

AIR	**Equation of State**	**Ideal Gas [39]** Equation (2.11)
	Reference density	1.225E-03 [g/cm^3]
	Gamma	1.4
	Adiabatic constant	0
	Pressure shift	0 [kPa]
	Reference Temperature	288.2 [K]
	Specific Heat	717.6 [J/kgK]
	Thermal Conductivity	0 [J/mKs]

Table 2.2. (Cont'd) Material Modeling – Air, C4

C4	**Equation of State**	**JWL [40]** Equation (2.10)
	Reference density	1.601 [g/cm^3]
	Parameter A	6.09770E+08 [kPa]
	Parameter B	1.295E+07 [kPa]
	Parameter R1	4.5
	Parameter R2	1.4
	Parameter W	0.25
	C-J Detonation velocity	8.19300E+03 [m/s]
	C-J Energy / unit volume	9 E+06 [kJ/m^3]
	C-J Pressure	2.8E+07 [kPa]
	Burn on compression fraction	0
	Pre-burn bulk modulus	0
	Adiabatic constant	0

Pressure histories are compared for each simulation. Four locations (gauge points) are selected to record medium properties. Zero being the detonation center, pressure histories for 100 mm, 200 mm, 300 mm and 400 mm are recorded (Figure 2.6).

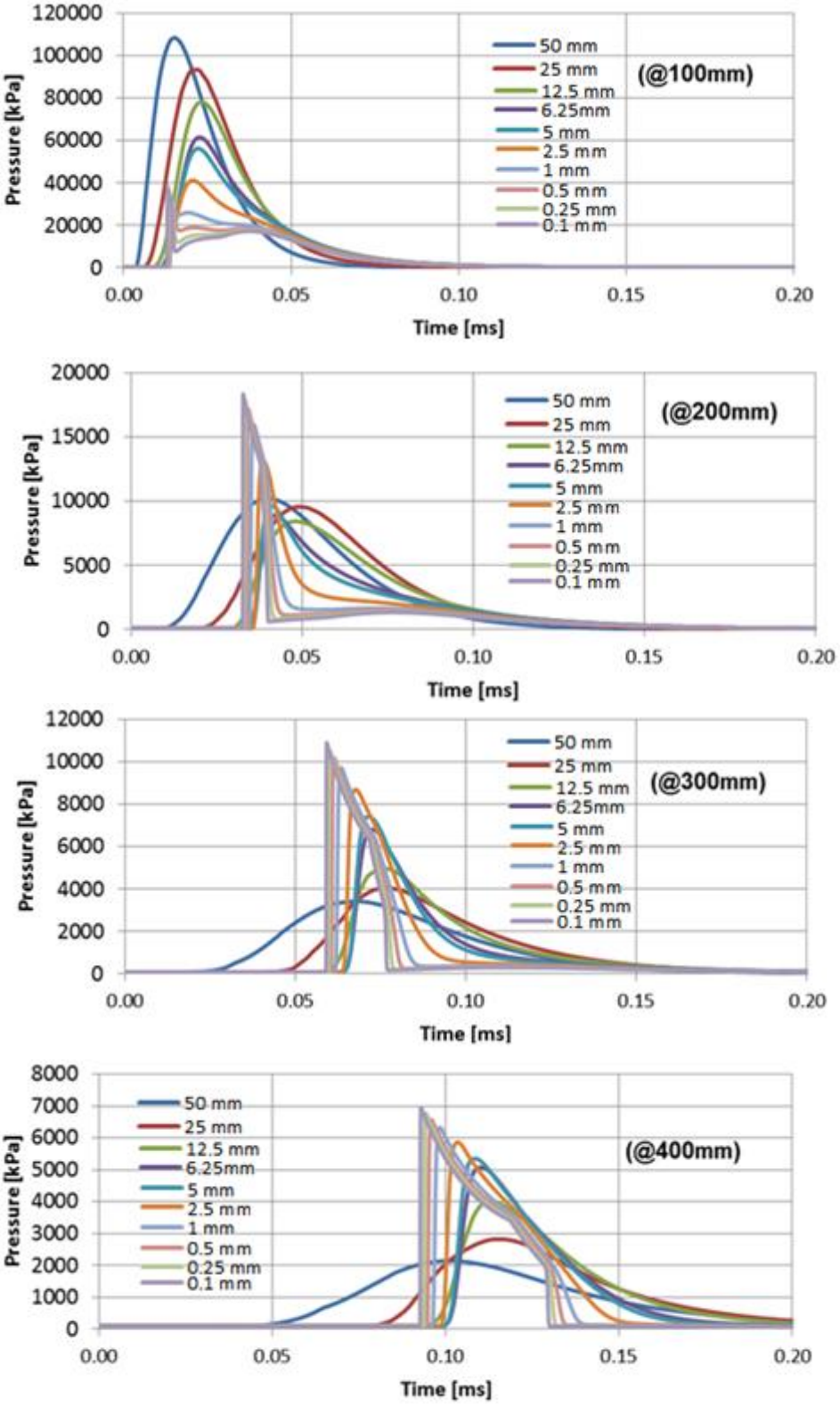

Figure 2.6. Pressure Histories at Different Locations

As it can be deduced from the figure above, pressure is predicted much higher with coarse models near the detonation center. Conversely, pressure is predicted much lower with coarse models far from the detonation center. This phenomenon occurs due to inaccurate calculations of very rapid changes in and near the detonation center in coarse models. Coarse models are not adequate to catch the parameter differentiations in space. The variation inside a single cell becomes too much to handle correctly, resulting a very rough estimate over that area. As the point of interested draws away from the detonation, near field factors are assumed to be diminished. In addition; to prevent any effect due to the outflow boundary condition, 400 mm distance is used to compare the peak pressures (Figure 2.7).

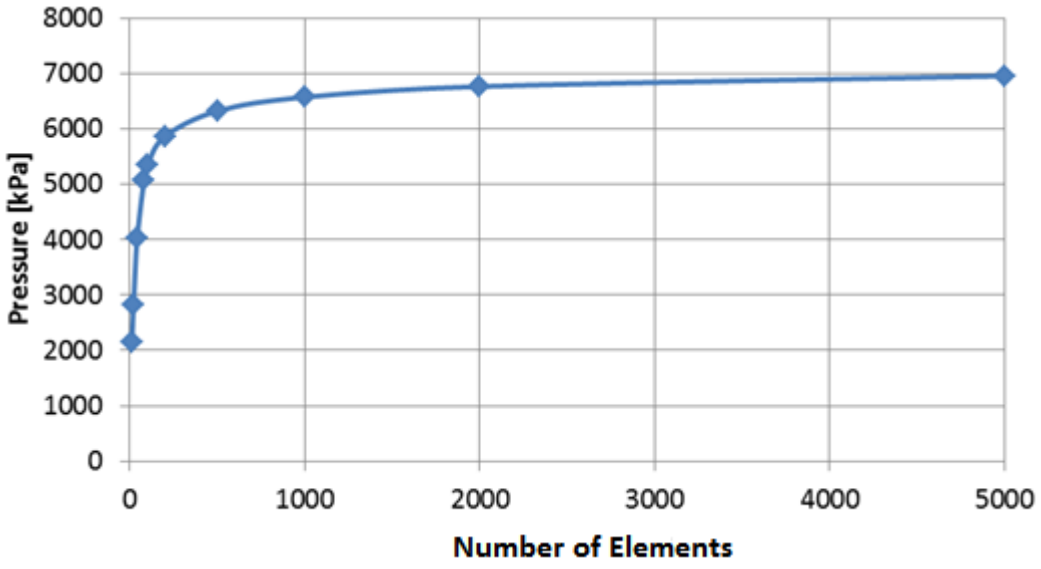

Figure 2.7. Peak Pressure Comparison

Results from 1000 elements to 5000 elements seem to be within a good range. In addition, pressure histories are almost coincident. Throughout this work, 0.1 mm and 1 mm mesh sizes are used. On the other hand, if mesh size bigger than 1 mm should be used due to other restrictions, it should be noted that under-estimation is predicted.

2.1.3.2. Remapping

Remapping is a widely used technique for blast calculations. The idea behind the method is the assumption of symmetry. Since the medium modeled in AUTODYN shows exactly the same properties everywhere, blast wave should propagate through it with the same velocity and pressure at the same distance to the center. This assumption is accurate if no obstacle is met on the way. Under the restrictions mentioned, initial analysis is carried out in one dimensional model (Figure 2.8).

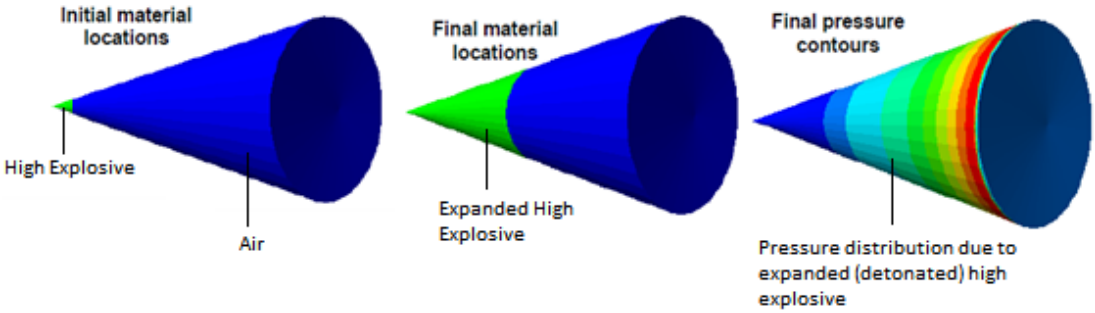

Figure 2.8. One Dimensinal Model

Primarily, problem should be evaluated in three stages depending on the structural geometry. Firstly, one dimensional calculation is performed according to the nearest obstacle to the detonation center. After that, results in one dimensional analysis are mapped into two dimensional problem. This action depends on the blast wave expansion. The calculation continues until the blast wave reaches any structure in two dimensional space. Finally, results of two dimensional analysis is mapped into three dimensional model (Figure 2.9).

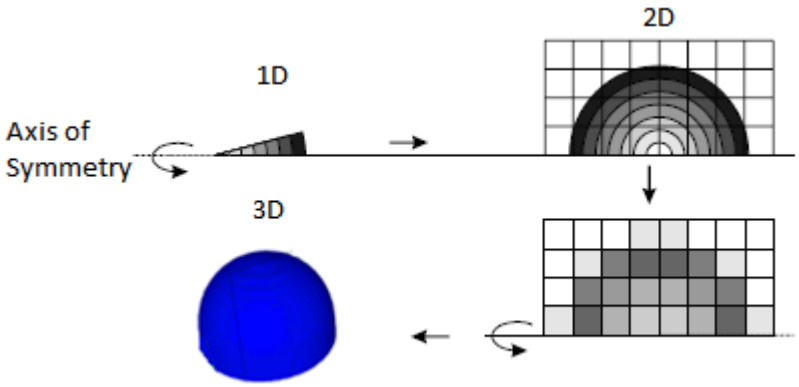

Figure 2.9. Mapping Sequence

To validate the method, two models are constructed. A 100 mm wedge is modeled for the one dimensional one and a 100 mm cube is modeled for three dimensional one using 1 mm cell size (Figure 2.10). In one dimensional domain, the opposite side of the detonation point is treated as outflow boundary to prevent any shock reflection. Similarly, all the surfaces are treated as outflow boundary in three dimensional domain. Calculations are performed from the detonation instant until the blast wave reaches 90 mm distance to avoid any boundary condition effect. The material properties are similar to the previous mesh sensitivity investigation: Ideal gas equation for air and JWL equation for C4. No remapping is used since the goal is to show one dimensional analysis can be performed instead of three dimensional until an interaction occurs. In theory, both models should estimate the same pressure history at the same distance.

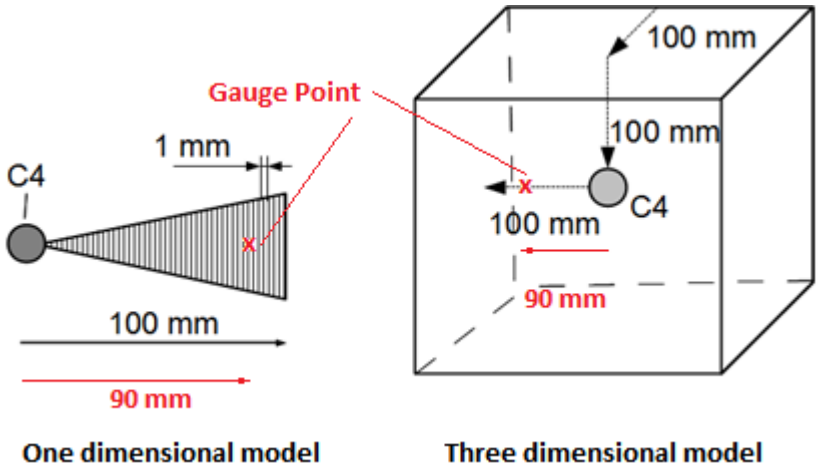

Figure 2.10. One Dimensional and Three Dimensional Models

The models are solved in AUTODYN. Peak pressures depending on the position of the gauges are recorded. Data starts from 30 mm since the radius of 150 g C4 charge itself is about 28 mm (Figure 2.11,Figure 2.12).

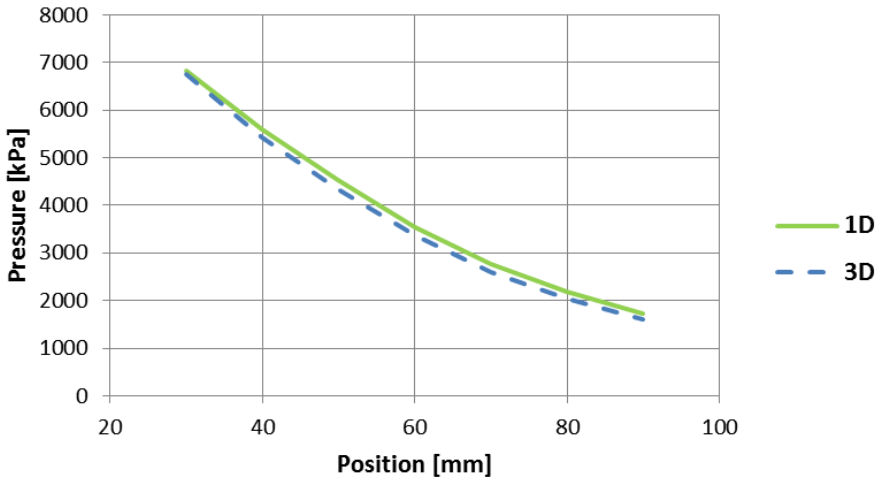

Figure 2.11. Position Dependent Peak Pressure Data for 1D and 3D

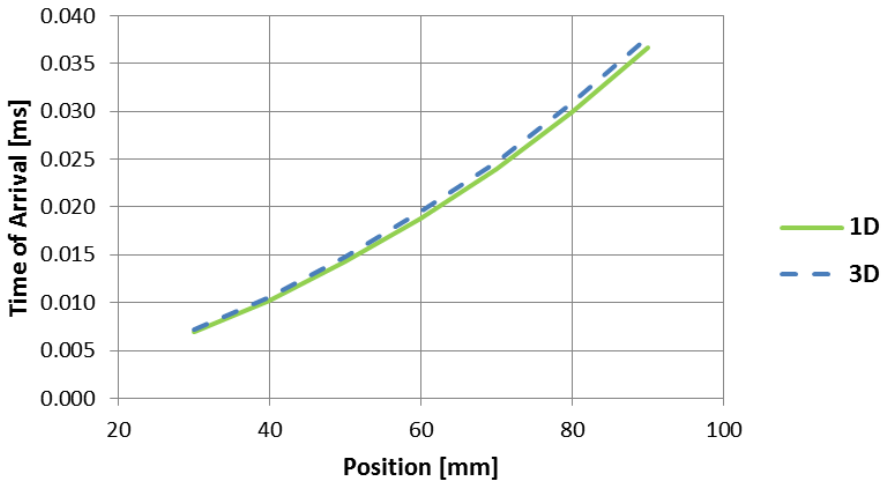

Figure 2.12. Position Dependent Arrival Time Data for 1D and 3D

Between 30 mm and 90 mm pressure difference reaches a maximum of 6.5% whereas arrival time difference in the same distance hits a maximum of 3.9%. Within the given problem definitions; 1D model is solved in 6 minutes and 3D model is solved in 402 minutes. Since the differences do not show any trend of increasing after 80 mm distance; it can be said that within known error margins, one dimensional analysis can be used considering the computational costs.

2.1.3.3. Numerical Investigation of Scaling Law

The other method employed to speed up the blast computation is the implementation of the scaling law into the hydrocode. Scaling law is also known as cube-root scaling or Hopkinson scaling. It is used in the literature extensively to minimize test costs by applying small scale setups. The method is proved to be accurate in many works from Baker [40], Esparza [41], Ripley et al. [42] and many more.

Practically, scaling law is used to relate the characteristic properties of the blast wave from an explosion of one energy level to another. According to the law, exactly the same pressure will occur at a given scaled distance which is defined by the ratio of true distance from a detonation and cube root of the charge weight.

$$Z = \frac{R}{W^{1/3}} \tag{2.12}$$

where Z is the scaled distance, R is the true distance, and W is the charge weight.

Various distances and charge weights may give the same scaled distance value. Actually, this flexibility makes the law so popular in the literature.

On the other hand; despite pressure being the same quantitatively, time axis should not be taken as same. Since the energy levels of different charges are not the same, the duration of the energy reliefs are not expected to be same. Hence, the time information from one energy level should be multiplied by some constant to be applicable to another energy level. The time proportion of the base energy level should be taken as 1 whereas the other energy level's constant is determined by the charge weight. Fortunately, it would be proportional to the cube root of the charge mass.

$$\frac{t_1}{(W_1)^{1/3}} = \frac{t_2}{(W_2)^{1/3}} \tag{2.13}$$

where t is the time parameter (can be selected as duration, arrival time etc.)

To validate the applicability of the law to AUTODYN, two models are constructed (Table 2.3).

Table 2.3. Scaling Law Models

Model Number	Charge Weight	Distance	Scaled Distance (Z)	Time Proportion Constant (t_1/t_2)
1	1	1	1	1
2	0.125	0.5	1	2

In theory, two models should give the same peak pressure since both having the same scaled distance. In addition; when the time axis of the smaller one is multiplied

using the proportion constant, pressure histories should coincide precisely. The results of the calculations are presented on the upcoming figure (Figure 2.13).

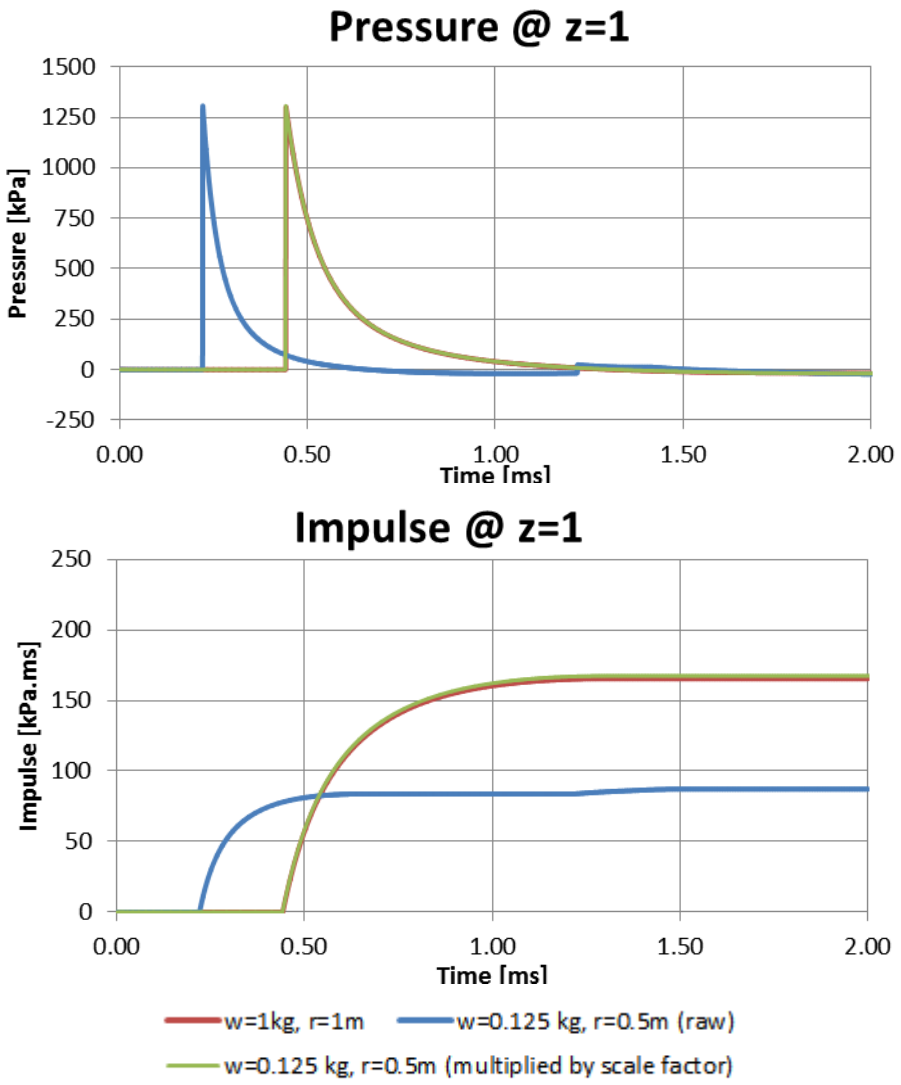

Figure 2.13. Scaling Law Computational Results

Model 1 and model 2 estimated the same peak pressure, and have identical histories which is expected. It should be noted that model 1 and 2 coincides, resulting an overlap of the computational outputs. As a result, it can be said that if one knows the proportion constant, scaling law is a powerful tool to reduce

computational costs by shrinking the models. In this work, scaling law is used extensively in numerical simulations.

2.2. Semi Empirical Method Used in Blast Calculations

The semi empirical method (BLASTX) employed for blast calculations during the work provides the blast environment in structures for both internal and external explosions. It uses fast running analytical/empirical models that are created by merging simplified blast physics and vast amount of experimental data. BLASTX treats the shock wave effects with a ray-based model that is integrated with the gas pressure-venting model. The blast is assumed to originate from spherical or cylindrical explosions where the walls of the room are treated as perfectly rigid reflecting surfaces that may allow gases to vent into other rooms by a certain opening. Since it was not possible to cover all the explosive types and ranges by experiment, BLASTX includes the data tables for 52 ranges and the most common explosives: C-4 and TNT charges. 1 kg charge is used as a standard charge weight where results for the other weights are obtained using the scaling law.

Wave forms are calculated by interpolation of tables of pressure, particle velocity, and density that were computed for 1 kg spheres.

At range R different from the 52 ranges of the tables, pressure, particle velocity, and density wave forms are interpolated as follows: Three ranges that surround R are determined. Peak shock overpressure (P_{SO}), arrival time (t_a), and positive phase duration (t_0) are computed by quadratic interpolation from these three ranges (Figure 2.14). Waveforms at the two closest ranges are then used. Time t (after detonation) is shifted in these waveforms to the arrival time computed for range R (same as multiplying time proportion constant). Positive durations of the pressure waveforms are shifted to the interpolated value at R. At times between the arrival time and the end of the positive phase, values of pressure, particle velocity, and density are linearly interpolated between the shifted waveforms.

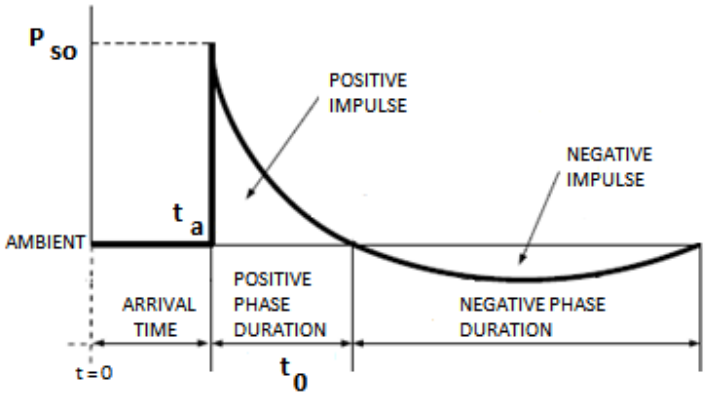

Figure 2.14. Ideal Blast Wave Form

At scaled ranges R beyond 20 $m/kg^{1/3}$, arrival time is extrapolated from the value at 20 $m/kg^{1/3}$ using the sound speed in air, and peak pressure and pulse duration are obtained from power law extrapolation. Let the subscript 20 denote values at the scaled range 20 $m/kg^{1/3}$. Then peak pressure is computed from the following equations:

$$for\ 20 < R \leq 40 \frac{m}{kg^{\frac{1}{3}}}, \quad P_{SO} = P_{20}(\frac{20}{R})^{1.37} \tag{2.14}$$

$$for\ R > 40 \frac{m}{kg^{\frac{1}{3}}}, \quad P_{SO} = P_{20}(\frac{20}{40})^{1.37}(\frac{40}{R})^{1.2} \tag{2.15}$$

Positive phase duration is calculated from

$$for\ R > 20 \frac{m}{kg^{\frac{1}{3}}}, \quad t_0 = t_{20}(\frac{R}{20})^{0.3} \tag{2.16}$$

Shock wave reflections off the walls of a room are computed using the procedure of the LAMB Code [43]. It is widely used in literature for shock addition. Each reflection from a wall is treated as a pulse originating from an imaginary source free-air explosion located behind the wall. The pressure at any point is a non-linear superposition of the direct shock and a contribution from an image source for each of an infinite series of reflections.

The procedure for computing a waveform is as follows: First, path lengths for rays of successively higher order reflections are generated. Arrival times, peak pressures, and the other waveform parameters are computed from for the scaled path lengths of each ray. Next, pressure, particle velocity, and density waveforms for each ray are calculated neglecting the presence of other rays. Finally, the pressure waveforms are combined using the LAMB non-linear shock addition rules to produce the total shock wave pulse [44].

- **Shock Addition Rule 1 – Conservation of Mass**

It is assumed that at a pointing space, the density, $\overline{\rho}$, is the ambient density, ρ_a, plus the sum of the overdensities, $\Delta\rho_i$, due to all shocks that have passed that point at a given time

$$\overline{\rho} = \rho_a + \sum_{i=1}^{N_s} \Delta\rho_i \qquad \textbf{(2.17)}$$

where N_s is the number of shocks.

- **Shock Addition Rule 2 – Conservation of Momentum**

$$\overline{\rho}\vec{V} = \sum_{i=1}^{N_s} \rho_i \vec{V}_i \qquad \textbf{(2.18)}$$

where $\vec{V}$ is the total material velocity, ρ_i is the density for shock i, and $\vec{V}_i$ is the particle velocity for shock i.

- **Shock Addition Rule 3 – Conservation of Energy**

The total overpressure from N_s shocks is

$$P = \sum_{i=1}^{N_s} P_i + \left[\frac{\gamma_0 + 1}{2}\right]\left[\frac{1}{2}\sum_{i=1}^{N_s} \rho_i \left|\vec{v}_i\right|^2 - \frac{\overline{\rho}}{2}\left|\vec{v}\right|^2\right] \qquad \textbf{(2.19)}$$

where P_i is the overpressure for shock i and γ_0 = Cp/Cv is the ratio of heat capacities (gamma) at ambient atmospheric pressure and temperature. In order to

improve the accuracy of the calculations for incident pressures above about 0.345 MPa, BLASTX uses a real gas variable gamma based on the sum of the P_i.

In the previous section, it was stated that BLASTX is a semi empirical program that employs physical relations and experimental data. Comparing BLASTX with CONWEP would reveal the differences between pure experimental interpolation and semi empirical approach. For this purpose, a simple problem is investigated: The reflected pressure 50 cm away from a certain charge in a free field explosion.

50,100 and 150 grams of spherical charges are selected to fulfill the purpose. Each scenario is calculated using both BLASTX and CONWEP.

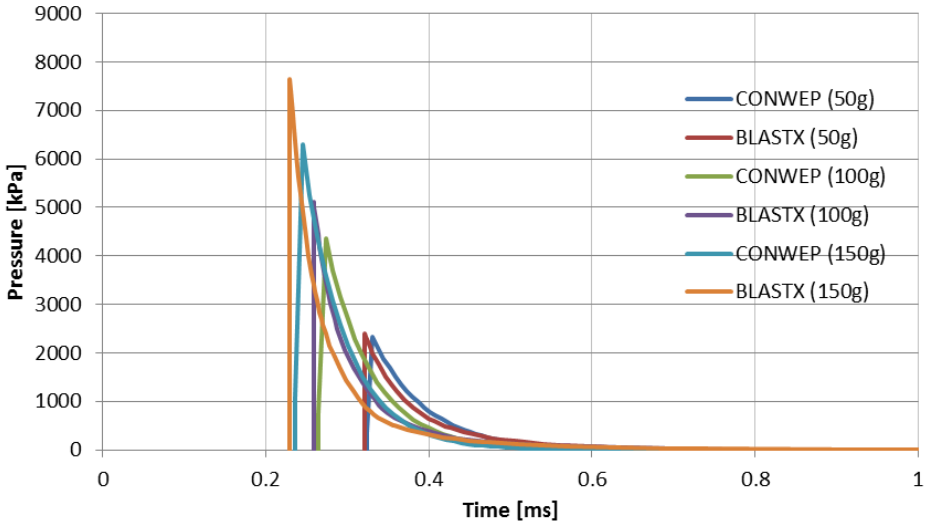

Figure 2.15. BLASTX and CONWEP Comparison

As a result, it is concluded that CONWEP underestimates the reflected pressure compared to BLASTX. In addition, the difference expands as the charge weight increases.

Free field explosion is chosen deliberately, since CONWEP has no ability to predict re-reflection waves. Due to that constraint, CONWEP is not suitable for internal explosions with several distinctive peaks.

2.3. Tolerance Analysis for Blast Tests

Every empirical or semi empirical method will suffer from some uncertainty inherently. It is almost impossible to overcome this difficulty due to their experimental foundations. Theoretically speaking, one should measure exactly the same pressure when a certain charge is detonated at a certain distance. However, there would be random cracks and tiny vacancies in the charge. In addition, although pressure gauges would be calibrated, it is not sufficient to get exactly the same pressure reading from different gauges located at the same distance.

Moreover, there would be test dependent factors affecting the measurements. Almost every test setup is designed for a specific test problem with a unique equipment combination. This variety itself creates a heterogeneous data set if one considers all the blast test data.

To demonstrate the gauge and test dependency of a pressure reading, a number of test data is compared below (Table 2.4). Several blast tests were conducted in the past; therefore a statistically significant number of test results can be assembled for this purpose.

Table 2.4. Various Blast Test Series [45]

Test Series	Number of Individual Measurements
Fabric Test 2	2
Divine Buffalo 1,9,19	40
Joist Tests 1-4	4
EMRTC CMU Tests	19
WINDAS Database	67
Swedish-Norwegian Tests	8
SAIC Barrier Tests	5
WES CMU 1-5	25
Divine Buffalo 21-24,28,29	20

The tests include a wide range of configurations and conditions. Some of the charges were cylindrical, others spherical, others hemispherical. However, by doing the necessary conversion procedures, one should find exactly the same pressure at the same scaled distance. But, Figure 2.16 clearly shows the spread and variety of the individual measurements.

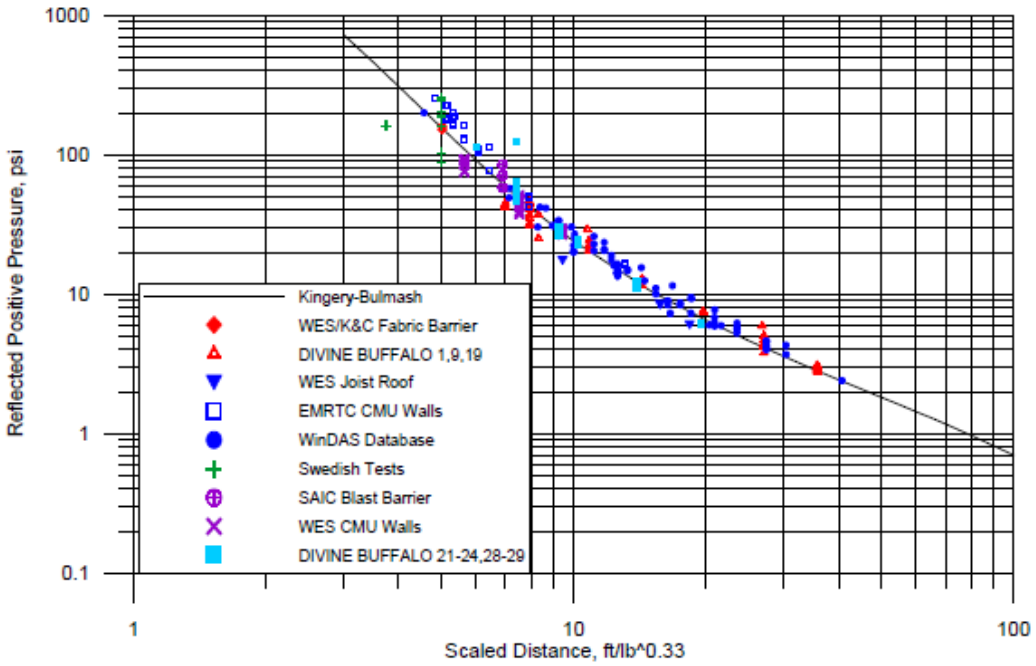

Figure 2.16. Test Data for Reflected Pressure [45]

Empirical and semi empirical methods use experimental data similar to this one.. In other words, a cloud of pressure data is reduced to a formula. This process yields an uncertainty employment in these blast prediction methods. On the other hand, another deduction can be made from another perspective: There are certain uncertainties in the blast overpressure measuring business.

In order to estimate the spread in the data, upper and lower bounds can be generated as follows

$$p_{upper} = p_{test}(M + 2stdev) \quad \textbf{(2.20)}$$

$$p_{lower} = p_{test}(M - 2stdev) \quad \textbf{(2.21)}$$

where $M$is the mean (best estimate), $stdev$ is the standard deviation and p_{test} is the experimental pressure data.

The curves for the upper and lower bounds reasonably constraint the data. Only very few individuals are left outside (Figure 2.17).

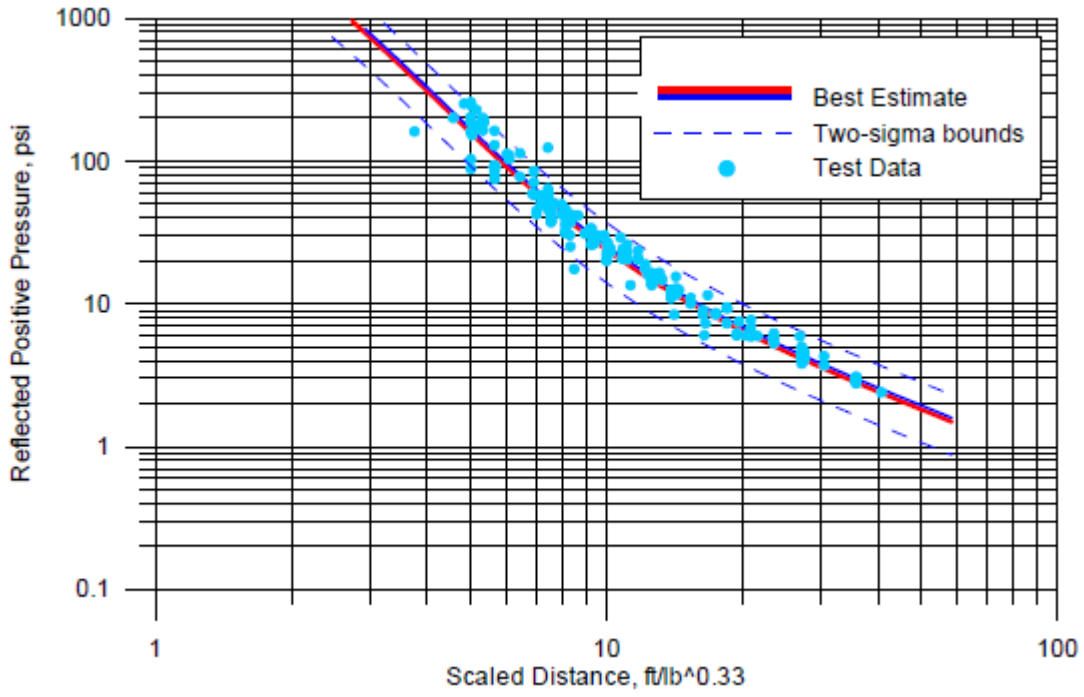

Figure 2.17. Two Sigma Bounds for Reflected Pressure [45]

Due to the compression introduced by the logarithmic scale, numeric magnitude of the upper and lower bounds are quite higher. The bounds are roughly at 0.7 and 1.5 times of the experimental data. Hence, -30% to +50% of uncertainty can be expected from any empirical method, or in other words, from any two test.

In addition, another study shows that data scatter ranged from ±10% at 63.5 cm to ±40% at smaller standoff for both peak and impulse using 226 grams of spherical C4 [46].

CHAPTER 3

ANALYSIS OF BLAST OVERPRESSURE

In this section, analysis of blast overpressure in a partially confined structure is performed. A test setup is constructed in order to compare the computational outputs with experimental results.

Firstly, problem under investigation is defined in detail. Next, modeling the problem using AUTODYN and BLASTX are explained individually. In addition, experimental part of the study is characterized by explaining pressure measurement methods, development process of the test setup and challenges in conduction of the trials. Finally, comparison of numerical, semi empirical and experimental results is depicted.

3.1. Definition of the Problem

In order to understand the blast loading in internal explosions, three problems with various venting areas are created. Each problem is examined by using three different charge weights that are detonated at the geometric center of the confined space.

Problems are constructed as 1 m^3 rigid wall cubicles with a square venting area on the top surface. Various edge lengths for the venting are employed to be able to expose the effects of pressure release in an internal explosion (Figure 3.1). Regardless of the calculation method, walls are assumed to be rigid. To satisfy this

assumption while constructing the experimental setup, steel plates and stiffeners are welded together. 50, 100 and 150 grams of Composition 4 (C4) high explosives are detonated exactly at the geometric center of the setup to get the same blast history on all of the side walls.

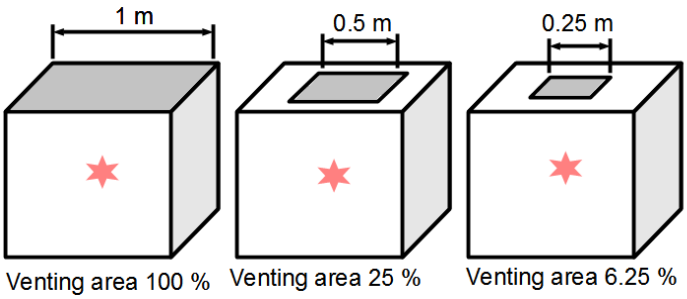

Figure 3.1. Problem Definition for the Analysis of Blast Overpressure

C4 high explosives are assumed to be spherical in order to eliminate the effects of the charge shape. Also, spherical charges allow the use of “remapping” technique during the computer modeling phase. Moreover, initiation point is crucial. Especially in small charges, one can avoid fluctuations due to off axis initiation by applying center initiation.

3.2. Modeling in Hydrocode

It was stated that scaling law is used in the literature extensively to minimize test costs by applying small scale setups. Same understanding can be applied to reduce the computational cost also.

The original problems employ 50,100 and 150 grams of C4 within $1m^3$ cubicles. By applying the scaling law, same blast histories can be obtained using different charge weights and distances.

Initially, the geometric parameters of the problem are specified (Figure 3.2).

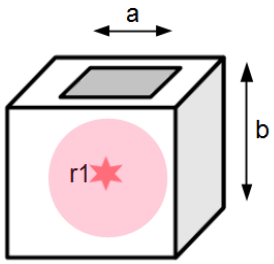

a: venting area edge length
b: problem edge length
r1: radius of C4

Figure 3.2. Parameters of the Problem

The geometric properties of the original problems are given in Table 3.1.

Table 3.1. Original Problems

	a [mm]	b [mm]	r1 [mm]	Charge	Scaled Distance
100% venting	1000	1000	19.5	50 g	1.357
25% venting	500	1000	19.5		1.357
6.25% venting	250	1000	19.5		1.357
100% venting	1000	1000	24.6	100 g	1.077
25% venting	500	1000	24.6		1.077
6.25% venting	250	1000	24.6		1.077
100% venting	1000	1000	28.2	150 g	0.941
25% venting	500	1000	28.2		0.941
6.25% venting	250	1000	28.2		0.941

Then, those parameters are scaled down in order to create a solution space that can be handled by any workstation. For this purpose, the small scale problem is chosen as 1/125 of the original one by volume. The geometric properties of the small-scaled problems are given in Table 3.2.

Table 3.2. Small Scaled Problems

	a [mm]	b [mm]	r1 [mm]	Charge	Scaled Distance
100% venting	200	200	3.91	0.4 g	1.357
25% venting	100	200	3.99		1.357
6.25% venting	50	200	3.99		1.357
100% venting	200	200	4.92	0.8 g	1.077
25% venting	100	200	4.92		1.077
6.25% venting	50	200	4.92		1.077
100% venting	200	200	5.63	1.2 g	0.941
25% venting	100	200	5.63		0.941
6.25% venting	50	200	5.63		0.941

Note that all the parameters except “scaled distance” are changed. This means the pressure histories should match when the time axis of the small-scaled solution is multiplied using the proportion constant. Since the small scale one is 1/125 of the original one, time proportion constant can be calculated as 5.

In addition to scaling law, remapping is also employed in hydrocode calculations. Initially, one dimensional calculation is performed up to 100 mm distance which is the nearest obstacle (wall) from the detonation center. This process is performed using 0.1 mm mesh size due to very small C4 radii in small scale. After that, results in one dimensional analysis are mapped into three dimensional problems which is actually a quarter of the problem space (Figure 3.3).

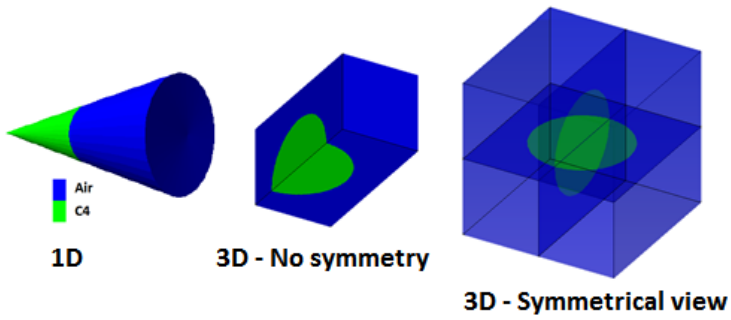

Figure 3.3. Modeling in AUTODYN - Remapping

Problem domain is a rectangular prism with dimensions 100 mm x 100 mm x 200 mm, since symmetry about two planes are employed. 1 mm mesh for the solution domain and 0.1 mm mesh for the one dimensional results are used whilst constructing the problems. Only difference between the problem domains is the boundary condition: All the outside surfaces are treated as rigid walls except the venting area on the top (Figure 3.4).

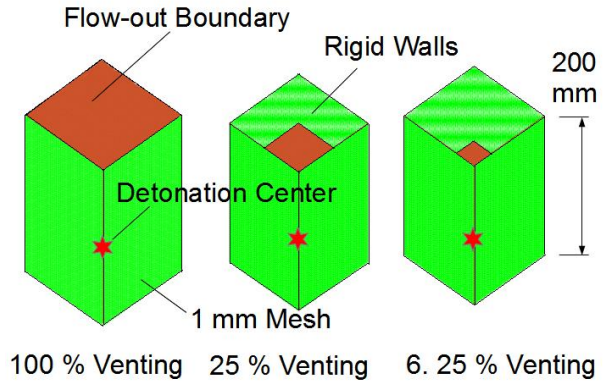

Figure 3.4. Modeling in AUTODYN – Symmetry

Apart from the geometric modeling, there is the material modeling. In this work, air, and C4 are used. The parameters were given in Section 2.1.3.1.

3.3. Modeling in Semi Empirical Method

Since it is a fast running computer program, the original problems given in Table 3.1 are modeled using BLASTX. Similarly, 50,100 and 150 grams of C4 explosives are detonated inside the structure. Consequently, blast histories at the center of rigid walls are recorded.

Geometrical properties are exactly the same with the original models (Figure 3.1). However, due to its empirical nature BLASTX does not include any material modeling. Since there is not any finite difference or finite element method employed that should include material behavior, material properties are integrated into its experimental database. BLASTX solely depends on its experimental database.

3.4. Challenges to Blast Pressure Measurement at Small Standoff

3.4.1. Friedlander Curve-Fitting

In this work, piezoelectric transducers are used. However, several attempts to measure reflected pressure concluded that transducer response is increasingly dominated by oscillatory noise as the charge standoff is reduced [46]. This drawback makes the measurement at close range very difficult. In addition, recorded pressure histories of identical tests may show significant variations (Section 2.3).

Although data is scattered, a sharp pressure increase followed by exponential decay (Figure 3.5) can be observed in any case.

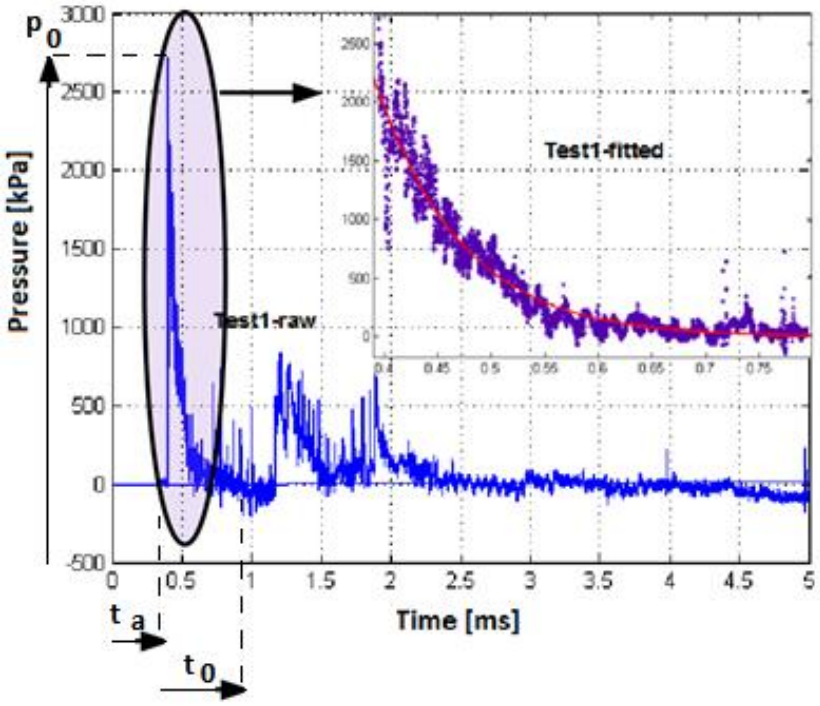

Figure 3.5. Reflected Pressure History (50g Charge Weight, 100% Venting Area, Test 1)

Some authors choose to fit a curve to the raw pressure data [46],[1]. Ideal pressure history is determined using that curve in order to compare with the raw experimental readings. Idealized blast wave form is a theoretical situation which cannot be fully satisfied under experimental situation. However, it is a parameter used in the literature to see the idealness of the blast wave. Friedlander-type curve (simple blast curve) is used to obtain ideal blast pressure history (Figure 3.6):

$$p = p_0\left(1 - \frac{(t - t_a)}{t_0}\right)e^{-\beta\frac{(t-t_a)}{t_0}} \quad \textbf{(3.1)}$$

where p is the overpressure, t is the time, t_a is the arrival time, t_0 is the positive blast pressure duration, p_0 is the peak overpressure, β is the decay constant.

In this equation, p_0 and β are calculated iteratively using MATLAB's curve-fitting toolbox.

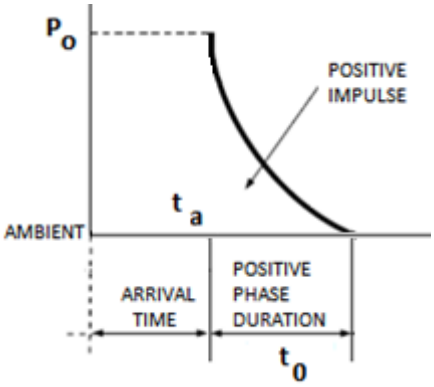

Figure 3.6. Idealized Blast Wave Form

In general, peak pressure is extracted from experimental data by finding the maximum pressure value numerically (Figure 3.7). Similarly, arrival time is found by locating first peak pressure.

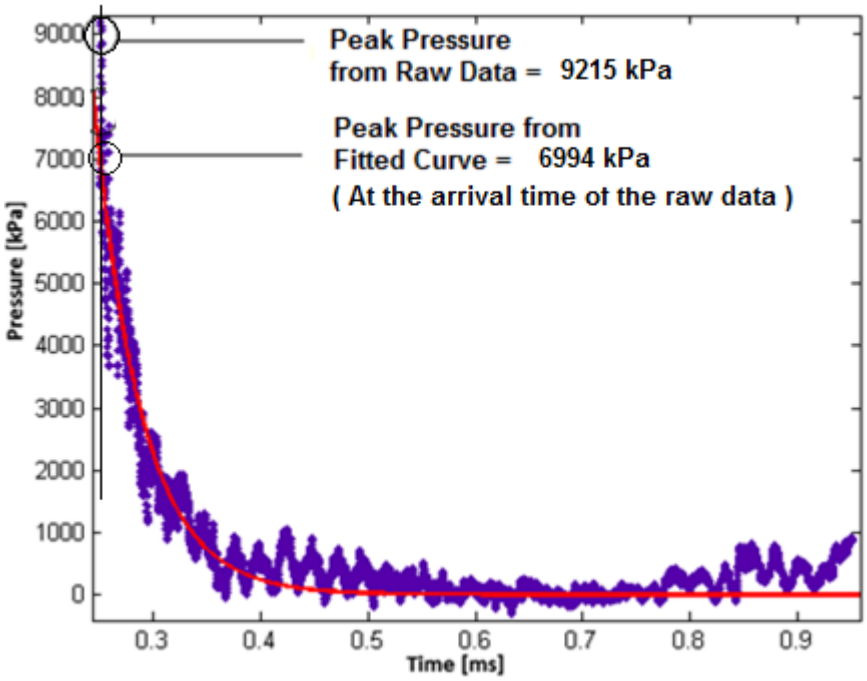

Figure 3.7. Peak Pressure Determination (150g Charge Weight, 100% Venting Area, Test 6)

Exponential fit process is applied to all of the test results. However, first peak pressure is considered only. Although ideal blast equation (Friedlander-type curve Eq. 3.1) could be applied to all the reflections in a blast wave, it is not much widely used in successive waves. Latter waves are corrupted due to reflections and other environmental effects. In addition, the duration of the successive blast waves cannot be extracted from the data due to emerged sections. Several assumptions are needed to do so, which results an unreliable curve fit after the first peak.

In conclusion, exponential fit is employed to estimate the “ideal” peak pressure. In order to see the difference in the raw and fitted data, both results are compared with the computational outputs.

3.4.2. Low-Pass Filtering

The main reason to the oscillatory data is the excitation of natural frequencies of the test setup. This kind of oscillations is seen when the load is applied face on by a blast wave. A very sharp pressure step excites the eigenfrequencies of the structure. Therefore, several oscillations are superimposed on the actual pressure signal.

In order to eliminate the unexpected sharp peaks in the pressure history, a filtering process is employed. Firstly, the frequency spectrum of a test data is examined. The frequency spectrum of a time-domain data is a representation of that data in the frequency domain. It is generated via Fourier transform. The Fourier transform of a function produces a frequency spectrum which contains all of the information about the original signal, but in a different form.

The Fourier transform of the test data (50g Charge Weight, Test1) suggests using a low-pass filter to reduce the amplitude of high frequency data points (Figure 3.8). The unwanted and unexpected high frequency peaks are assumed to be created by the test setup. Therefore, by filtering those data points, one should get a smoother blast pressure history.

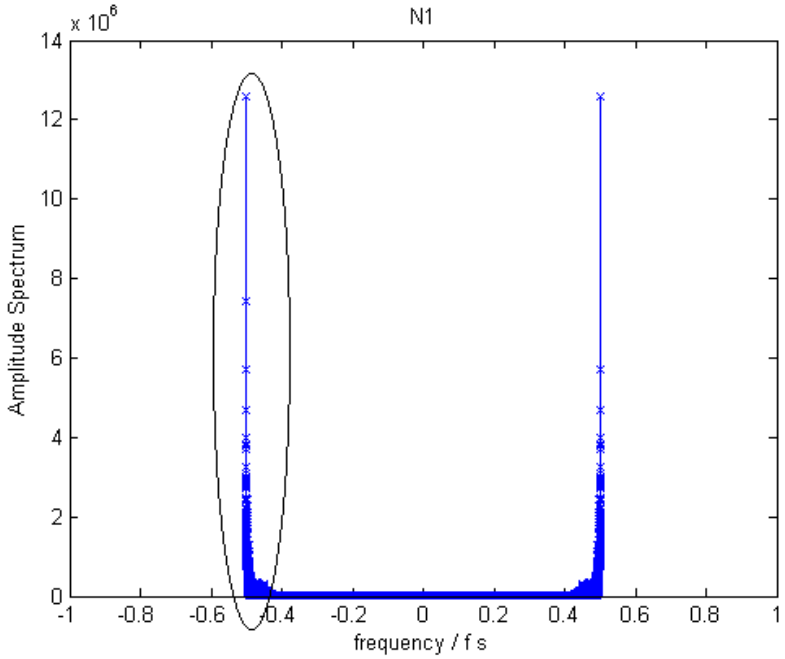

(a)

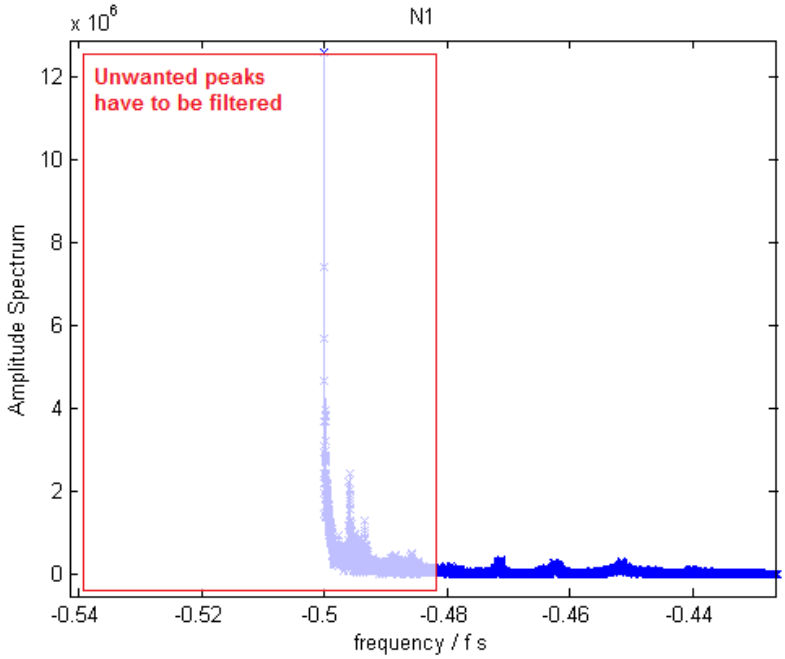

(b)

Figure 3.8. (a) Frequency Spectrum of a Test Data (150 g Charge Weight, Test 1) (b) Enlarged View of Unwanted High Frequency Peaks

A low-pass filter passes low-frequency data but attenuates reduces the amplitude of data with frequencies higher than the cutoff frequency. The actual amount of reduction for each frequency varies from filter to filter.

The MATLAB code is written to perform filtering operations (APPENDIX – F). In order to preserve the blast overpressure phenomenon, the cutoff frequency is calculated using the first peak duration which is roughly 0.2 ms (5000 hz). In data acquisition systems, generally 10 times the frequency of the phenomenon is enough to represent the fast varying data [51]. Conversely, to create a low-pass filter that removes oscillations the same approach can be used. In our case, 50 kHz cutoff frequency is used.

Using “butter” function of MATLAB, test results are filtered. An example of a filtered data is given below (Figure 3.9).

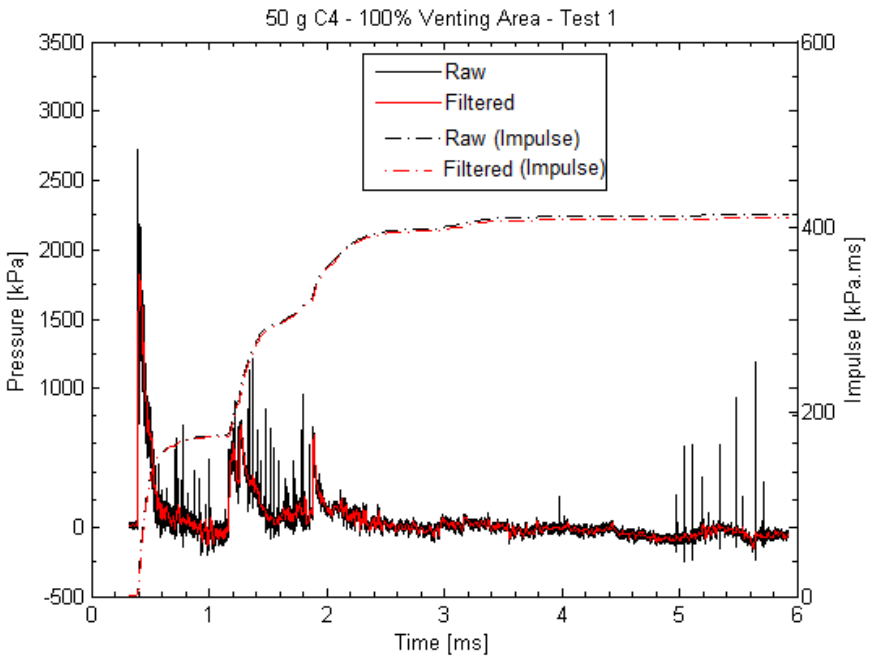

(a)

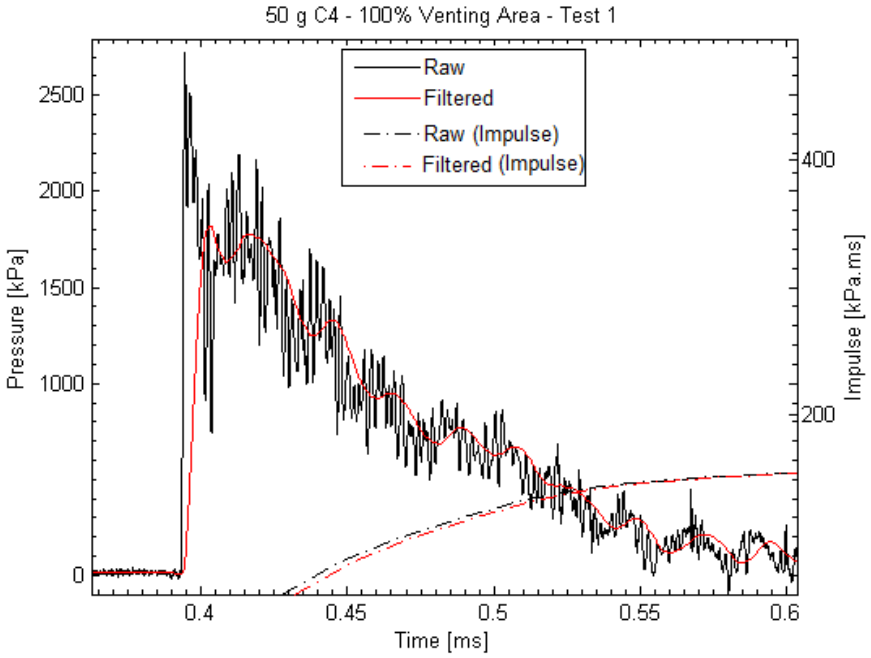

(b)

Figure 3.9. (a) Filtered Test Data (50g Charge Weight, 100% Venting Area, Test 1) (b) First Peak (Enlarged) (c) Second Peak (Enlarged)

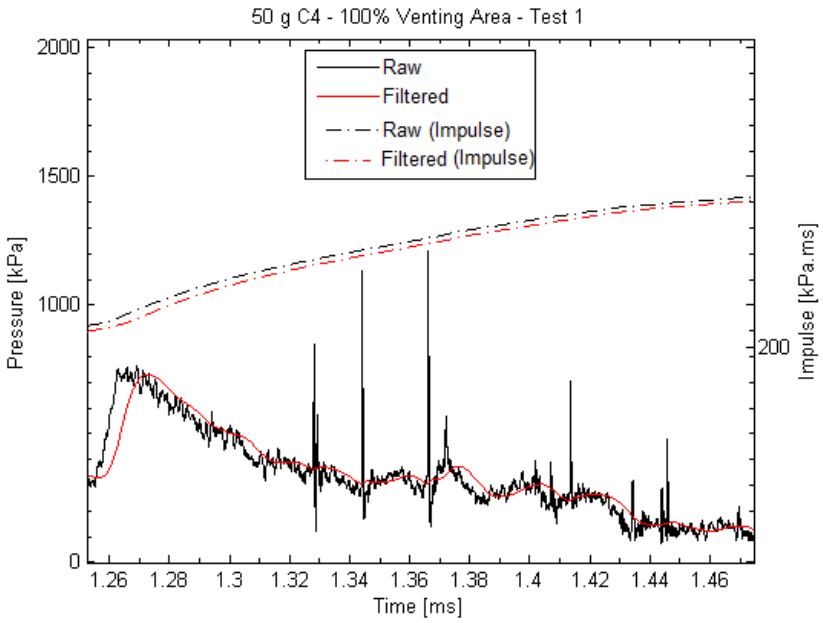

(c)

Figure 3.9. (Cnt'd) (a) Filtered Test Data (50g Charge Weight, 100% Venting Area, Test 1) (b) First Peak (Enlarged) (c) Second Peak (Enlarged)

Note that, the impulses (total area under the pressure curves) are almost the same. The close gap between the integrals (impulses) can be interpreted as removal of sharp oscillations and preserving the behavior of the blast phenomenon.

3.5. Test Method

It was stated that three different charge weights are used: 50 g, 100g, and 150 g. By applying simple volume calculation one may calculate the chaotic radii where the detonation products may reach according to Baker's 10 radii rule (Table 3.3).

Table 3.3. Chaotic Radii

Charge Weight [g]	Charge Radii [mm]	Chaotic Radii [mm]
50	19.5	195
100	24.6	246
150	28.2	282

According to the results, it can be said that oscillations due to product gases may be negligible since the transducers are located 50 cm away from the detonation center.

In order to reduce the oscillations as much as possible, another preventive action is taken by selecting a pressure transducer with a high resonant frequency. PCB 102B3 type transducer is used which is specifically designed for reflected blast wave measurements. It is exceptionally fast (1μs response time), has a 500 kHz resonant frequency and measures up to 69 MPa. However, to show these properties fully, it is advised to use flush-mounting technique (Figure 3.10).

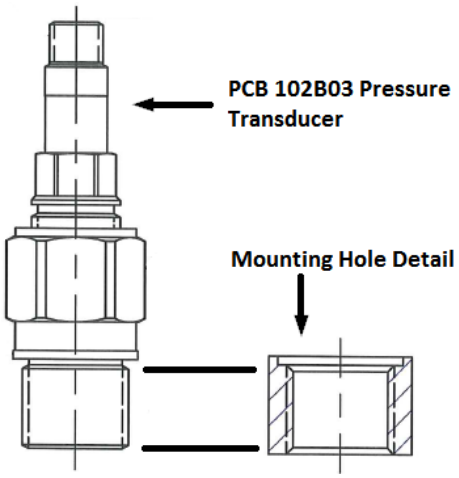

Figure 3.10. Pressure Transducer

Along with the various charge weights, three different venting areas are employed. In the calculation side, this makes a total of 9 analyses. However, at least three experiments have to be conducted to overcome repeatability issues.

3.6. Test System

In order to create a test system several calculations are performed. Deflections at the center of the walls are recorded for different thicknesses by detonating various charges. From 5 mm to 20 mm, dynamic responses are observed for 50 grams to 750 grams of C4 high explosive. Similar to the rest of the work, charges are detonated at the center of the cubicle (Figure 3.11). Steel plates are bonded

together. At the top, outflow boundary condition is applied. Calculations are performed using fully coupled AUTODYN.

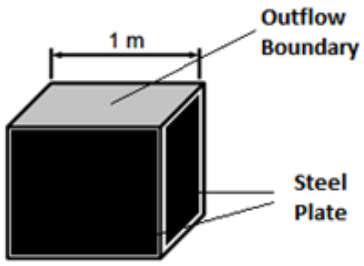

Figure 3.11. Steel Plate Response Model (Schematic)

To set a baseline, dynamic deflection process is observed by detonating 750 grams of C4 inside a cubicle with a thickness of 5 mm and 20 mm initially. The maximum deflections at the center of the wall are given below respectively (Figure 3.12).

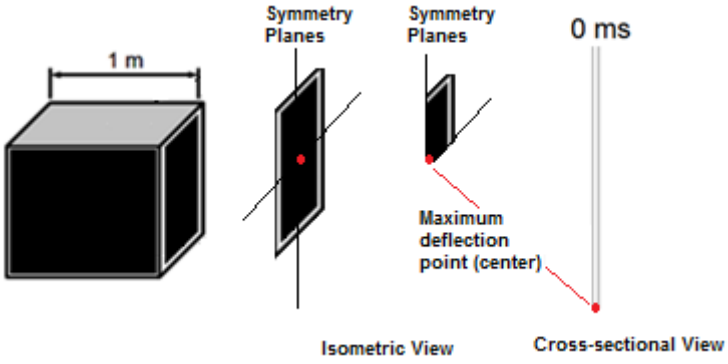

(a)

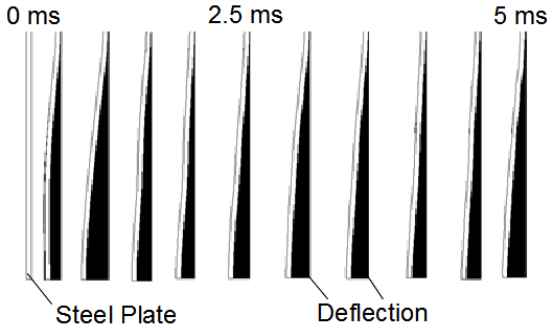

(b)

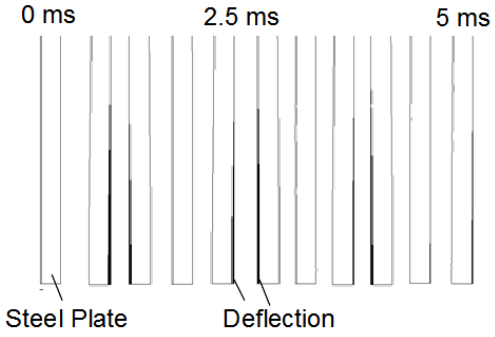

(c)

Figure 3.12. (a) Maximum Deflection Point of a Plate (b) Dynamic Response of 5 mm Plate (c) Dynamic Response of 20 mm Plate

It can be seen that 5 mm thick steel cubicle shows substantial deflection compared to 20 mm thick one that shows minor structural changes. In addition, 5 mm thick steel plates show plastic behavior and are unable to recover to its original position. Since the structure should recover itself, it can be concluded that 750 grams of C4

should be reduced. Afterwards, various plate thicknesses are investigated using 50,100 and 150 grams of C4. According to those results, a test setup is designed (Figure 3.13).

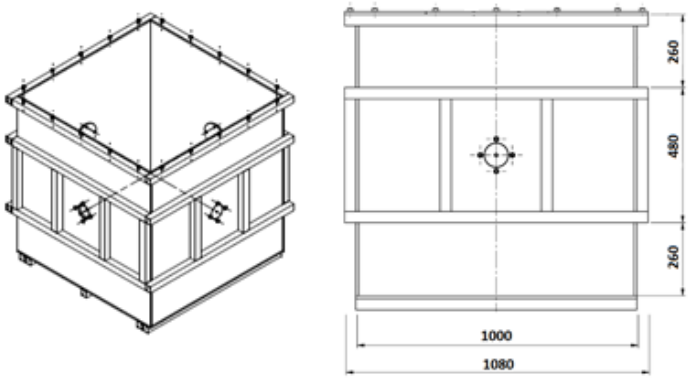

Figure 3.13. Test Setup Design

Along with the results of several plate thicknesses, the result of the final test setup is presented (Figure 3.14).

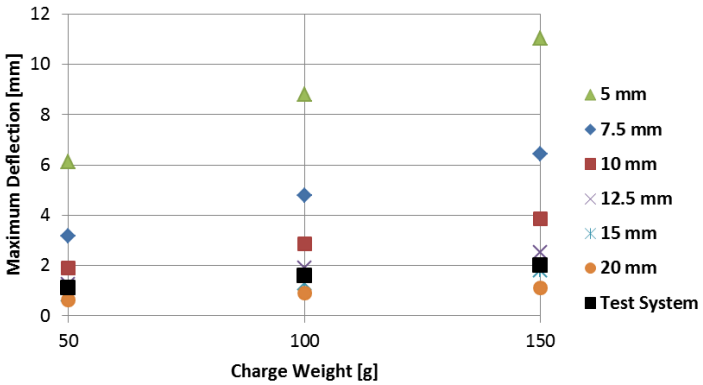

Figure 3.14. Maximum Deflection for Various Charge Weights

During the modeling process, it was assumed that all the steel members are bonded together and the top surface is fully vented. Fully coupled AUTODYN solution

technique is employed. In addition, remapping is used where one dimensional solution continues until the blast wave reaches any structure, and results are mapped into three dimensional domain.

After evaluating the results, at first glance the 20 mm steel plate would be the best choice. But due to heavy structural design it would not be reasonable. Also, its mobility and price would be unacceptable. As an alternative, the use of stiffeners to support the plates is decided. So, a cubicle with 10 mm thickness and 40x40x4 mm stiffeners are applied near the center of the side walls. This approach strengthened the system considerably. As a result, the test system seems to be better than 12.5 mm steel plate configuration. It deflects less than 2 mm if 150 g C4 is used.

3.7. Comparison of the Results

In this section, comparison of numerical (AUTODYN), semi empirical (BLASTX) and experimental results is depicted. Experimental results are available only for 100% venting area configuration due to equipment malfunction and faulty production of the test setup. Three different charge weights are tested for at least three times.

In addition, numerical and semi empirical codes are also compared. BLASTX solves a typical blast problem like the ones investigated in 1 minute; meanwhile AUTODYN spends 4 days approximately. It can be said that BLASTX is thousands times faster than AUTODYN. In the upcoming sections, computational results are examined extensively.

Test setup is constructed as outlined in the earlier sections. Technical drawings are given in the appendix (APPENDIX – E). Also, a steel tripod is used to hang the C4 and to make sure that C4 detonates right at the geometric center, plastic ropes are used as guides and aluminum electrical capsule is used to initiate the detonation. In this work, spherical C4 blocks are shaped by hand with an acceptable tolerance. The tolerance in the mass was as low as 1 g. A photo is given below in order to give a general idea about the pretest preparations (Figure 3.15).

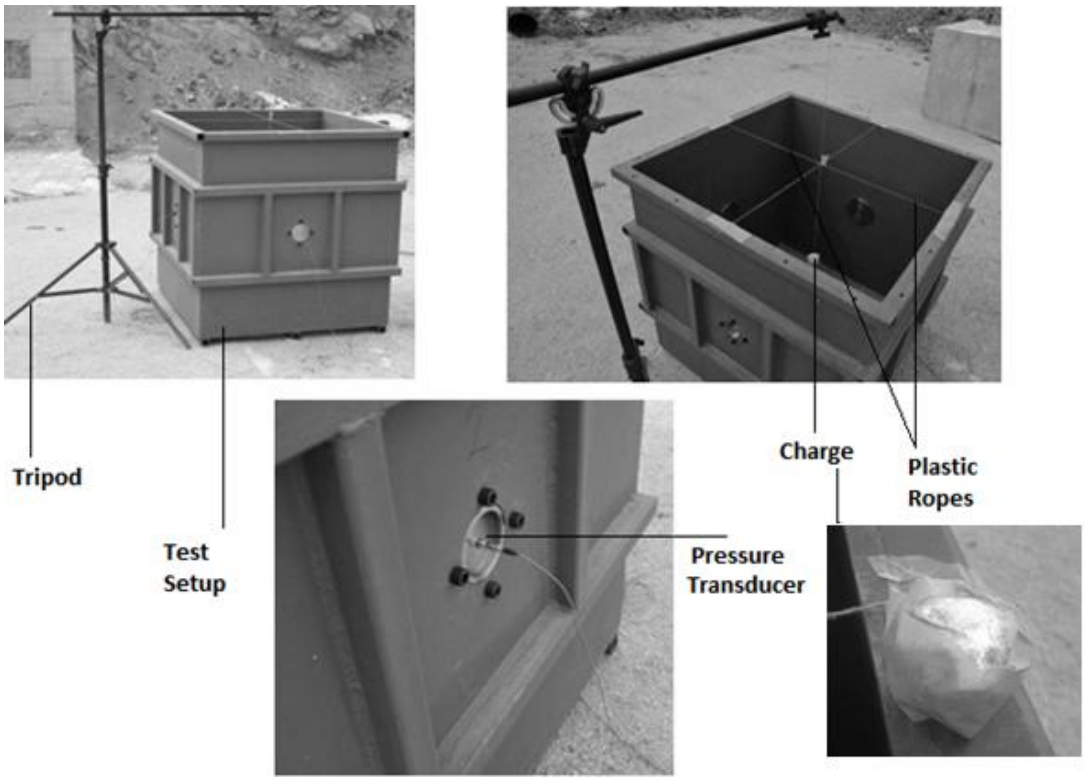

Figure 3.15. Test Setup for 100% Venting Area

A typical pressure versus time data obtained from Test 1 using 50 grams of C4 and 100% venting area is previously shown in Figure 3.5 and Figure 3.9. The rest of the test results are presented in the appendix (APPENDIX – B, APPENDIX – C) in detail. Only the important parameters like peak pressure, arrival time and impulse are considered in this section.

Calculations results and experimental data are compared into two categories. Firstly, first and second peak pressures and impulse are compared regarding the scaled distance. Since the location of the pressure gauges are fixed, scaled distance can be interpreted as charge weight also. Secondly, same results are presented in a different way to see the effects of venting area. For 100% venting area (VA), test data is compared with computational results. For 25% and 6.25% VA, computational outputs are evaluated within each other.

Scaled distance is a parameter of scaling law (Eq. 2.12). It is the ratio of the true distance, and the charge weight. In the literature, blast overpressure results are

generally presented using scaled distance. Since various distances and charge weights may give the same scaled distance value, one may use the data for several cases.

For the first peak pressure parameter, BLASTX and AUTODYN computed exactly the same values within each other regardless of the venting area (Figure 3.16). Since there is not any obstacle or boundary change on the blast wave path until the first contact, it is expected to observe the same pressure for various venting area. On the other hand, first peak pressure increases when the scaled distance decreases (in other words when the charge weight increases). Due to the higher energy output of heavy charge weights, first peak pressures are predicted much higher.

Test data dispersion related to the first peak pressure is close for 50 and 100 g. However, data for 150 g is much more scattered. In addition, it can be said that filtered (low-pass) and fitted test (Friedlander curve) data appear under the raw data while showing similar behavior. The fitted data is calculated distinctively higher than the filtered data but both approaches smoothen the first peaks yielding lower pressures.

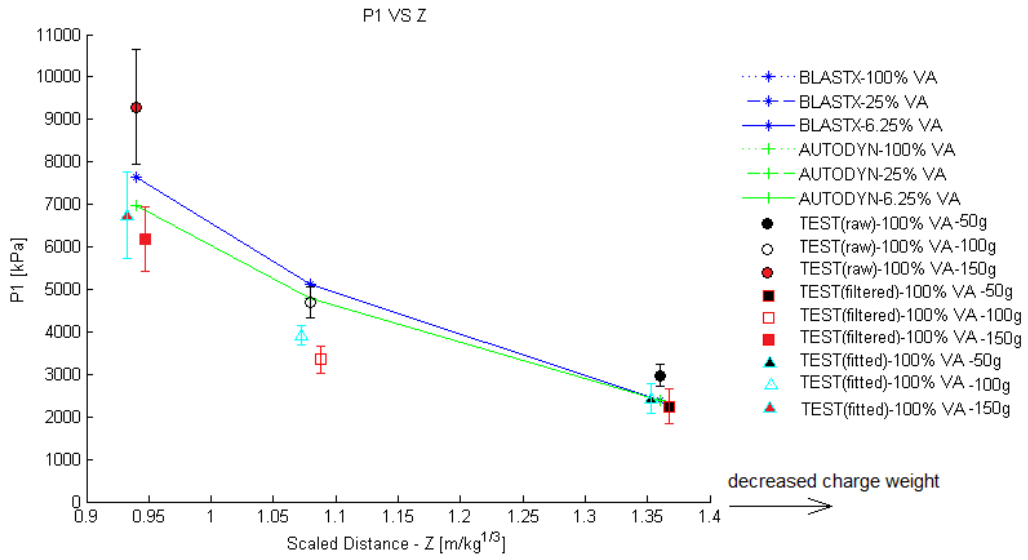

(a)

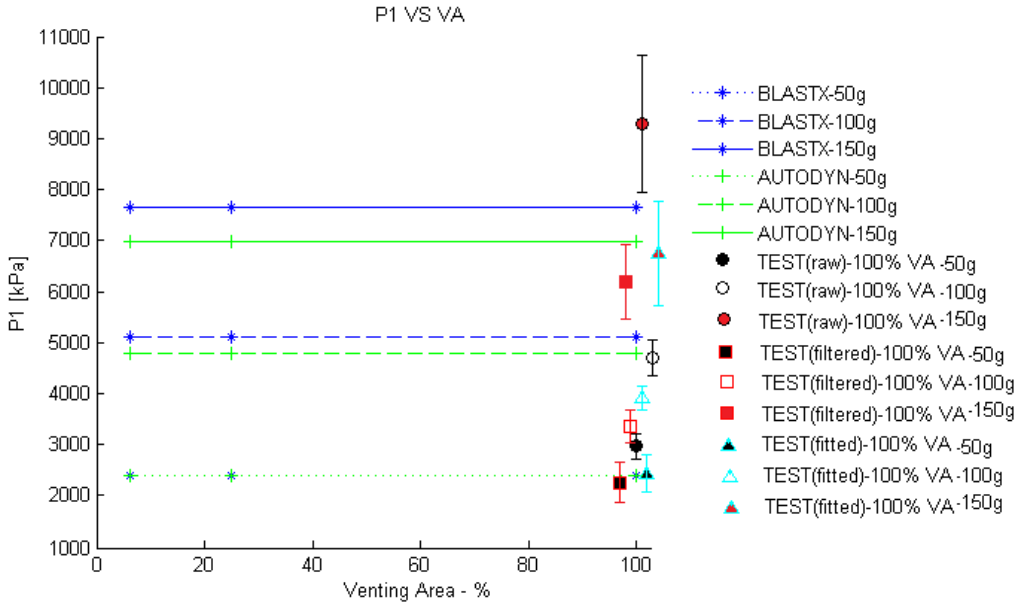

(b)

Figure 3.16. (a) First Peak Pressure vs. Scaled Distance (b) First Peak Pressure vs. Venting Area

For the arrival time of first peak, similar to the pressure parameter, BLASTX and AUTODYN predict the same quantities for different venting areas (Figure 3.17). Time parameter is dependent only to the charge weight. On the other hand, arrival time of first peak increases as the scaled distance increases. Due to the lower

energy output of lighter charge weights, time parameters are predicted much longer. Test data is more dispersed for 50 g charge weight. In addition, a constant relation can be observed between raw and filtered test data.

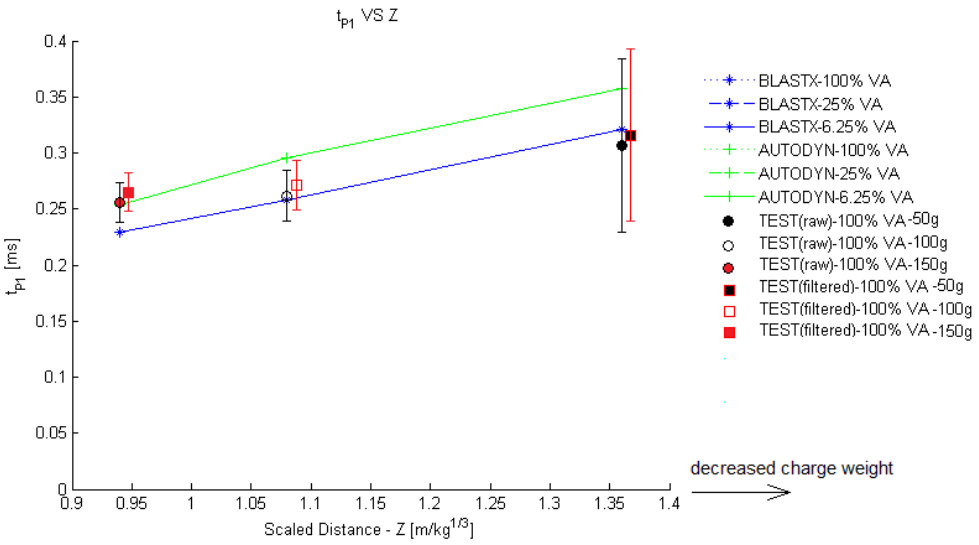

(a)

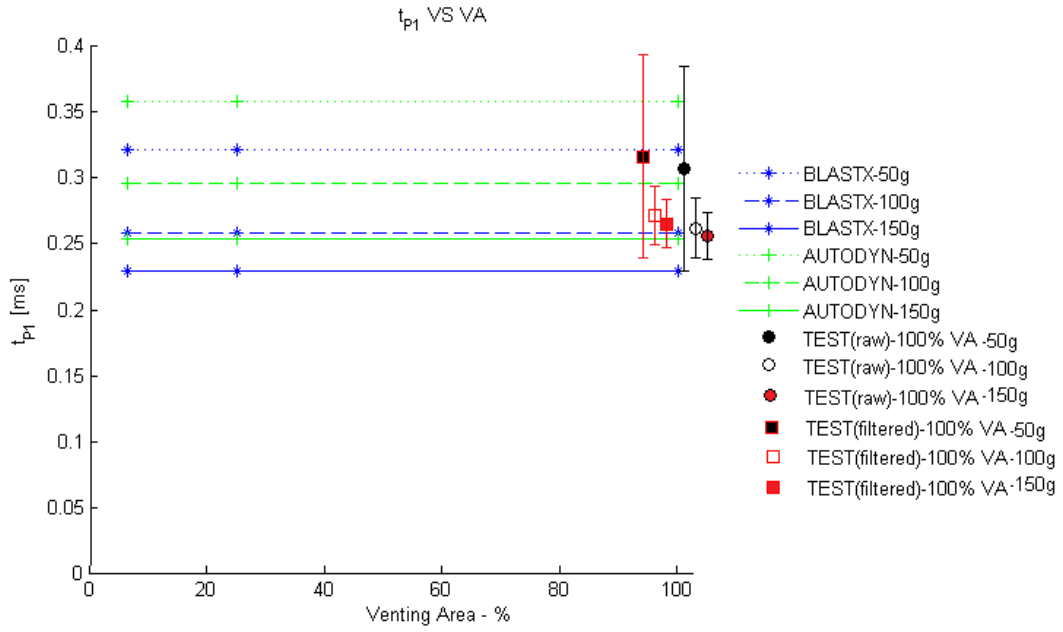

(b)

Figure 3.17. (a) Arrival Time of First Peak vs. Scaled Distance (b) Arrival Time of First Peak vs. Venting Area

Second peak pressure parameter has a distinct relation with venting area and scaled distance. Since re-reflection blast wave path and amplitude are strongly depended on boundary conditions, results are diversified accordingly.

It can be observed that second peak pressure decreases as the scaled distance increases (Figure 3.18). This behavior is similar to the first peak pressure parameter. Due to the relatively low energy release by lighter charge weights, lower reflection peaks are expected. On the other hand, similar trend can be seen for the venting area comparison. However, the rate of reduction is minor this time.

A convergence can be detected for the increased scaled distance which is especially observed from the test and BLASTX results. Test data and computational outputs become closer.

For the second peak pressure, test data are distinctively separated from the computational results – especially AUTODYN. The reason is the test setup. Although it was assumed to be a quasi-rigid structure to comply with the rigid wall assumption in calculations, still a certain amount of energy is absorbed by its elasticity. Due to the rigid wall boundary condition, blast wave does not interact with the structure.

Although both computational methods employ rigid wall boundary, AUTODYN predictions are higher than BLASTX's with a vast margin. It can be explained by the outflow boundary condition applied on the AUTODYN model. The other side of the boundary reflects a certain amount of the blast wave back to the domain until the material in a cell completely flows out. As a result, reflected pressures are over predicted. The solution to this drawback is bigger or finer domain which is not possible for this kind of problems due to the computational costs.

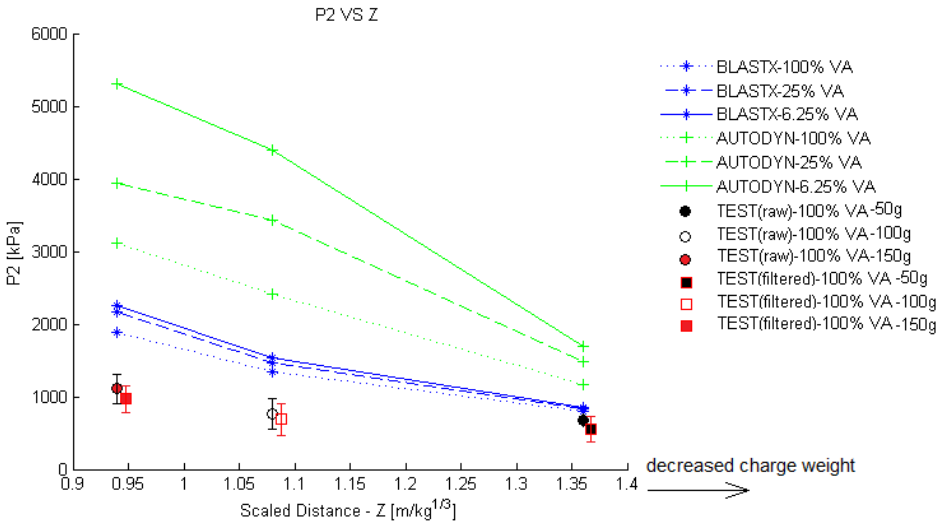

(a)

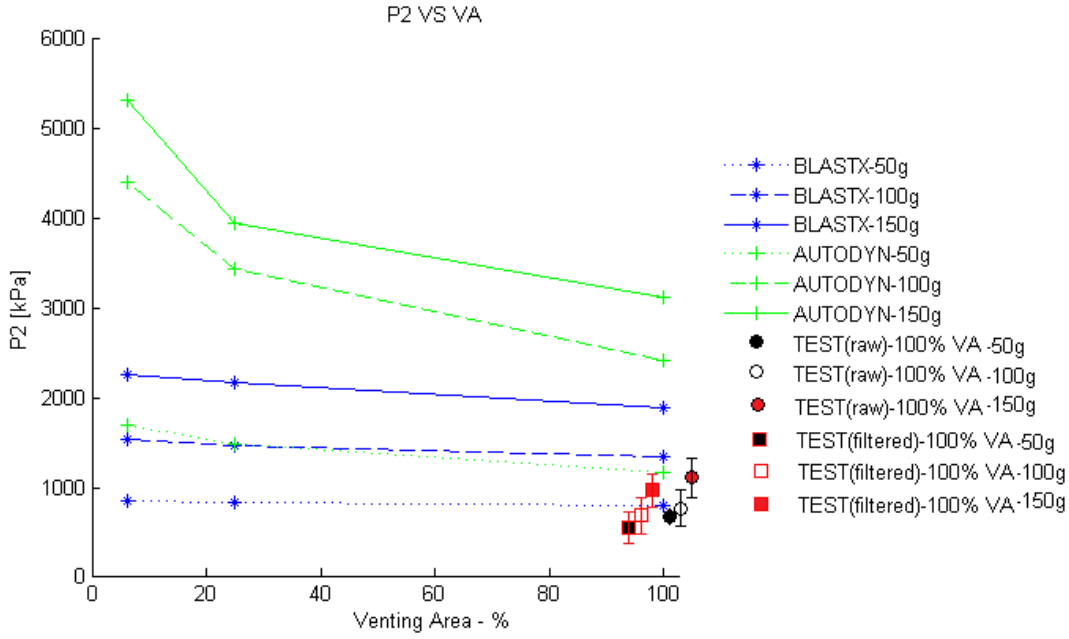

(b)

Figure 3.18. (a) Second Peak Pressure vs. Scaled Distance (b) Second Peak Pressure vs. Venting Area

For the arrival time of the second peak, computational outputs show linear increase as the scaled distance increases (Figure 3.19). On the other hand, no distinct dependability related to venting area is observed for both AUTODYN and BLASTX.

There are negligable differences for different venting areas in AUTODYN results that are occurred due to different boundaries in the models. Since AUTODYN is a numerical tool, boundary conditions affect all the parameters during a computation. In this case, various venting area conditions affected the results.

The test results for 100g and 150g seem to be similar. However, due to the enormous data dispersion in the time parameters one may not reach to a specific conclusion about experimental results.

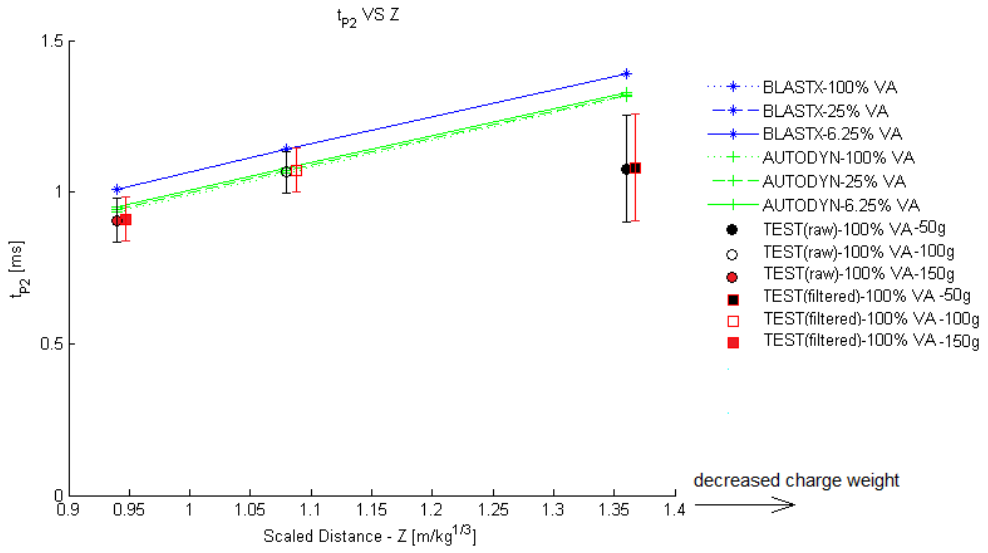

(a)

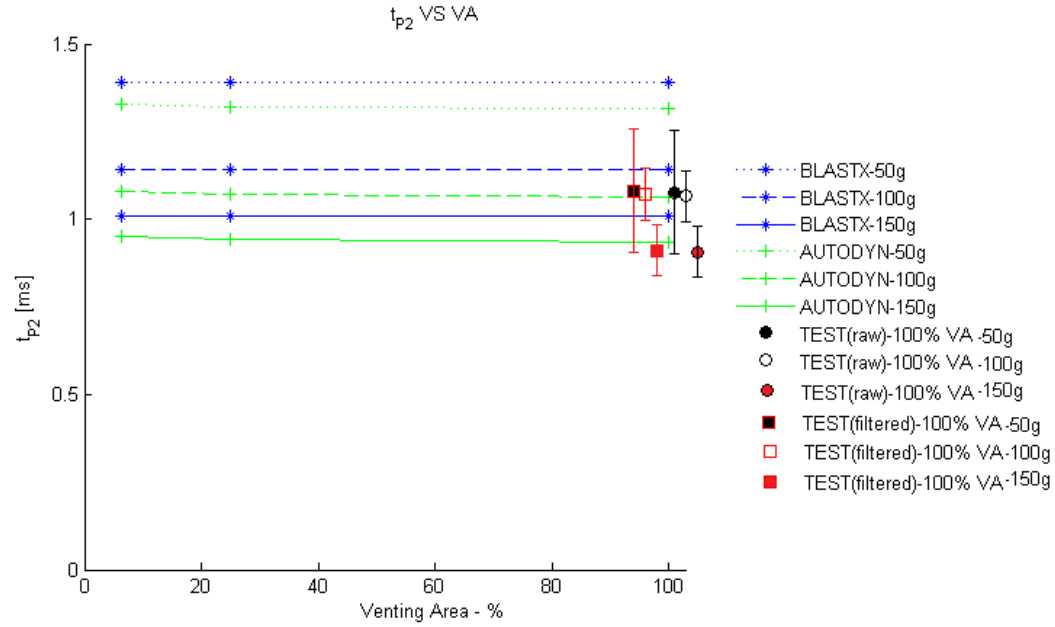

(b)

Figure 3.19. (a) Arrival Time of Second Peak vs. Scaled Distance (b) Arrival Time of Second Peak vs. Venting Area

The last parameter used for the result comparison is the total positive impulse. Impulse represents the energy transferred to the structure. It is calculated by taking the integral of positive part of the pressure histories. This procedure is performed using “trapz” function in MATLAB (trapezoidal numerical integration).

Due to the low energy levels in light charges, the total impulse decreases with scaled distance (Figure 3.20).

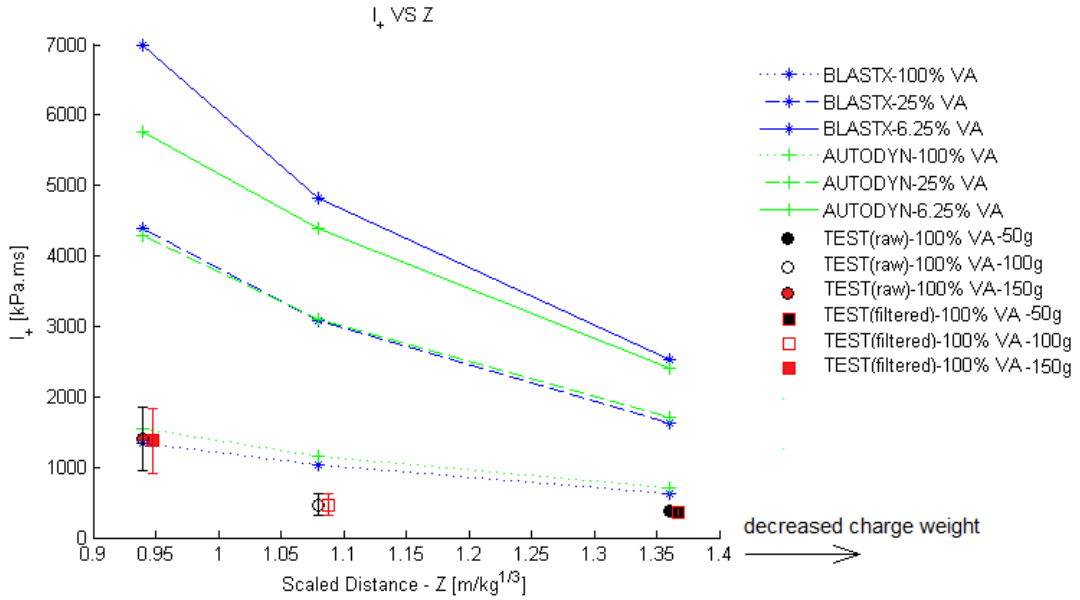

(a)

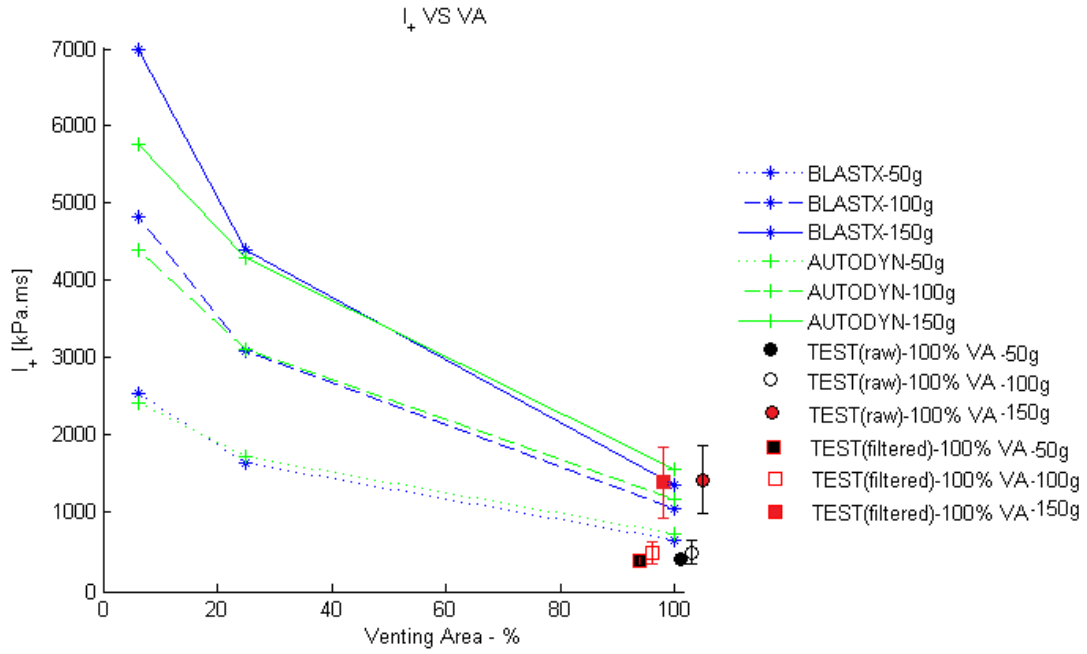

(b)

Figure 3.20. (a) Positive Impulse vs. Scaled Distance (b) Positive Impulse vs. Venting Area

Impulse strongly depends on venting area. The re-reflection waves occur many times in more confined spaces. Therefore, it takes much time to release the high pressurized medium out of the structure. Consequently, more energy is transferred to the structure with smaller venting area. To expose this effect, impulse calculations are performed using different time scales depending on the venting area: 6 ms for 100% venting area, 8 ms for 25% venting area and 10 ms for 6.25% venting area. The idea behind those time limits is explained in the following section.

The difference between the experimental data and computational predictions is quite distinct that cannot be ignored. In order to analyze the reason behind, test setup and its quasi-rigid assumption is investigated.

3.8. Elasticity Investigation of the Test Setup

To investigate the difference caused by the elasticity of the test setup, fully coupled modeling (Figure 3.21) is employed rather than solving by an Euler domain under the assumption of rigid wall (Figure 3.4). In this method, fast moving air interacts with the metallic structure. Due to the interaction some of the blast energy is expended for the elastic deformation of the steel (Section 3.6).

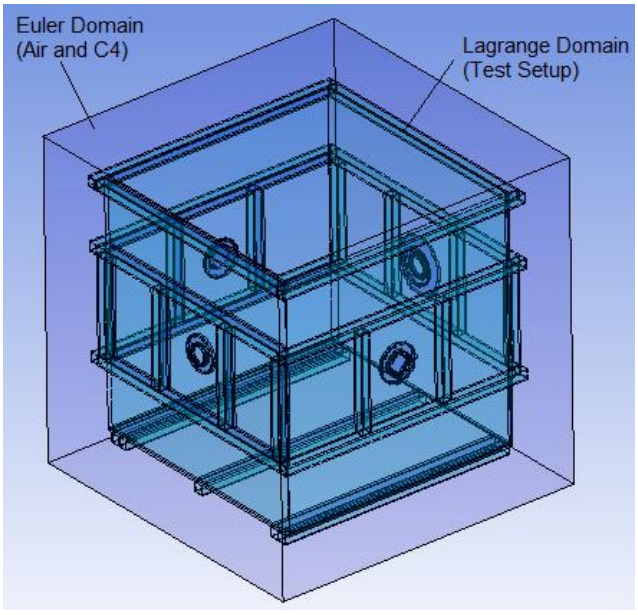

Figure 3.21. Fully Coupled Modeling for 100% Venting Area

AISI 1006 Steel presented in AUTODYN's material library is used to model the test setup. Shock model is preffered for the equation of state and Johnson Cook parameters are used for the strength modeling (Table 3.4).

Table 3.4. Material Modeling- AISI 1006 Steel

Equation of State	**Shock [41]** Equation (2.9)
Reference density	7.896 [g/cm^3]
Gruneisen coefficient	2.17
Parameter C1	4569 [m/s]
Parameter S1	1.49
Parameter Quadratic S2	0 [s/m]
Relative volume, VE/V0	0
Relative volume, VB/V0	0
Parameter C2	0 [m/s]
Parameter S2	0
Reference Temperature	300 [K]
Specific Heat	452 [J/kgK]
Thermal Conductivity	0 [J/mKs]
Strength	**Johnson Cook**
Shear Modulus	8.18000E+07 [kPa]
Yield Stress	3.50000E+05 [kPa]
Hardening Constant	2.75000E+05 [kPa]
Hardening Exponent	0.36
Strain Rate Constant	2.20000E-02
Thermal Softening Exponent	1
Melting Temperature	1.81100E+03 [K]
Ref. Strain Rate (/s)	1
Strain Rate Correction	1st Order

For 50, 100 and 150 grams of C4; fully coupled calculations are performed using 100%, 25% and 6.25% venting area test setup. On the venting side (top face), outflow boundary condition is applied. Since this kind of modeling approach requires too much computational time, parallel processing technique is applied using AUTODYN: Models are divided into 8 to 10 pieces.

The fully coupled results are compared with Eulerian results and experimental outputs for the 100% venting area (Figure 3.22).

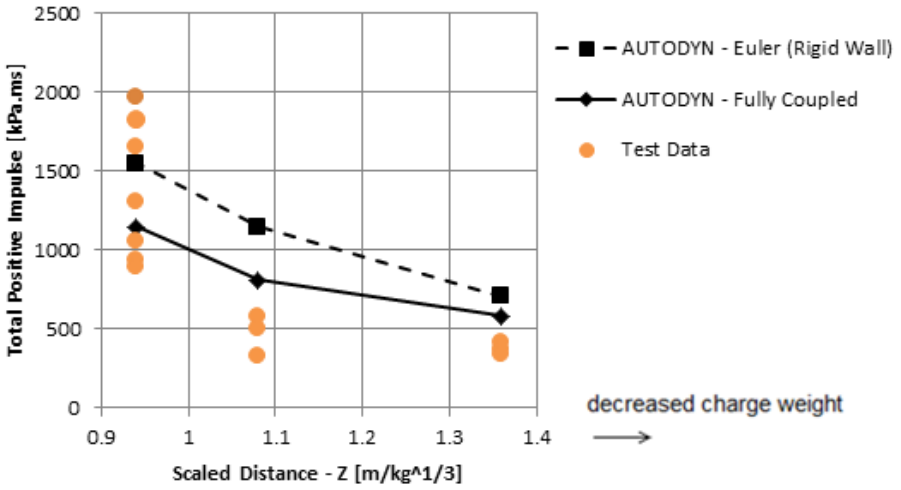

(a)

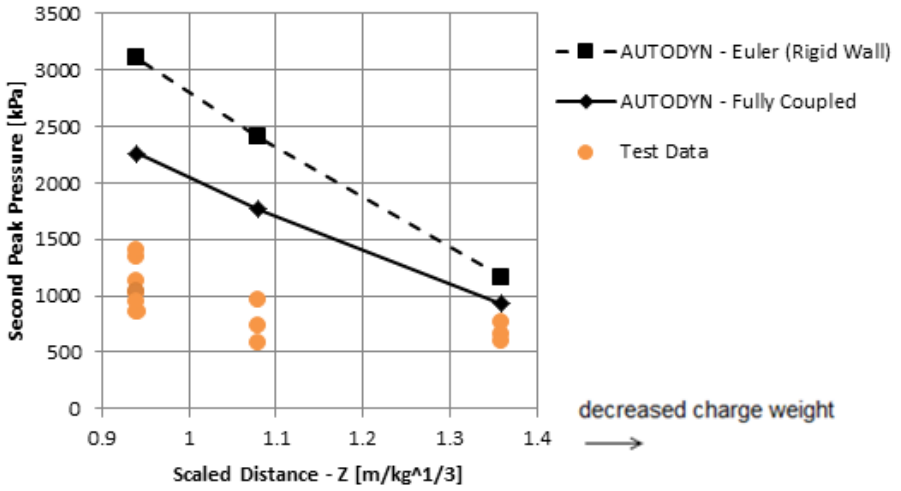

(b)

Figure 3.22. (a) Total Positive Impulse Comparison (100% Venting Area) (b) Second Peak Pressure Comparison (100% Venting Area)

It can be said that test setup was not built rigid enough to reflect the blast waves perfectly. Although the maximum deflection prediction is small (Section 3.6) and ignorable in the structural point of view, the decreased total impulse in fully coupled method shows that considerable of the blast energy is absorbed by the test setup.

From another perspective, it can be seen that the difference between the Eulerian calculation and fully coupled method decreases as the scaled distance increases. For smaller charges, test setup shows higher rigidity as expected.

In addition to the impulse comparison, second peak pressure comparison also gives useful information about the elasticity of the test setup (Figure 3.22). After the initial blast wave, successive peak pressures are predicted considerable lower than the Eulerian calculation in the fully coupled solution due to the energy loss during the structure interaction. However, fully coupled results are still higher than experimental results due to the flow out boundary condition explained in the previous section.

Time dependent impulse data is also investigated during the comparison of Eulerian and fully coupled methods (Figure 3.23, Figure 3.24, Figure 3.25, Figure 3.26). Due to the rigid wall assumption, the dissipation of blast energy takes much longer in the Eulerian approach. The re-reflection waves occur too many times because of “perfect reflection”. However, fully coupled method lets the interaction of air (blast wave) and the steel structure. Some deflection occurs due to the interaction (Section 3.6) and consequently, some amount of the blast energy is absorbed by the test structure.

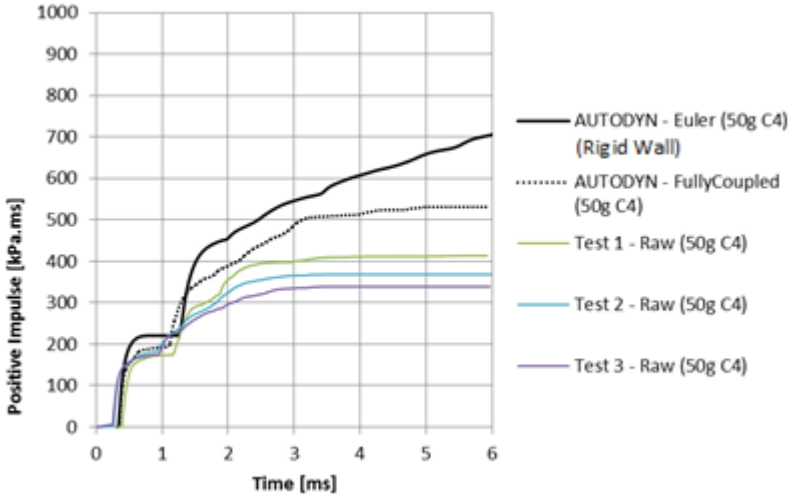

Figure 3.23. Positive Impulse Comparison for 50 g Charge Weight (100% Venting Area)

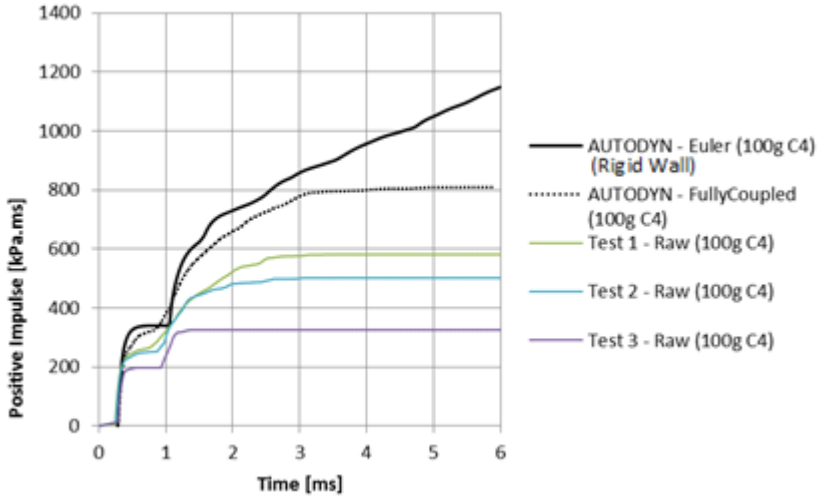

Figure 3.24. Positive Impulse Comparison for 100 g Charge Weight (100% Venting Area)

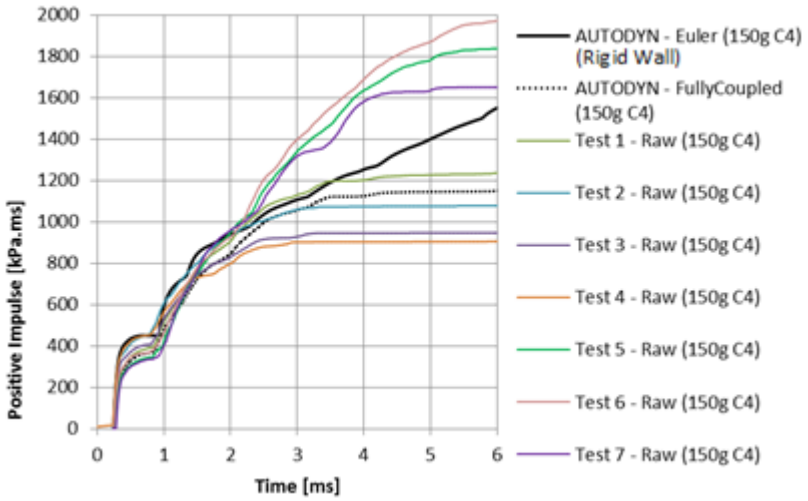

Figure 3.25. Positive Impulse Comparison for 150 g Charge Weight (100% Venting Area)

For 100% venting area, by looking at experimental results and fully coupled predictions it can be said that the blast energy diminishes in 5 to 6 ms (Figure 3.23, Figure 3.24, Figure 3.25).

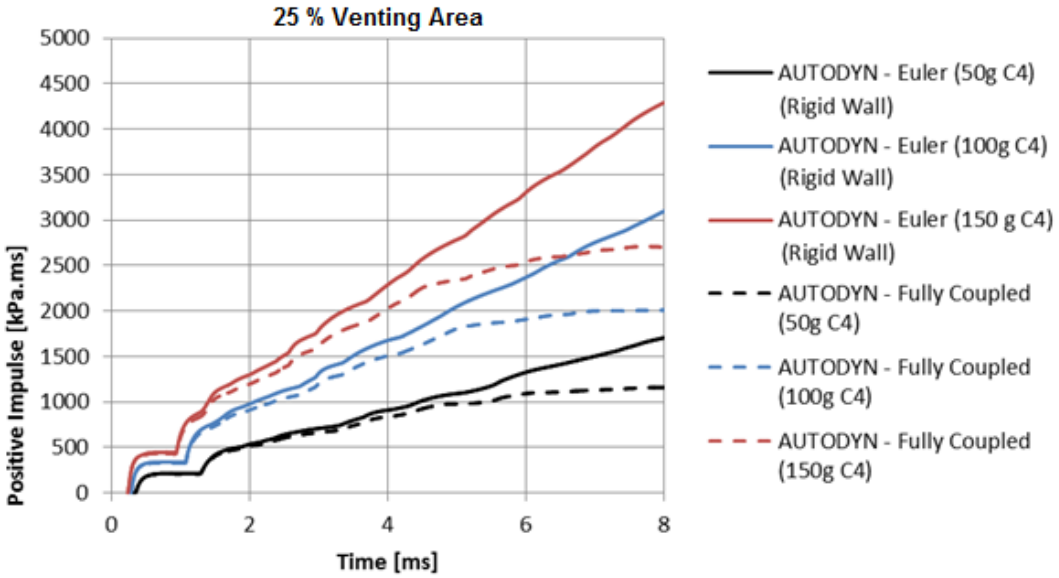

(a)

Figure 3.26. (a) Positive Impulse Comparison for 25% Venting Area (b) Positive Impulse Comparison for 6.25% Venting Area

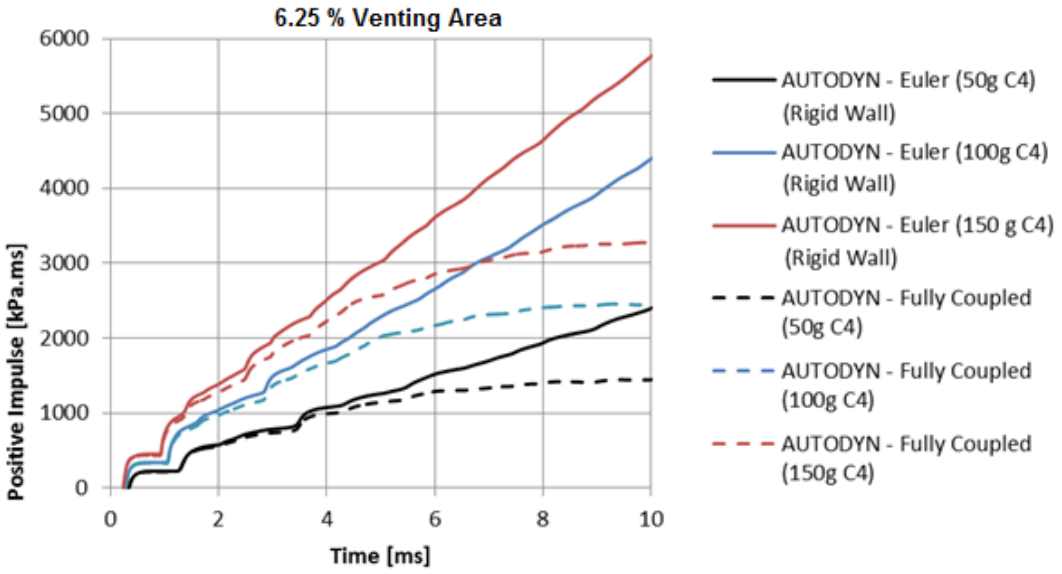

(b)

Figure 3.26 (Cont'd) (a) Positive Impulse Comparison for 25% Venting Area (b) Positive Impulse Comparison for 6.25% Venting Area

For 25% and 6.25% venting area, it can be said that the blast energy is transferred completely in 8 and 10 ms respectively (Figure 3.26).

The difference between the Eulerian and fully coupled predictions is elevated with the confinement. Due to the increased interaction process in highly confined models, more energy is absorbed by the structure.

CHAPTER 4

ANALYSIS OF DYNAMIC RESPONSE TO BLAST LOADING

In the previous section, the prediction capabilities of AUTODYN and BLASTX are investigated. For the analysis of dynamic response to blast loading, one should know the amount of uncertainty caused by the blast calculation. Comparison of blast parameters of computational and experimental results for 100% venting area is presented below (Table 4.1).

Table 4.1. (a) Comparison of Computational Predictions with Raw Experimental Averages (b) Comparison of Computational Predictions with Filtered Experimental Averages

(a)

	50 g Charge Weight		**100 g Charge Weight**		**150 g Charge Weight**	
	AUTODYN	**BLASTX**	**AUTODYN**	**BLASTX**	**AUTODYN**	**BLASTX**
P_1	-20%	-20%	2%	9%	-25%	-18%
P_2	72%	19%	215%	75%	180%	70%
Impulse	89%	68%	145%	120%	11%	-5%

Table 4.1. (Cnt'd) Comparison of Computational Predictions with Raw Experimental Averages (b) Comparison of Computational Predictions with Filtered Experimental Averages

(b)

	50 g Charge Weight		100 g Charge Weight		150 g Charge Weight	
	AUTODYN	**BLASTX**	**AUTODYN**	**BLASTX**	**AUTODYN**	**BLASTX**
P_1	6%	6%	43%	52%	13%	23%
P_2	112%	46%	250%	95%	222%	95%
Impulse	95%	73%	149%	123%	13%	-3%

AUTODYN and BLASTX calculate the most important blast parameter – First Peak Pressure – within acceptable limits. However, latter blast wave and total positive impulse are considerably different than experimental data for both methods.

4.1. Definition of the Problem

After investigating the accuracy of the blast solving tools, one can consider the dynamic response to blast loading. To do so, AUTODYN is used as the structural solver whilst BLASTX and AUTDYN are used for the blast calculation (Table 4.2).

Table 4.2. Dynamic Response Calculation Methods

Method		**Structural Solver**	**Blast Solver**
1	Fully Coupled	AUTODYN	AUTODYN
2	Hybrid Method	AUTODYN	BLASTX

In the first method, AUTODYN solves the problem using fully coupled interaction algorithm. Both blast overpressure and structural response is calculated within the same problem definition. On the other hand, second problem employs BLASTX which solves the blast loading for a given time. Then, the output is applied as dynamic pressure boundary condition on the structural problem in AUTODYN.

In order to compare the accuracy of two methods, the same example problem is solved and tested. A 2 m^3 deformable steel cubicle (3 mm thickness) with 1 m^2 square venting area on the top surface is constructed as a test setup (Figure 4.1).

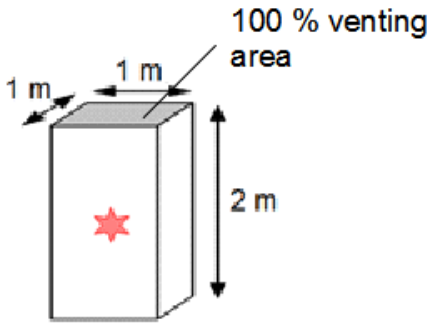

Figure 4.1. Problem Definition for the Analysis of Dynamic Response

In this setup, stiffeners are not employed to avoid any compromise in the deflection process. Moreover, 50 grams of C4 high explosive is detonated at the geometric center of the setup to get the same dynamic response on all of the side walls. Similar to the test setup in the previous chapter, center initiation is used.

4.2. Modeling in Fully Coupled Method

Euler solver, Lagrange solver and Euler-Lagrange interaction are used for the fully coupled method dynamic response calculation.

Structure is a rectangular prism with dimensions 1 m x 1 m x 2 m. Note that, Euler space (air) is modeled significantly larger than the steel test setup. In order to predict the deformation correctly, the deflected parts of the setup should also stay within the air. By doing so, solution domain is expanded to a prism with dimensions 1.3 m x 1.3 m x 2 m (Figure 4.2).

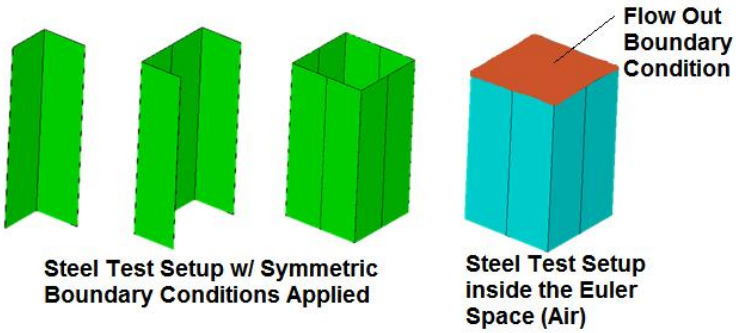

Figure 4.2. Modeling in AUTODYN

Remapping is also used in these problems. Initially, one dimensional calculation is performed up to 500 mm distance which is the nearest obstacle (steel plate) from the detonation center. After that, result is mapped into three dimensional problem which is actually a quarter of the problem space. Moreover, outflow boundary condition is employed for the venting surface

In this work, air, C4 and steel materials are used. Detailed information about the material models and parameters are given in the earlier sections (Table 3.4).

4.3. Modeling in Hybrid Method with BLASTX

In the hybrid method, BLASTX and AUTODYN are used together. Initially, BLASTX calculates the blast pressure history on the steel plates. Note that BLASTX is not able to solve any deformation, meaning that the predicted blast history does not contain any information caused by deformed boundaries. Then those outputs are applied as dynamic pressure boundary condition on the structural problem defined in AUTODYN. The advantage of this method is the less complicated hydrocode problem definition which requires less computational power. Since, no interaction is solved, and only Lagrange solver is used for the structural response problem, this method requires less computational resources. On the other hand, rigid boundary condition assumption made in BLASTX is the drawback of the method.

The tricky part of coupling BLASTX and AUTODYN is the application of the pressure history as a boundary condition. It was stated that BLASTX works pointwise. It does not calculate pressure history for the entire problem. Predefined points are considered only. This kind of approach conflicts with the AUTODYN' solving scheme

that asks for pressure data for each element. In order to overcome this difficulty, steel surfaces are divided into equivalent 25 cmx25 cm sections (Figure 4.3).

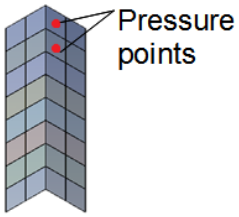

Figure 4.3. Section Division for Hybrid Method

The pressure on the center of each square is calculated by BLASTX. Then, it was assumed that pressure is distributed uniformly over the squares. 32 different blast histories are applied as dynamic pressure boundary conditions. At last, AUTODYN solves the structural problem conditions - a rectangular prism with dimensions 1 m x 1 m x 2 m - with several boundaries.

4.4. Test Setup

Test setup is constructed by welding 3 mm thick steel plates with steel frames together. Welding process is performed for both frames outside and plates inside. In order to prevent the distortion due to heat and uneven cooling process of welding that is not applied continuously. However, despite the efforts still some negligible distortion is observed (Figure 4.4).

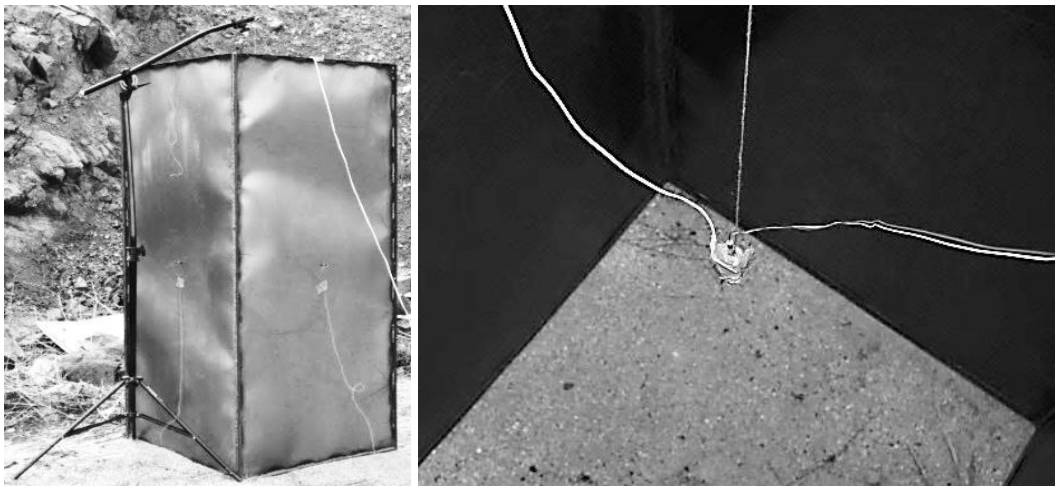

Figure 4.4. Test Setup

Similar to the previous tests, a steel tripod is used to lower the C4, and plastic ropes are used as guides to make sure that C4 detonates right at the geometric center. 50 grams of C4 is shaped by hand with an acceptable precision. Again, aluminum electrical capsule is used to initiate the detonation.

4.5. Comparison of the Results

Fully coupled AUTODYN and hybrid methods' computational outputs are compared with the experimental data. Computational models are solved for 20 ms. After 20 ms, the chaotic situation inside the prism is eradicated (Figure 4.5). A fully coupled AUTODYN technique is employed where the top surface is treated as outflow boundary and steel plates are assumed to be bonded together. The frames are ignored for simplicity.

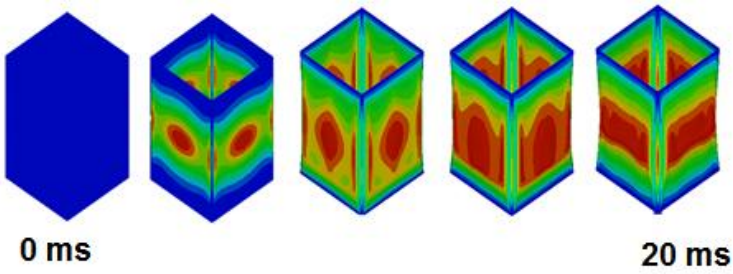

Figure 4.5. Computational Results

According to the computer simulations, the distortion of the prism can be categorized as significant deformation on the plates and slight bending on the frames. The same physical responses are also observed during the test (Figure 4.6).

Figure 4.6. Test Setup (After the test)

In this work, the deformation of the steel plates is considered only. Especially, the maximum deflection at the center of the plate is compared (Figure 4.7). The schematic cross sectional view of the maximum deflection plane in theory is given below. Note that, maximum deflection is expected on the quarters.

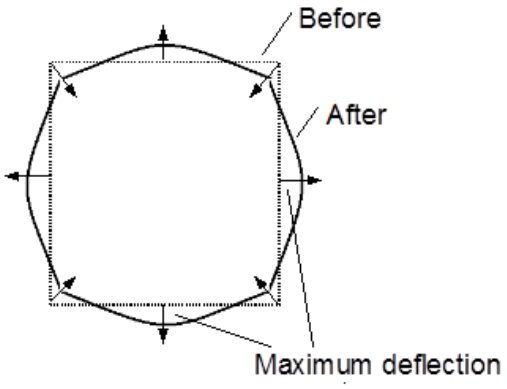

Figure 4.7. Maximum Deflection Plane (Expected)

Despite the circular expectation, test results show some inconsistencies in the outer contour. In order to fully understand the cross sectional plane of the maximum deflection, the prism is cut into two halves (Figure 4.8).

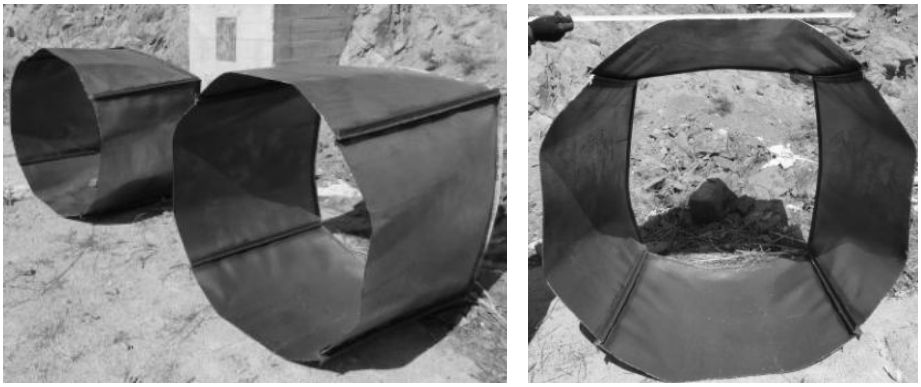

Figure 4.8 Test Setup (Cross sectional view)

High resolution pictures of the cross section are taken after the test. Using image processing technique, the exact contour is plotted and compared with the original prism (Figure 4.9). First, imaginary centers of original and deformed bodies are constructed using a rectangle and a circle respectively. Then, centers are superposed to determine the deflection.

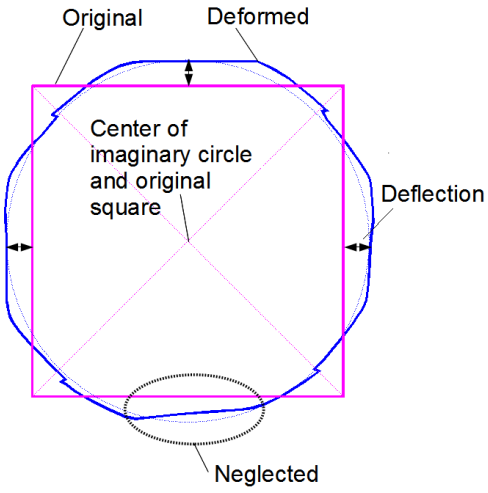

Figure 4.9. Image Processing

Deflection values on the quarters for three edges are considered. The bottom edge was compromised during the cutting process. The average value for the deflection is found as 82 mm.

Next, computational results are compared with the experimental data. It can be said that hybrid method predicts slightly higher than the fully coupled method due to the rigid wall assumption of BLASTX while computing the blast histories. The energy dissipation caused by the distortion of the structure is ignored. Hence, the effect of detonation overestimated. In general, computerized methods calculate within acceptable limits (Table 4.3).

Table 4.3. Comparison of the Results

Method	Final Deformation	Difference	Computational Time
Fully Coupled	90 mm	10%	6 days
Hybrid Method	102 mm	24%	2 hours
Test	82 mm	Reference Data	

The modeling in hybrid method takes considerably much time – approximately two times higher. On the other hand, the computational requirements are substantially low. It took almost a week to solve the problem in fully coupled method, whereas 4 hours was needed for the whole process in the hybrid method. Since the preparations for the hybrid method is more complex, 2 hours is spent for that purpose.

It should be noted that 3 mm thickness is chosen on purpose to observe the deflection very well and especially to expose the drawback of the hybrid method: rigid wall assumption while computing the blast histories. However; despite the large deformation, the overestimation of the hybrid method can be considered as acceptable. Considering the slight overestimation, the hybrid method can be used if the acceptable tolerance of deflection is not critical. In addition, it can be also said

that the hybrid method is “safer” than the fully coupled method which makes it suitable for safety predictions.

Finally, an analysis is carried out in order to expose the effect of first peak pressure in the final deformation. To do so, an additional AUTODYN model is prepared that blast loading is removed after the end of the first blast wave (~1 ms). Consequently, final deformation after the first peak is compared with the final deformation after the whole process.

Table 4.4. Comparison of the Results

Method	Final Deformation After the First Peak	Ratio with the Whole Blast History
Fully Coupled	59 mm	65 %
Hybrid Method	55 mm	54 %

It can be concluded that, for the thin metallic structures, first peak pressure and its duration provides a significant portion of the total deformation. The remaining smaller portion of the deformation is occurred due to the successive blast waves. This result is consistent with the total load profile simplification in the literature for the reflected overpressure in internal explosions (Figure 4.10).

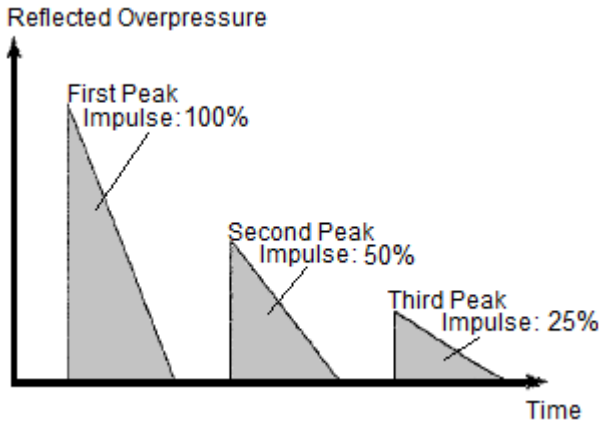

Figure 4.10. Load Profile Simplification for Internal Explosion [50]

CHAPTER 5

CONCLUSION AND FUTURE WORK

5.1. Discussion of the Results and Conclusion

The design of a structure is crucially important especially if it has a possibility to be exposed to any kind of internal explosion. In this study, blast overpressure and dynamic response to blast loading are investigated.

In the scope of this study, firstly, theoretical backgrounds of computational procedures are presented. The basic principles of the hydrocodes (e.g. AUTDOYDN) and the numerical applications are explained in detail. Next, semi empirical methods (e.g. BLASTX) are reviewed. Afterwards, a unique way of coupling these two methods is also taken under consideration. In addition, a tolerance analysis is presented in order to show the variance in test results.

Secondly; during the analysis of blast overpressure, partially confined structures are examined. In this investigation; structural parts are assumed to be rigid. A test setup is used for experimental purposes. This section starts with the definition of the problems under investigation. Then, computational results obtained from BLASTX and AUTODYN are compared with the experimental data. It is observed that; first peak pressure show good agreement with the experimental data whereas arrival time of first peak pressure, arrival time of second peak pressure and positive impulse predictions are distinctively separated. The difference in the environmental conditions is the main reason for the dispersion of experimental data. In addition, the size of the aluminum electrical capsule may alter the results since small charges are involved in this study.

The rigidity of the test setup is also investigated. By comparing Eulerian (under the assumption of rigid wall, structure is ignored) and fully coupled methods (blast wave and structure interaction is accounted), it was observed that some amount of energy is absorbed by the steel structure.

After investigating the accuracy of blast calculation methods, the dynamic response to blast loading is investigated. In this work, AUTODYN is used as the structural solver whereas BLASTX and AUTODYN are used for the blast calculation. Two types of solution procedures are tracked. In the first method, AUTODYN solves the problem using fully coupled interaction policy. Both blast overpressure and structural response are calculated within the same problem definition. On the other hand, second method employs BLASTX that solves the blast history for a given time. The pressure data is applied as dynamic pressure boundary condition on the structural problem in AUTODYN. In this study, a deformable test setup is constructed. A relatively delicate structure is deliberately chosen to observe the deflection and to expose the disadvantage of the hybrid method: rigid wall assumption while computing the blast histories. However; despite the large deformation, the hybrid method predicts close to fully coupled AUTODYN and experimental output. It can be said that the hybrid method can be used for safety predictions due to slight overestimation.

Finally, although the methods introduced in this study are the known best methods in computing interior explosion behavior, they have observed weaknesses in computational results as shown in this thesis. It can be concluded that when these methods are used in the prediction of blast loading, a degree of possible error margin should be taken into consideration.

5.2. Future Work

A hybrid method to estimate the dynamic response to blast loading is developed in the scope of this work. The method is proven to be quite acceptable for the given test setup. However; this study can be extended with the following items suggested:

- Different structural materials can be analyzed to provide better rigidity.
- Tests are performed for only 100% venting area; the same procedure can be pursued for 25% and 6. 25% venting areas. It is highly recommended to

stock redundant equipment to solve electronic malfunction and faulty production issues.

- Test setup can be modified so that vibration isolation techniques are employed for the gauge mountings.
- This work is completed within certain constraints. By doing substantially more tests and computations for various charge weights, one can see the boundaries of the method.
- Various blast pressure gauges can be selected to see if there is any gauge dependent errors.
- Time dependent deflection comparison can be performed.
- The hybrid method can be improved to solve problems with complex geometries.
- The accuracy of computational methods in latter blast waves can be improved by defining an improved boundary condition.

REFERENCES

[1] Rahman, S., Timofeev, E., “Pressure Measurements in Laboratory-Scale Blast Wave Flow Fields”, Review of Scientific Instruments, Vol. 78, 2007

[2] Kevorkian, S., Duriez, N., Loiseau, O., “Laboratory Scale Tests for Internal Blast Loading”, Structures Under Shock and Impact XI, pp.128-134, 2010

[3] Baylot, J. T., Bevins T. L., “Effect of Responding and Failing Structural Components on the Airblast Pressures and Loads on and Inside of the Structure, Computers and Structures, Vol. 85, pp.891-910, 2007

[4] Remennikov, A. M., “A Review of Methods for Predicting Bomb Blast Effects on Buildings”, Journal of Battlefield Technology, 2003

[5] Nurick, G. N., Martin J. B., “Deformation of Thin Plates Subjected to Impulsive Loading – A Review Part 1: Theoretical Considerations”, International Journal of Impact Engineering Vol. 8, No. 2, pp.159-170, 1988

[6] “TM 5-1300 Structures to Resist the Effects of Accidental Explosions”, Departments of the Army, the Navy, and the Air Force, 1990

[7] Joachim, E. C., “Prediction of Airblast Pressures from Explosions in Underground Magazines”, US Army Engineer Waterways Experiment Station, 1994

[8] Joachim, E. C., “Evaluation of the BlastX3.5 Computer Model for Explosion Blast Analysis and Siting of Underground Magazines”, US Army Engineer Waterways Experiment Station, 1996

[9] Benselama, A. M., William-Louis, M. J. P., Monnoyer, F., “1D–3D Mixed Method for the Numerical Simulation Of Blast Waves in Confined Geometries”, Journal of Computational Physics, 2009

[10] Olovsson, L., Hanssen, A.G., Borvik, T., Langseth, M., “A Particle-Based Approach to Close-Range Blast Loading”, European Journal of Mechanics A/Solids, 2009

[11] Rose, T.A., “An Approach to the Evaluation of Blast Loads on Finite and Semi-Infinite Structures”, PhD Thesis, Engineering Systems Department, Cranfield University

[12] Van den Berg, A. C., “BLAST: A Compilation of Codes for the Numerical Simulation of the Gas Dynamics of Explosions”, Journal of Loss Prevention in the Process Industries, 2008

[13] Rigas, F., Sklavounos, S., “Experimentally Validated 3-D Simulation of Shock Waves Generated By Dense Explosives in Confined Complex Geometries”, Journal of Hazardous Materials, 2005

[14] Chapman, T.C., Rose, T.A., Smith, P.D., “Blast Wave Simulation using AUTODYN-2D: A Parametric Study”, International Journal of Impact Engineering, Vol. 16, pp.777-787, 1995

[15] Fairlie, G.E., “The Numerical Simulation of High Explosives using AUTODYN-2D & 3-D”, Institute of Explosive Engineers 4th Biannual Symposium, 1998

[16] Birnbaum, N.K., Clegg, R.A., Fairlie G.E., Hayhurst, C.J., Francis, N. J., “Analysis of Blast Loads on Buildings”, Century Dynamics Incorporated

[17] Luccioni, B., Ambrosini, D., Danesi, R., “Blast Load Assessment using Hydrocodes”, Engineering Structures, Vol. 28, pp. 1736-1744, 2006

[18] Trelat, S., Sochet, I., Autrusson, B., Cheval, K., Loiseau, O. “Impact of a Shock Wave on a Structure on Explosion at Altitude”, Journal of Loss Prevention in the Process Industries, Vol. 20, pp. 509-516, 2007

[19] Zhou, X.Q., Hao, H., “Prediction of Airblast Loads on Structures Behind a Protective Barrier”, International Journal of Impact Engineering, Vol. 35, pp. 363-375, 2008

[20] Zyskowski, A., Sochet, I., Mavrot, G., Bailly, P., Jerome, R., “Study of the Explosion Process in a Small Scale Experiment – Structural Loading”, Journal of Loss Prevention in the Process Industries, Vol. 17, pp. 291-299, 2004

[21] Nyström, U., Gylltoft, K., “Numerical Studies of the Combined Effects of Blast and Fragment Loading”, International Journal of Impact Engineering, Vol. 36, pp. 995-1005, 2009

[22] Shi, Y., Hao, H., Li, Z., “Numerical Simulation of Blast Wave Interaction with Sturucture Columns”, Shock Waves, Vol. 17, pp. 113-133, 2007

[23] Safari, K. H., Zamani, J., Khalili, S. M. R., Jalili, S., “Experimental, Theoratical, and Numerical Studies on the Response of Square Plates Subjected to Blast Loading”, The Journal of Strain Analysis for Engineering Design, 2011

[24] Randers-Pehrson, G., Bannister, K.A., “Airblast Loading Model for DYNA2D and DYNA3D”, U.S. Army Research Laboratory, 1997

[25] Wong, W. T., “An Internal Blast Analysis of a Steel Box Member”, Canadian Journal of Civil Engineering, Vol. 36, pp. 1332-1339, 2009

[26] Weibull, H. R. W., “Pressures Recorded in Partially Closed Chambers at Explosion of TNT Charges”, Royal Swedish Fortifications Administration Stockholm, Sweden, 1968

[27] Hokanson, J. C., Esparza, E. D., Baker, W. E., Sandoval, N. R., “Internal Blast Measurements in a Model of Pantex Damaged Weapons Facility”, Southwest Research Institute, 1982

[28] Smith, P. D., Mays, G. C., Rose, T. A., Teo, K. G., Roberts, B. J., “Small Scale Models of Complex Geometry for Blast Overpressure Assessment”, International Journal of Impact Engineering, Vol. 12, pp. 345-360, 1992

[29] Jacinto, A. C., Ambrosini, R. D., Danesi, R. F., “Experimental and Computational Analysis of Plates Under Air Blast Loading”, International Journal of Impact Engineering, Vol. 25, pp. 927-947, 2001

[30] Boyd, S. D., “Acceleration of a Plate Subject to Explosive Blast Loading – Trial Results”, Department of Defense, Australia, 2000

[31] Edri, I., Savir, Z., Feldgun, V. R., Karinski, Y. S., Yankelevsky, D. Z., “On Blast Pressure Analysis Due to a Partially Confined Explosion: I. Experimental Studies”, International Journal of Protective Structures, Vol. 2, 2011

[32] Chan, P. C., Klein, H. H., “A Study of Blast Effects Inside an Enclosure”, 62nd Shock and Vibration Symposium, 1991

[33] Bass, C., Davis, M., Rafaels, K., Rountree, M., Harris, R., M., Sanderson, E., Andrefsky, W., Zielinski, M., “A Methodology for Assessing Blast Protection in Explosive Ordnance Disposal Bomb Suits”, International Journal of Occupational Safety and Ergonomics, Vol. 11, No. 4, pp. 347–361, 2005

[34] Bauwens, C., R., Chao, J., Dorofeev, S., V., “Effect of Hydrogen Concentration on Vented Explosion Overpressures from Lean Hydrogen-Air Deflagrations”, International Journal of Hydrogen Energy, Vol. 1, No. 7, pp., 2012

[35] Loiseau, O., Cheval, K., Kevorkian, S., “Laboratory Scale Tests for the Assessment of Solid Explosive Blast Effects”, Towards Convergence of Technical Nuclear Safety Practices in Europe (EUROSAFE)

[36] Smith, A., C., Sapko, M., J., “Detonation Wave Propagation in Underground Mine Entries”, National Institute of Occupational Safety and Health, USA

[37] Collins, G.S., “An Introduction to Hydrocode Modeling”, 2002

[38] AUTODYN Training Course, 2005

[39] AUTODYN Theory Manual, Revision 4.3

[40] Baker, W. E., Westine, P. S., Dodge, F. T., “Similarity Methods in Engineering Dynamics: Theory and Practice of Scale Modeling”, Elsevier, 1991

[41] Esparza, E. D., Baker, W. E., Oldham, G. A., “Blast Pressures Inside and Outside Suppressive Structures”, Southwest Research Institute, Department of the U.S. Army, 1975

[42] Ripley, R. C., Von Rosen, B., Ritzel D.V., Whitehouse, D. R., “Small-Scale Modeling of Explosive Blasts in Urban Scenerios”, Martec Ltd, Canadian Explosives Research Lab, Dyn-FX Consulting Ltd

[43] Needham, C. E., Whittwer, L: A., “Low Altitude Multiple Burst (LAMB) Models”, Air Force Weapons Laboratory, Kirtland AFB, 1975

[44] Britt, J. R., Ranta, D. E., Joachim, C. E., “BLASTX Code, User Manual”, 2001

[45] Bogosian, D., Ferritto, J., Shi, Y., “Measuring Uncertainty and Conservatism in Simplified Blast Models”, 30th Explosive Safety Seminar, 2002

[46] Veldman, R. L., Nansteel, M. W., Chen, C. C.-T., “Measurement of Blast Reflected Overpressure at Small Charge Standoff with Tourmaline Piezoelectric Transducers”, 26th International Symposium on Ballistics, 2011

[47] Rogers, G. F. C., Mayhew, Y. R., "Thermodynamic and Transport Properties of Fluids, SI Units"

[48] Dobratz, B.,M., Crawford, P.,C., "LLNL Explosives Handbook", 1985

[49] G. R. Johnson and W. H. Cook, "A Constitutive Model and Data for Metals Subjected to Large Strains, High Strain Rates, and Temperatures", 7th International Symposium on Ballistics, 1983

[50] Baker, W. E., “Explosions in Air”, University of Texas Press, 1973

[51] MATLAB Theory Manual, 2012

APPENDIX – A

TABULATED RESULTS FOR BLAST OVERPRESSURE

Table A.1. Tabulated Results for 100% Venting Area

100% Venting Area						
Charge Weight	**Method**	**P_1 [kPa]**	**t_{P1} [ms]**	**P_2 [kPa]**	**t_{P2} [ms]**	**I [kPa.ms]**
50 g	AUTODYN	2380	0.357	1166	1.316	706
	BLASTX	2389	0.321	803	1.390	627
	Test 1 (raw)	2722	0.394	764	1.269	413
	Test 2 (raw)	3021	0.269	667	0.934	368
	Test 3 (raw)	3161	0.256	601	1.026	339
	Test 1 (filtered)	1823	0.403	730	1.273	408
	Test 2 (filtered)	2440	0.278	454	0.941	353
	Test 3 (filtered)	2479	0.266	468	1.029	327

Table A.1. Tabulated Results for 100% Venting Area (Cont'd)

100 g	AUTODYN	4800	0.296	2404	1.064	1149
	BLASTX	5105	0.258	1335	1.140	1031
	Test 1 (raw)	4320	0.245	579	1.123	581
	Test 2 (raw)	4939	0.254	970	0.990	501
	Test 3 (raw)	4827	0.286	742	1.086	325
	Test 1 (filtered)	3450	0.255	474	1.130	575
	Test 2 (filtered)	3584	0.264	878	0.994	486
	Test 3 (filtered)	3029	0.295	706	1.095	324
150 g	AUTODYN	6966	0.254	3106	0.935	1550
	BLASTX	7641	0.229	1879	1.010	1336
	Test 1 (raw)	11100	0.258	1347	0.902	1398
	Test 2 (raw)	10875	0.240	1399	0.891	1083
	Test 3 (raw)	9391	0.252	1023	0.818	946
	Test 4 (raw)	8671	0.236	1128	0.898	917
	Test 5 (raw)	8403	0.272	869	0.835	1837
	Test 6 (raw)	9215	0.251	1045	1.030	1975
	Test 7 (raw)	7413	0.282	948	0.953	1659
	Test 1 (filtered)	6484	0.267	1064	0.908	1307
	Test 2 (filtered)	7246	0.248	1243	0.896	1056
	Test 3 (filtered)	6584	0.264	878	0.826	938
	Test 4 (filtered)	6274	0.245	999	0.902	894
	Test 5 (filtered)	5600	0.281	757	0.856	1809
	Test 6 (filtered)	6164	0.260	986	1.034	1971
	Test 7 (filtered)	4976	0.291	835	0.957	1655

Table A.2. Tabulated Results for 25% Venting Area

25% Venting Area						
Charge Weight	**Method**	**P_1 [kPa]**	**t_{P1} [ms]**	**P_2 [kPa]**	**t_{P2} [ms]**	**I [kPa.ms]**
50 g	AUTODYN	2380	0.357	1474	1.319	1706
	BLASTX	2389	0.321	839	1.390	1636
100 g	AUTODYN	4800	0.296	3429	1.073	3096
	BLASTX	5105	0.258	1469	1.140	3079
150 g	AUTODYN	6966	0.254	3944	0.942	4292
	BLASTX	7641	0.229	2159	1.010	4383

Table A.3. Tabulated Results for 6.25% Venting Area

6.25% Venting Area						
Charge Weight	**Method**	**P_1 [kPa]**	**t_{P1} [ms]**	**P_2 [kPa]**	**t_{P2} [ms]**	**I [kPa.ms]**
50 g	AUTODYN	2380	0.357	1698	1.327	2398
	BLASTX	2389	0.321	855	1.390	2519
100 g	AUTODYN	4800	0.296	4393	1.079	4393
	BLASTX	5105	0.258	1528	1.140	4824
150 g	AUTODYN	6966	0.254	5302	0.949	5761
	BLASTX	7641	0.229	2262	1.010	6986

APPENDIX – B

COMPUTATIONAL RESULTS

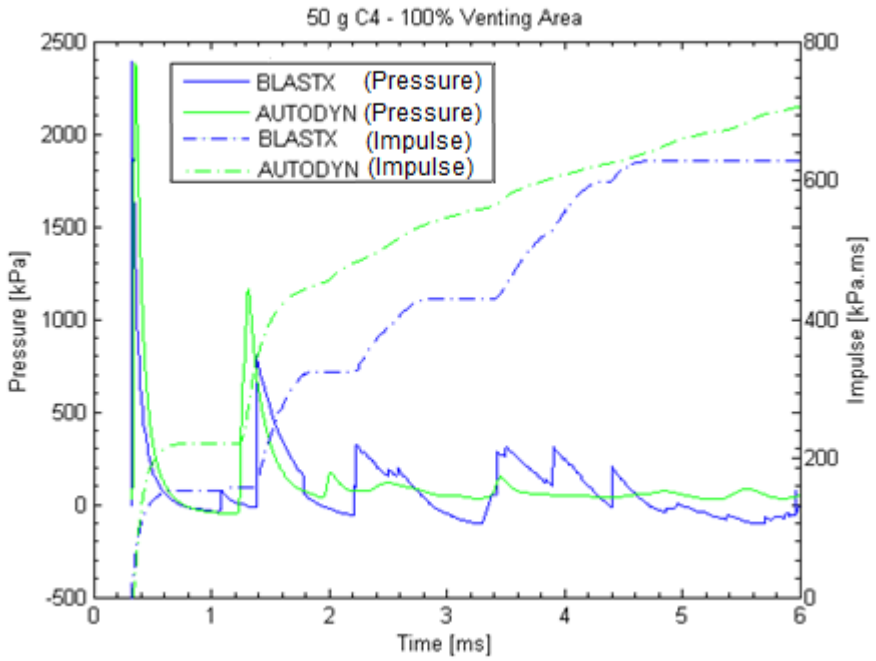

Figure B.1. Computational Results – 50 g Charge Weight, 100% Venting Area

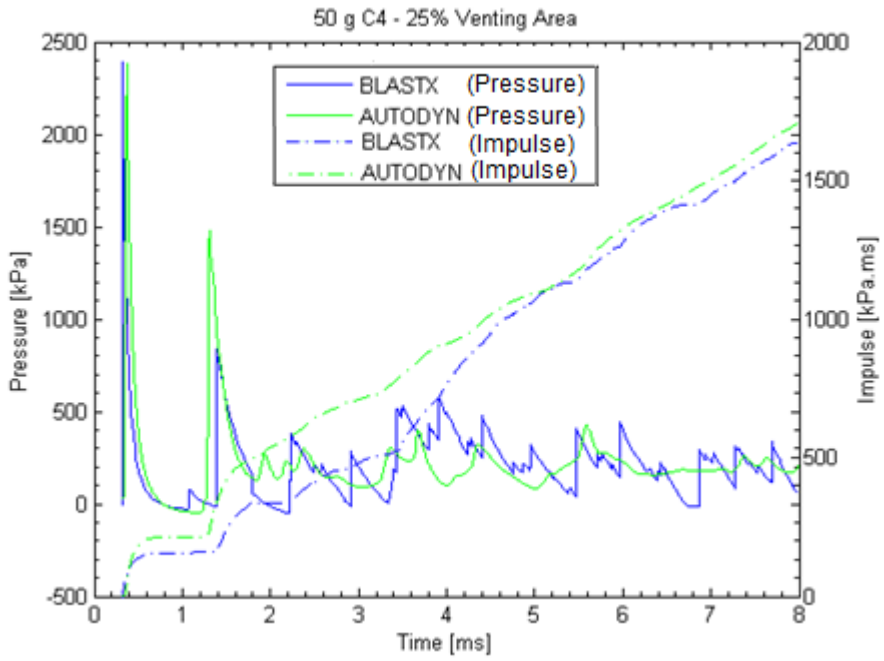

Figure B.2. Computational Results – 50 g Charge Weight, 25% Venting Area

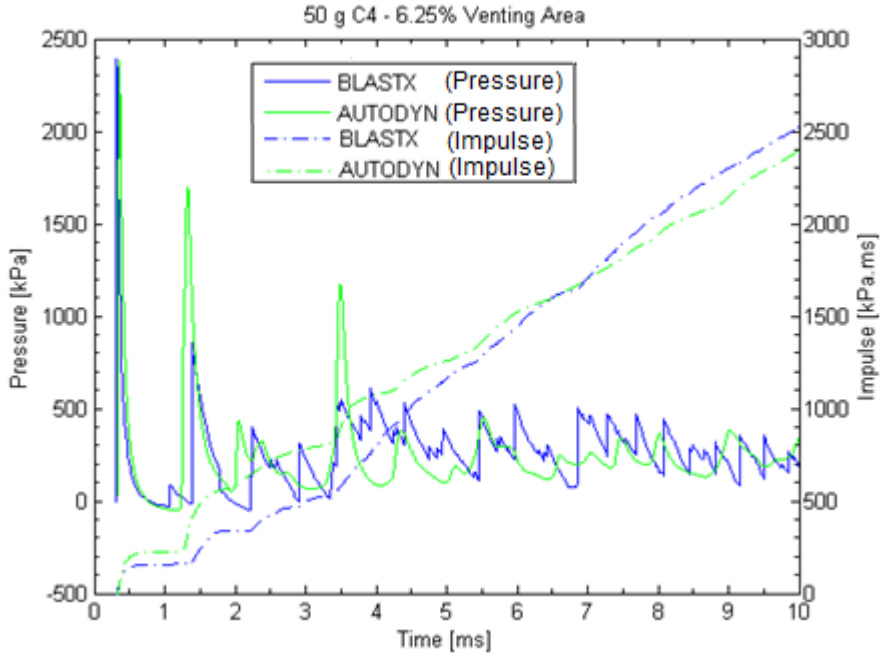

Figure B.3. Computational Results – 50 g Charge Weight, 6.25% Venting Area

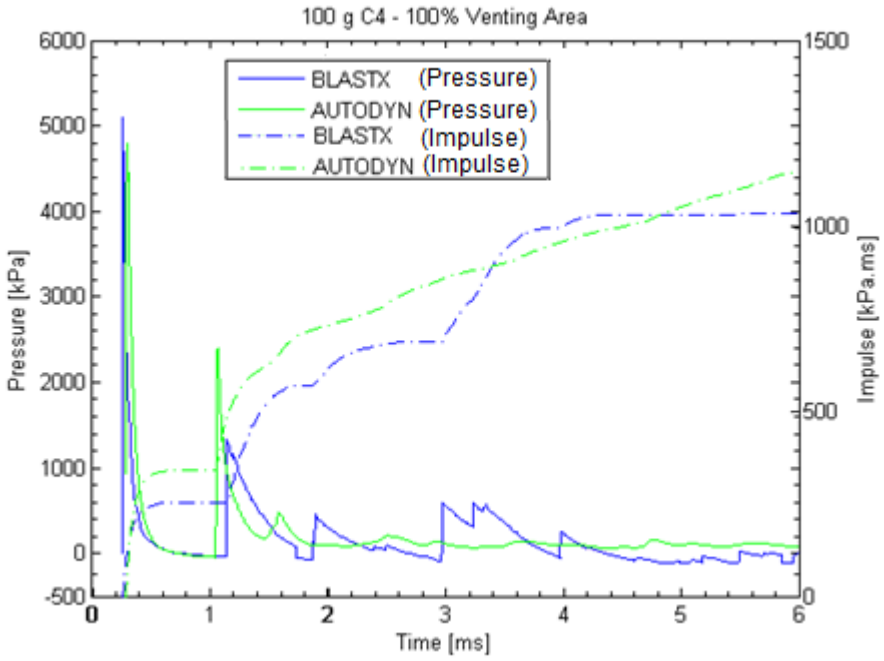

Figure B.4. Computational Results – 100 g Charge Weight, 100% Venting Area

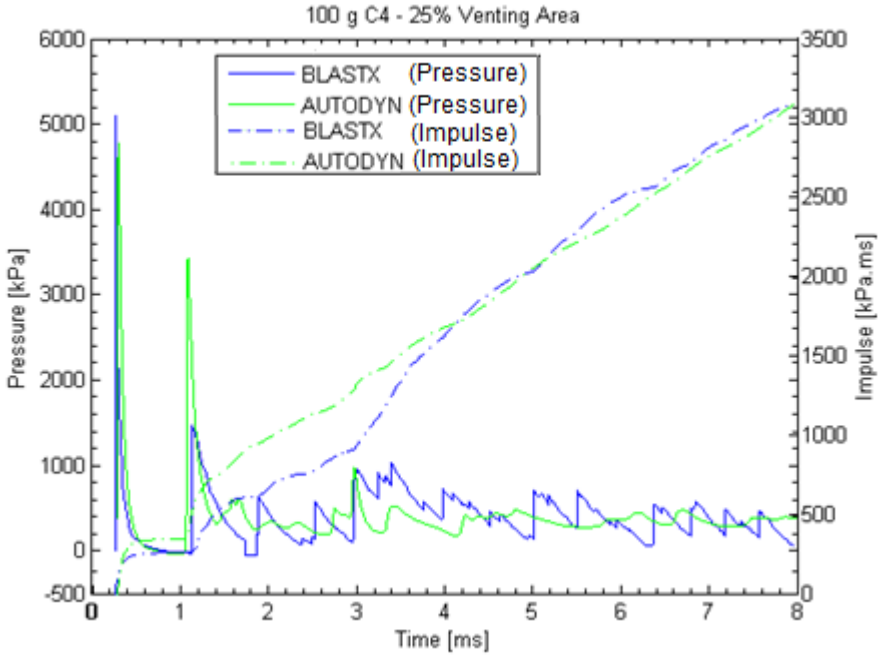

Figure B.5. Computational Results – 100 g Charge Weight, 25% Venting Area

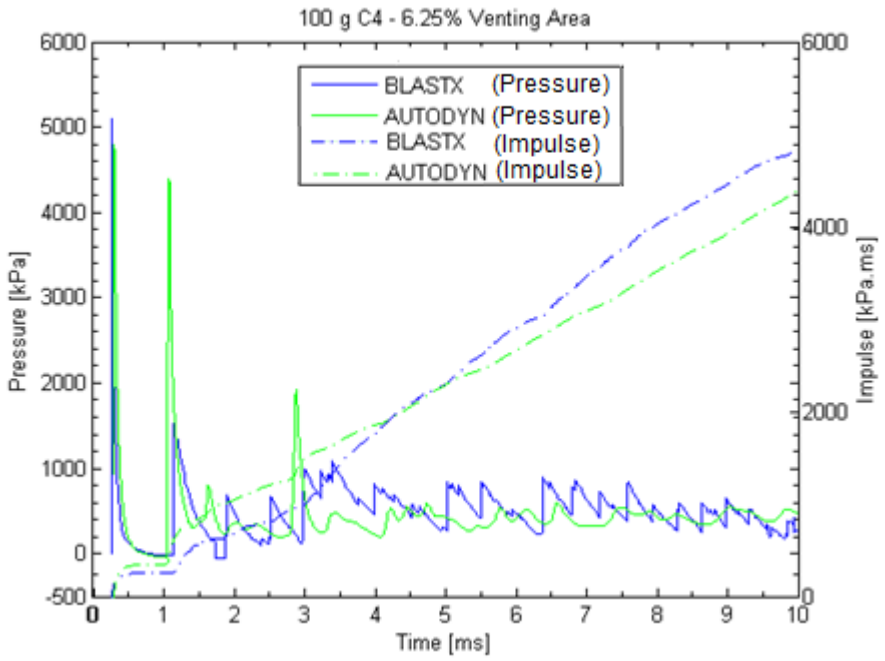

Figure B.6. Computational Results – 100 g Charge Weight, 6.25% Venting Area

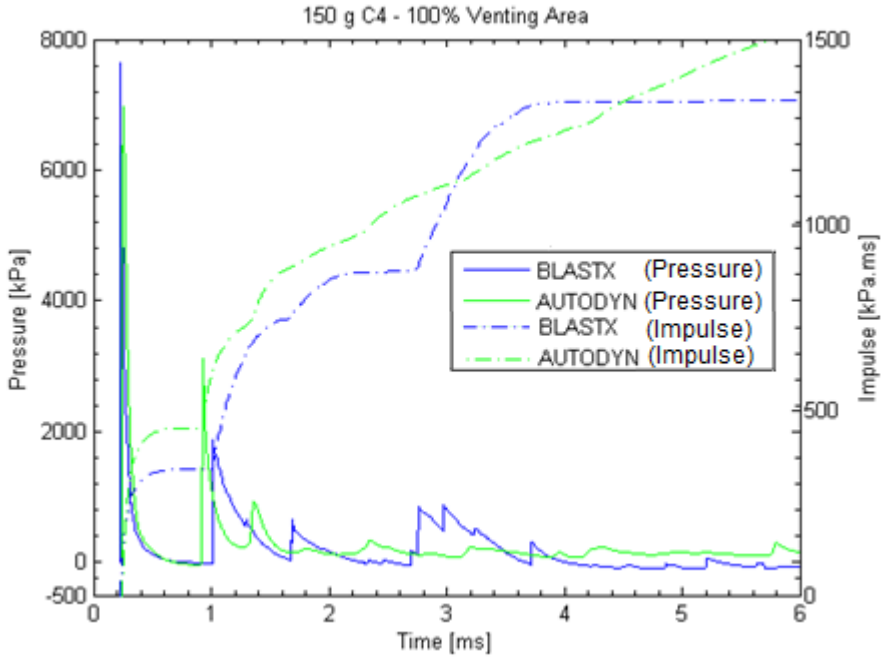

Figure B.7. Computational Results – 150 g Charge Weight, 100% Venting Area

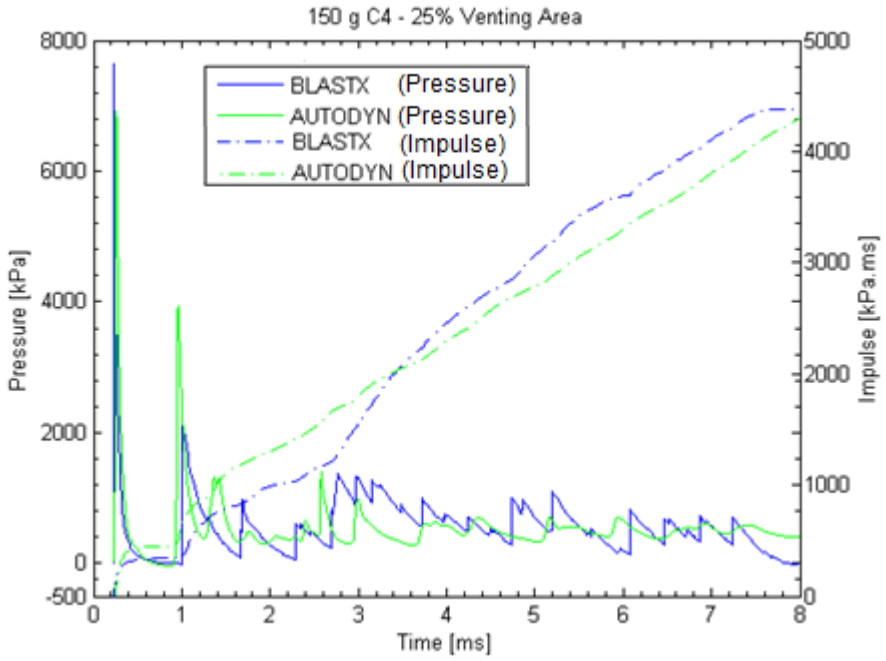

Figure B.8. Computational Results – 150 g Charge Weight, 25% Venting Area

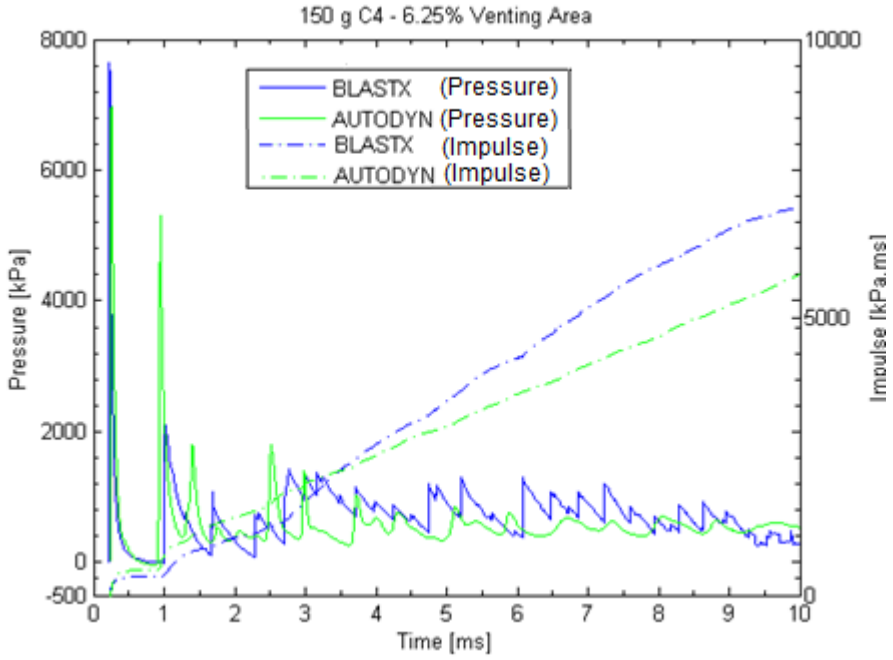

Figure B.9. Computational Results – 150 g Charge Weight, 6.25% Venting Area

APPENDIX – C

FILTERED TEST RESULTS: 100% VENTING AREA

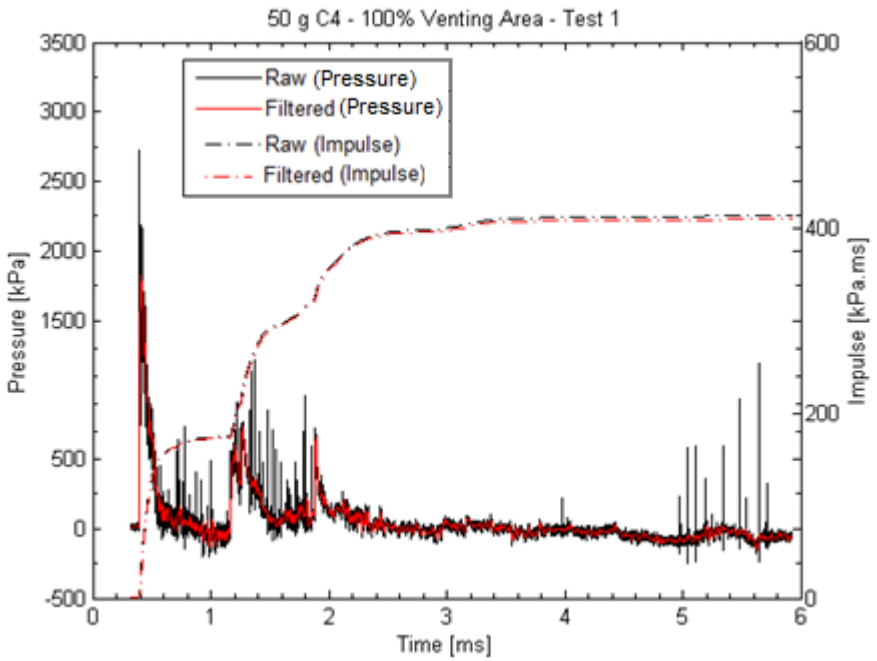

Figure C.1. Test 1 Data (50 g Charge Weight, 100% Venting Area)

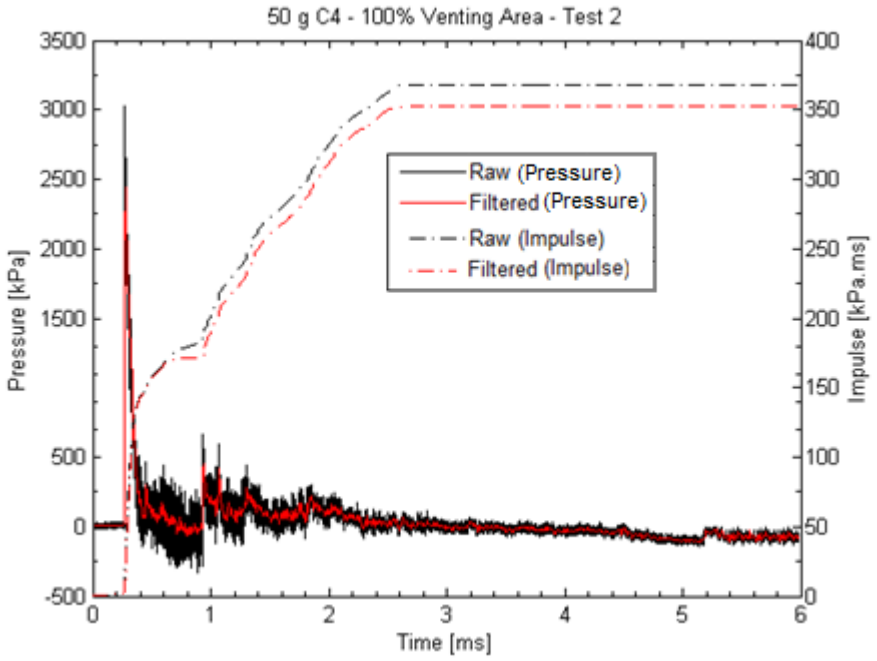

Figure C.2. Test 2 Data (50 g Charge Weight, 100% Venting Area)

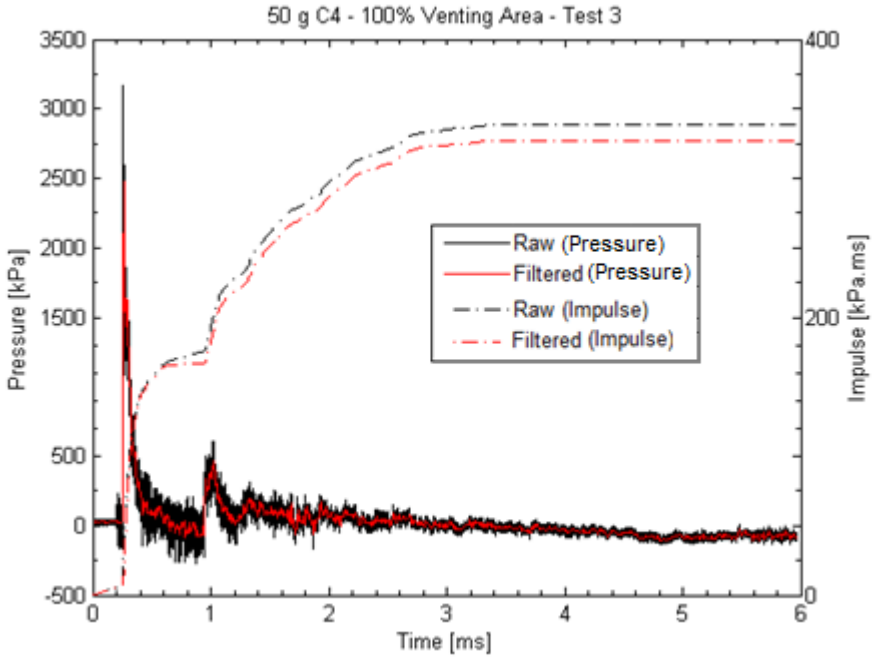

Figure C.3. Test 3 Data (50 g Charge Weight, 100% Venting Area)

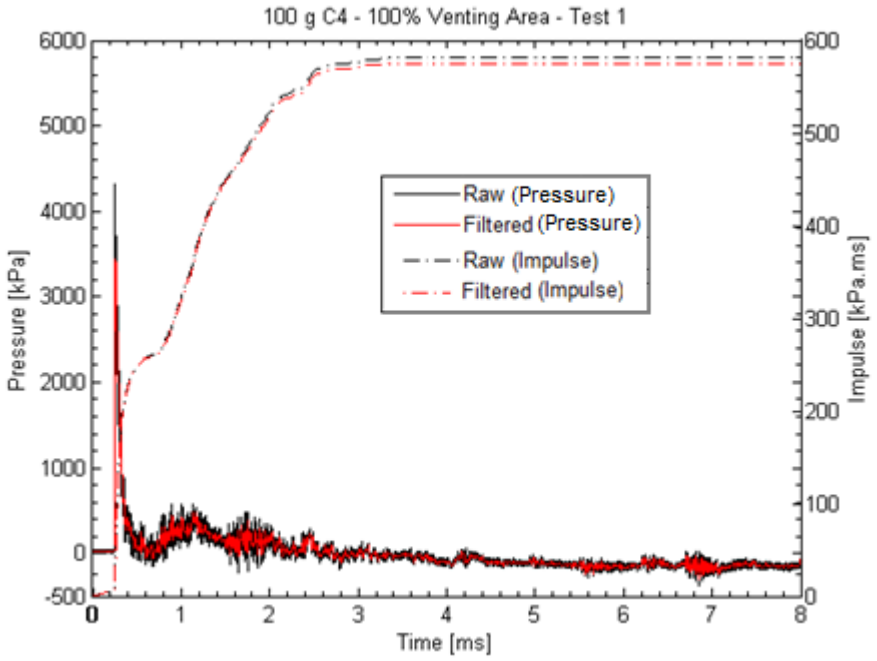

Figure C.4. Test 1 Data (100 g Charge Weight, 100% Venting Area)

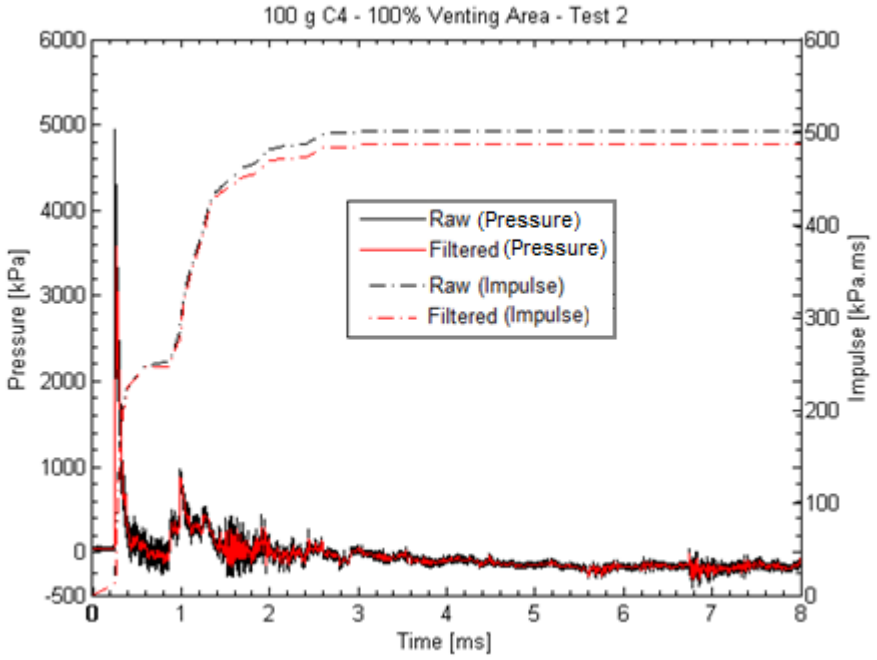

Figure C.5. Test 2 Data (100 g Charge Weight, 100% Venting Area)

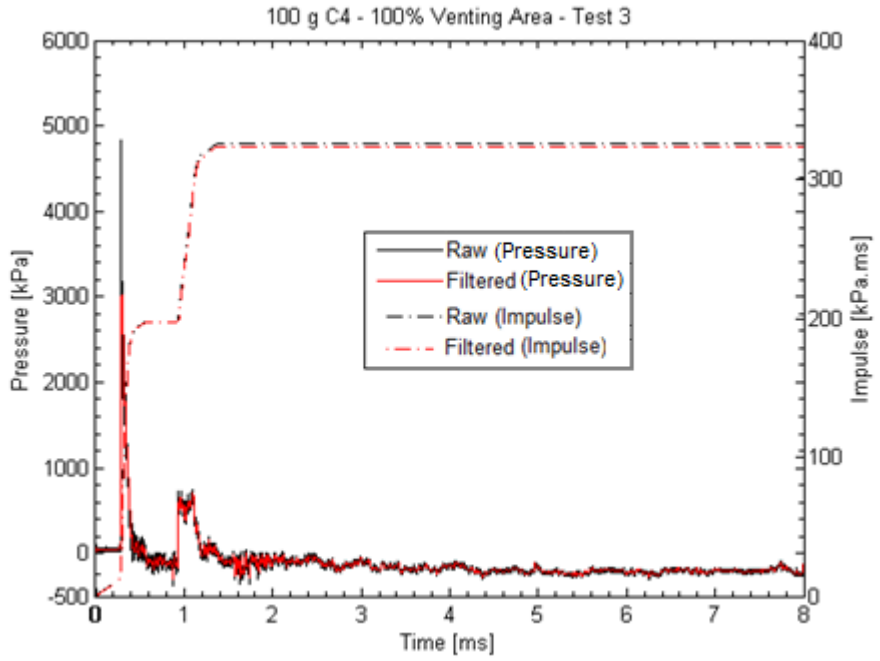

Figure C.6. Test 3 Data (100 g Charge Weight, 100% Venting Area)

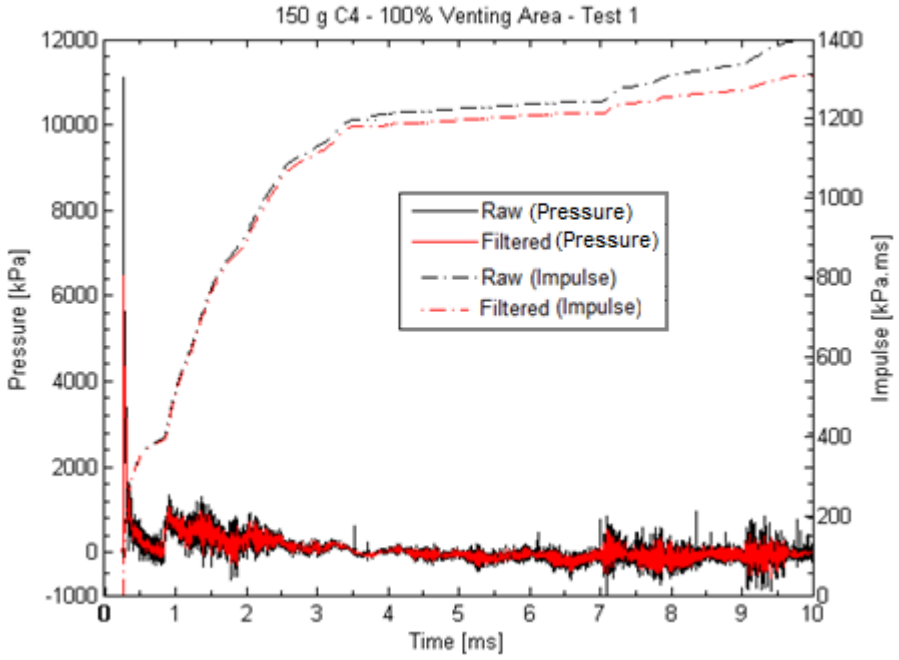

Figure C.7. Test 1 Data (150 g Charge Weight, 100% Venting Area)

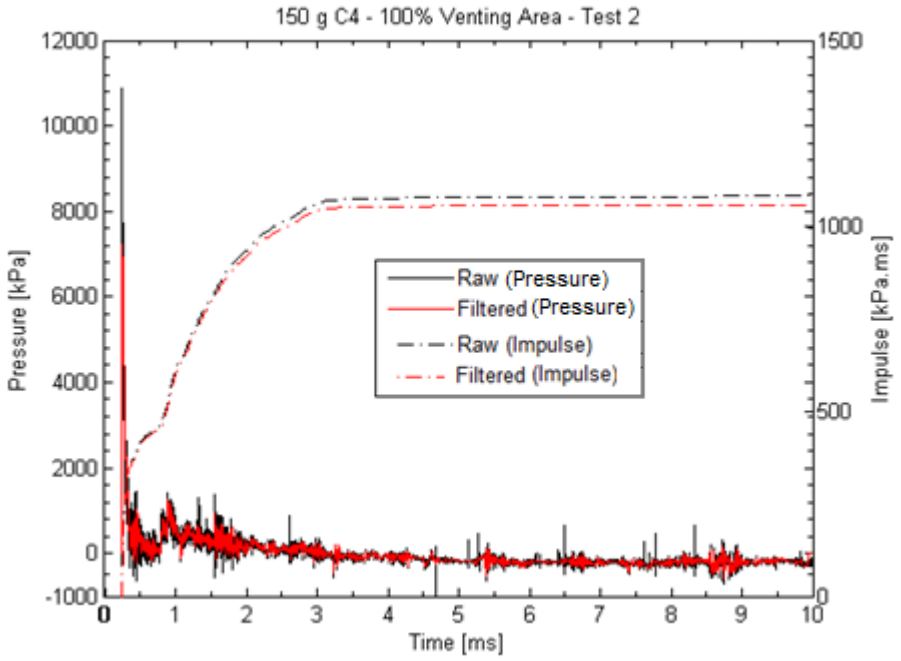

Figure C.8. Test 2 Data (150 g Charge Weight, 100% Venting Area)

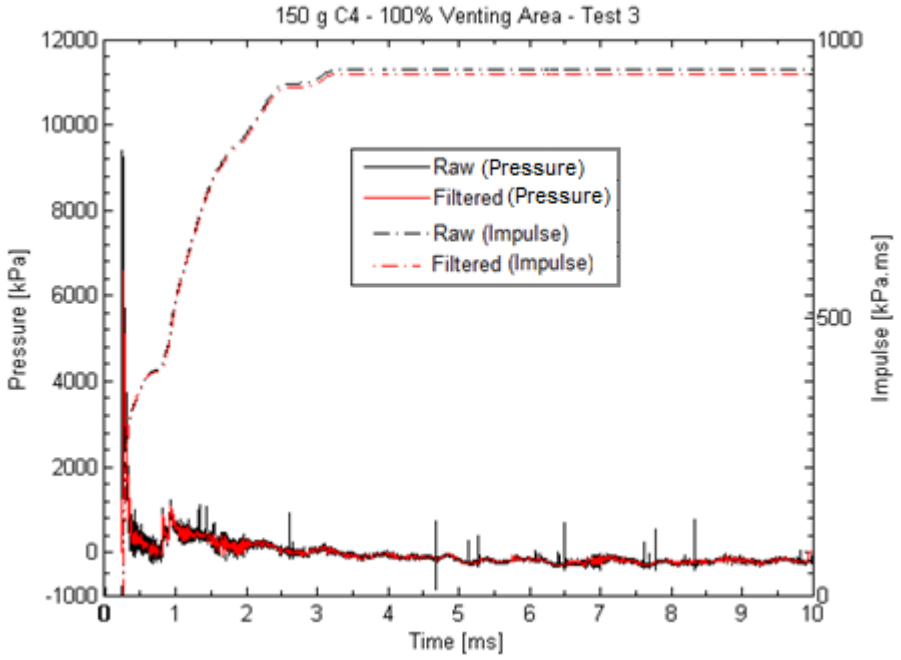

Figure C.9. Test 3 Data (150 g Charge Weight, 100% Venting Area)

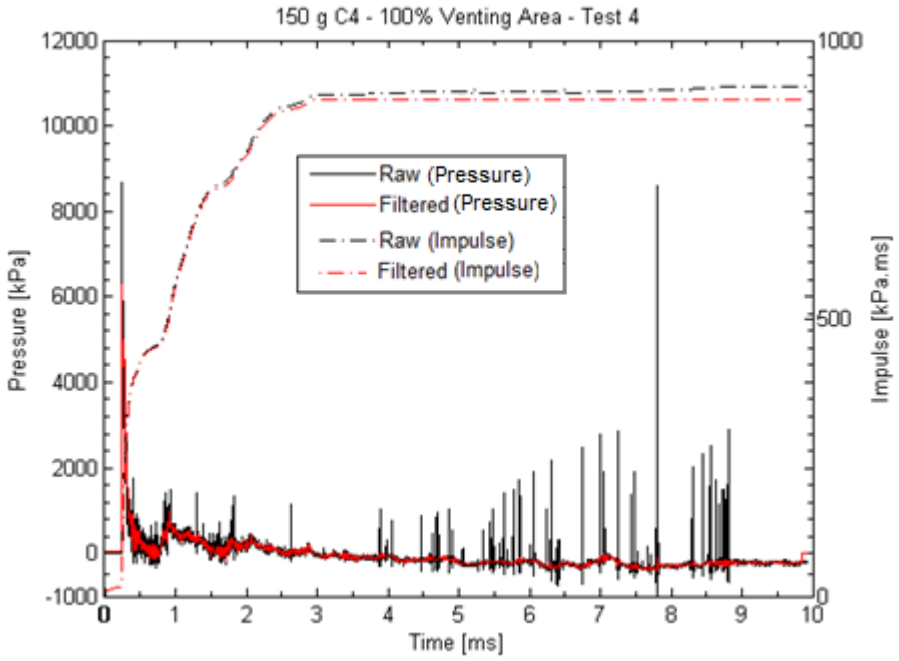

Figure C.10. Test 4 Data (150 g Charge Weight, 100% Venting Area)

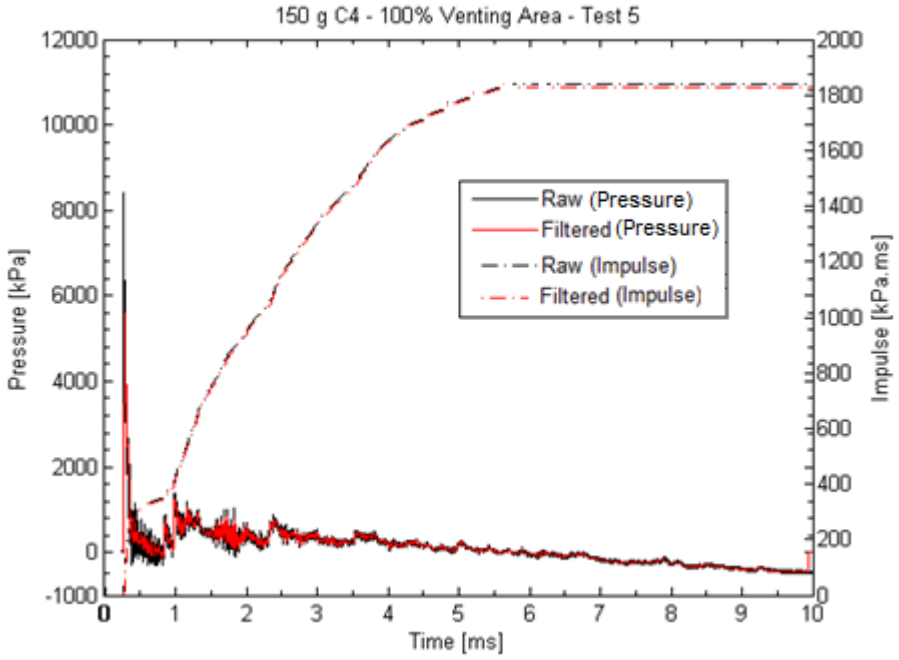

Figure C.11. Test 5 Data (150 g Charge Weight, 100% Venting Area)

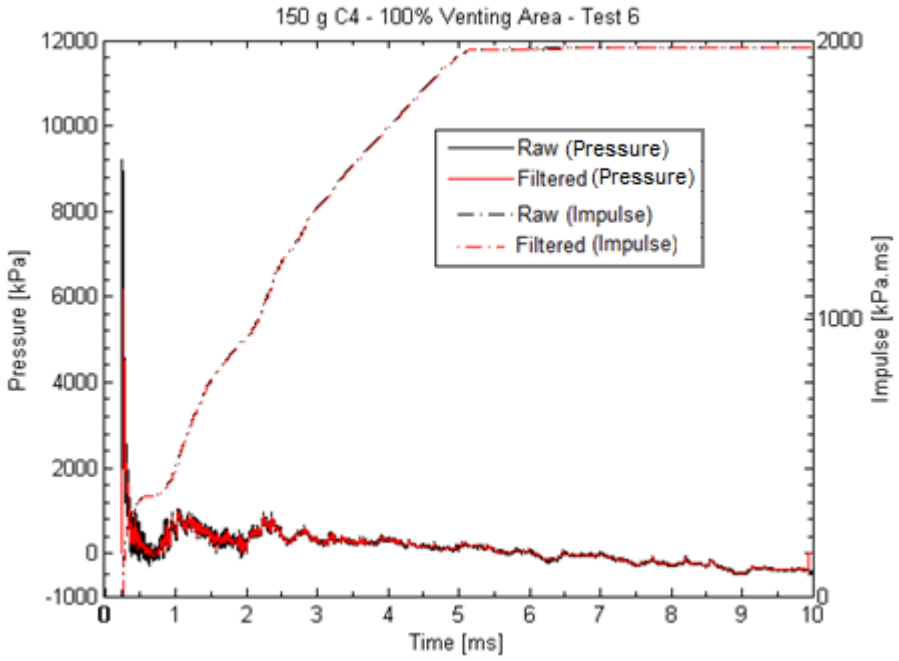

Figure C.12. Test 6 Data (150 g Charge Weight, 100% Venting Area)

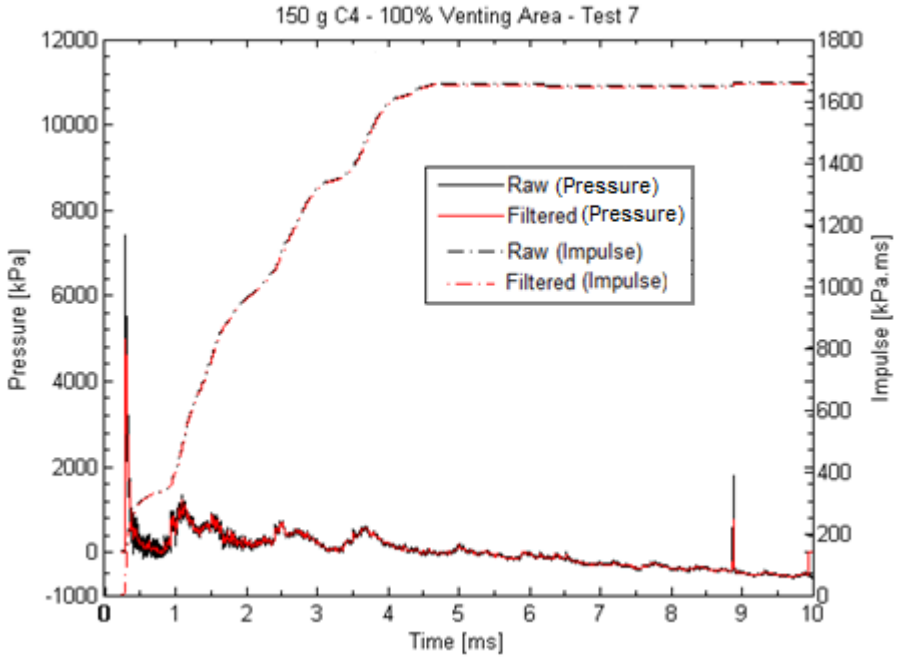

Figure C.13. Test 7 Data (150 g Charge Weight, 100% Venting Area)

APPENDIX – D

FITTED TEST RESULTS: 100% VENTING AREA

For fitting purposes, time boundaries for each charge weight are selected. It is an assumption to start the iteration process.

- **50 g**

Data between 0 – 0.65 ms is used for fitting purposes

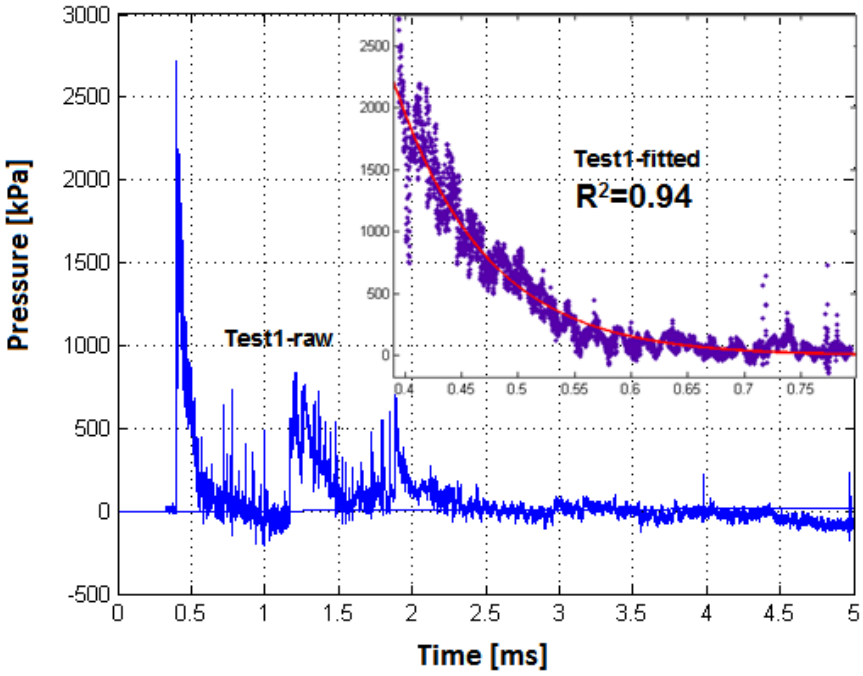

Figure D.1. Test 1 Data (50 g Charge Weight, 100% Venting Area)

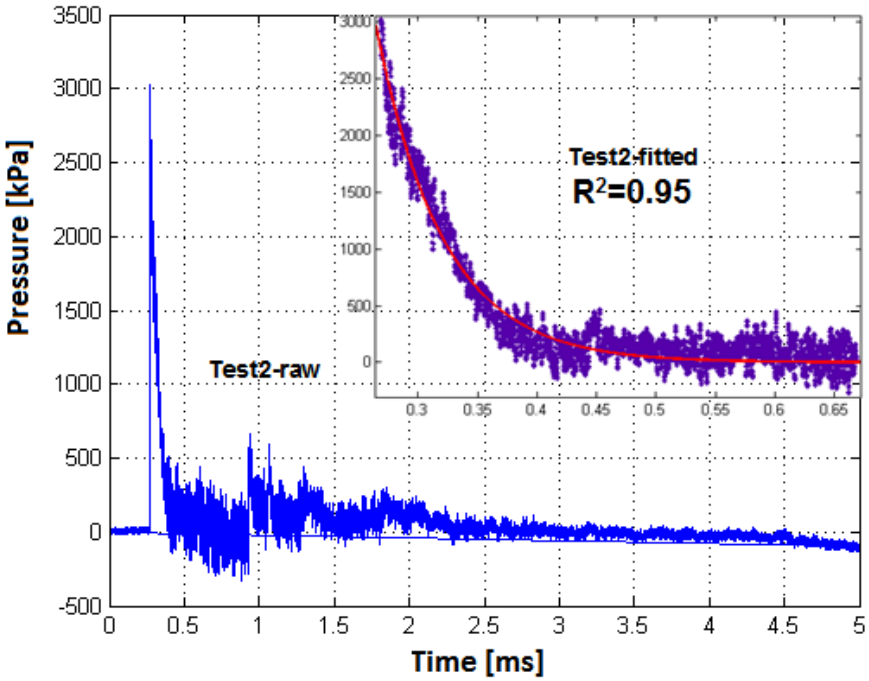

Figure D.2. Test 2 Data (50 g Charge Weight, 100% Venting Area)

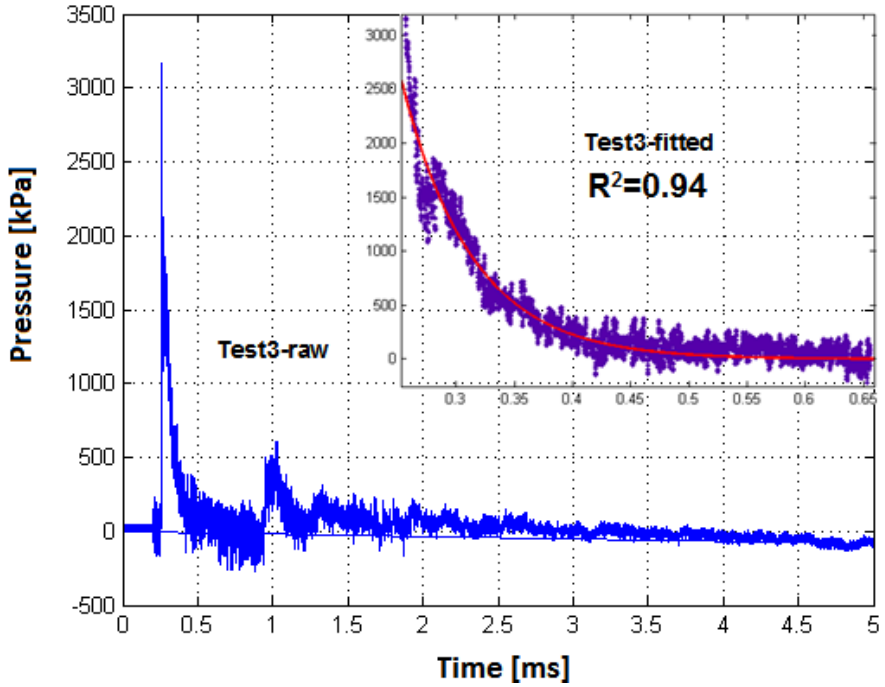

Figure D.3. Test 3 Data (50 g Charge Weight, 100% Venting Area)

- **100 g**

Data between 0 – 0.8 ms is used for fitting purposes

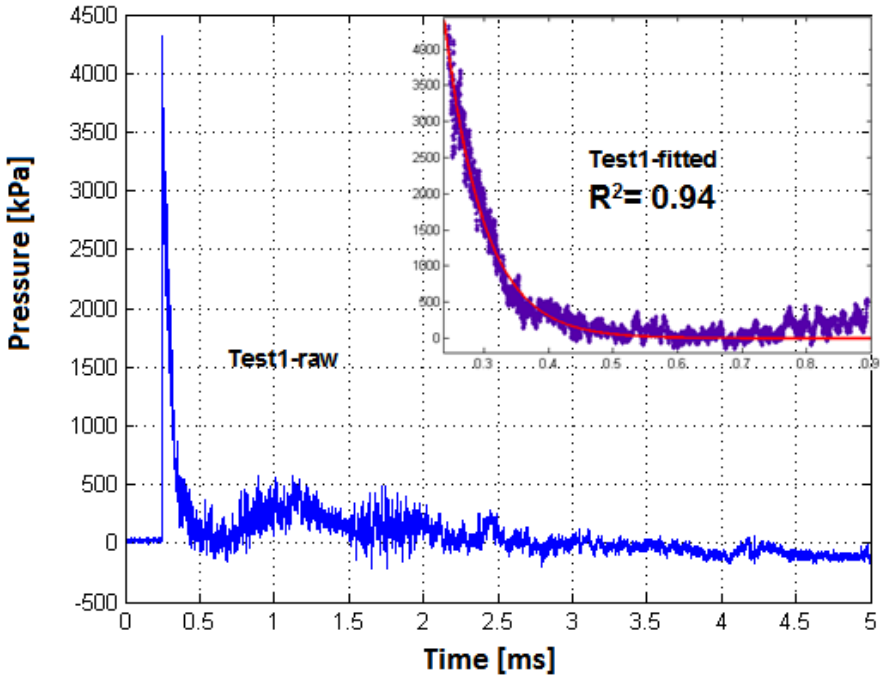

Figure D.4. Test 1 Data (100 g Charge Weight, 100% Venting Area)

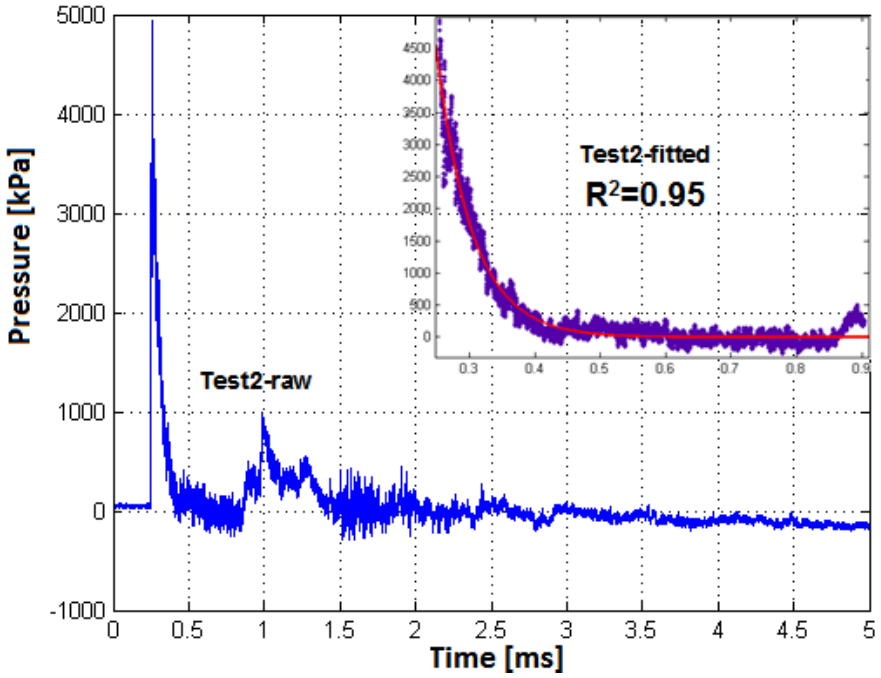

Figure D.5. Test 2 Data (100 g Charge Weight, 100% Venting Area)

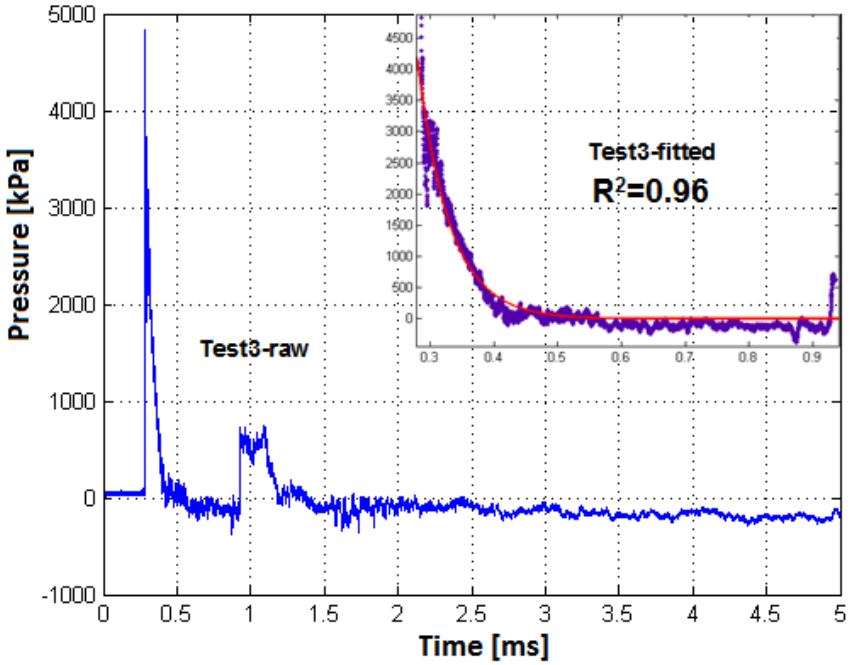

Figure D.6. Test 3 Data (100 g Charge Weight, 100% Venting Area)

- **150 g**

Data between 0 – 0.8 ms is used for fitting purposes

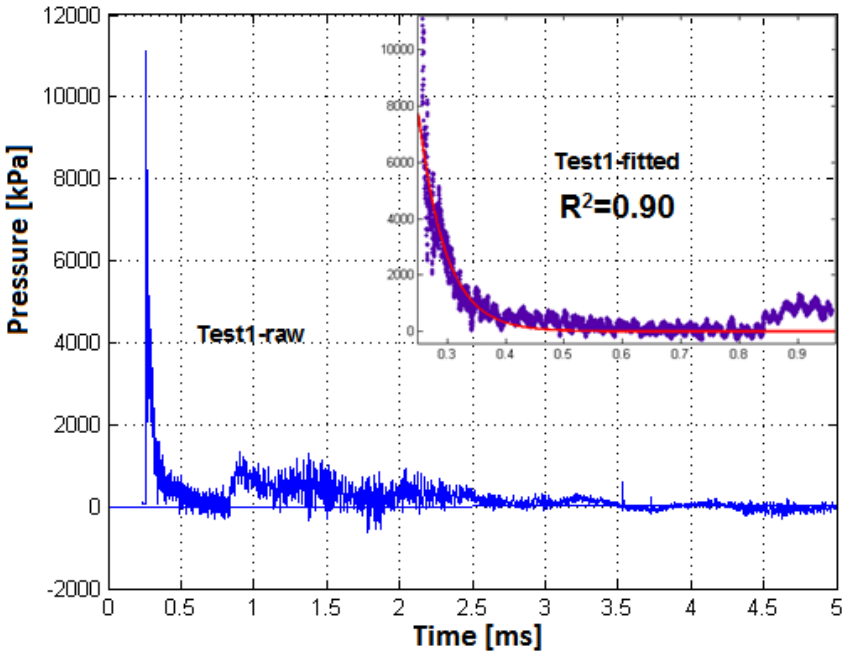

Figure D.7. Test 1 Data (150 g Charge Weight, 100% Venting Area)

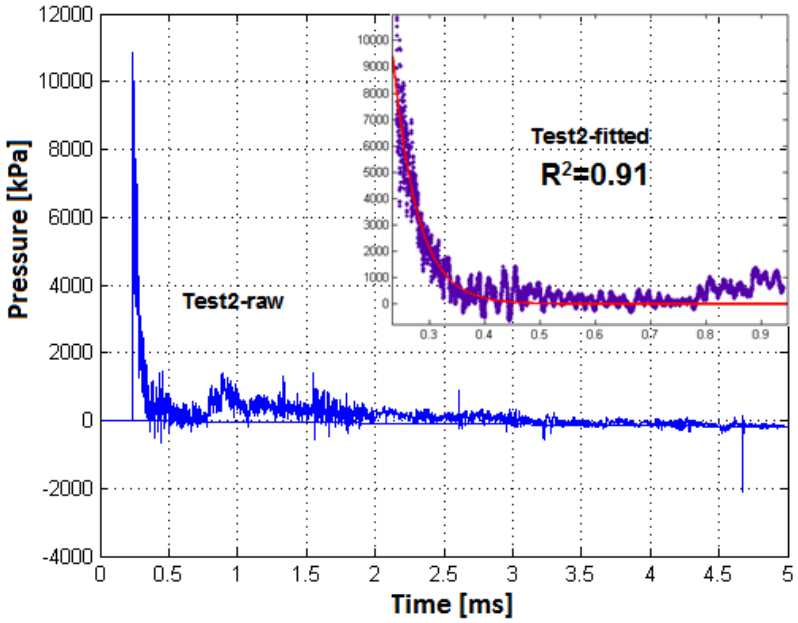

Figure D.8. Test 2 Data (150 g Charge Weight, 100% Venting Area)

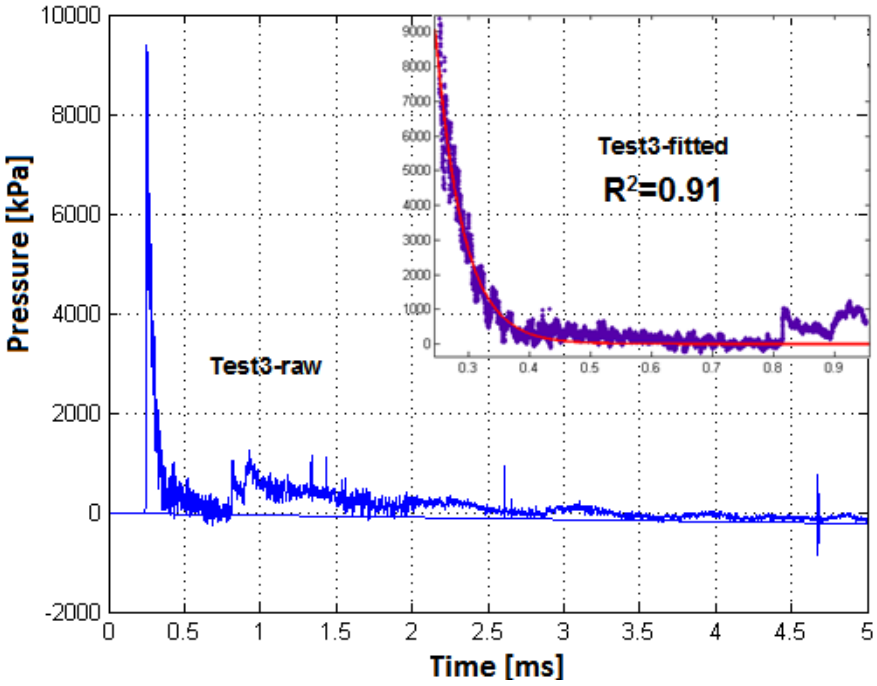

Figure D.9. Test 3 Data (150 g Charge Weight, 100% Venting Area)

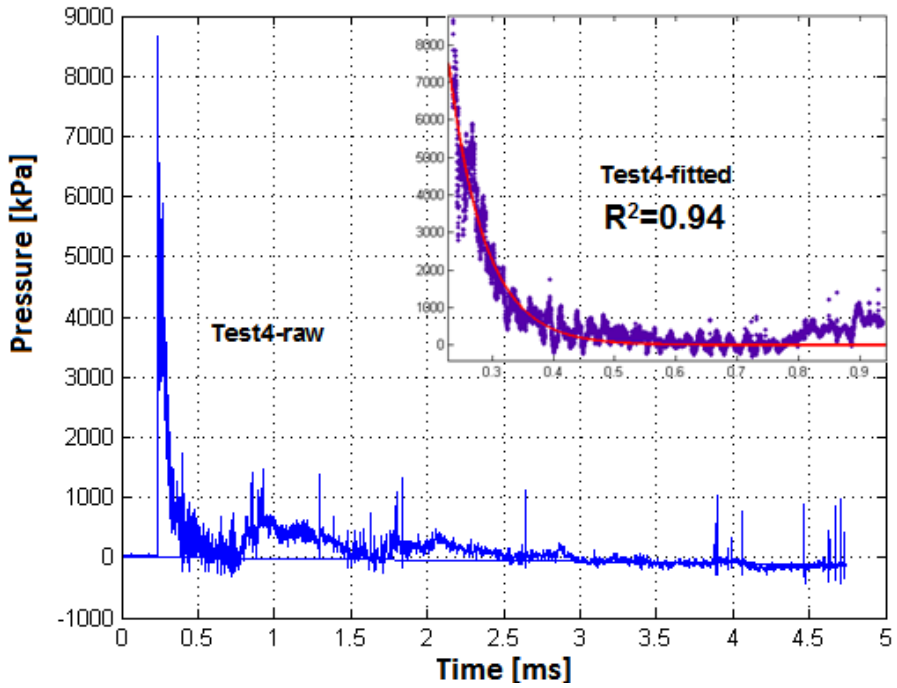

Figure D.10. Test 4 Data (150 g Charge Weight, 100% Venting Area)

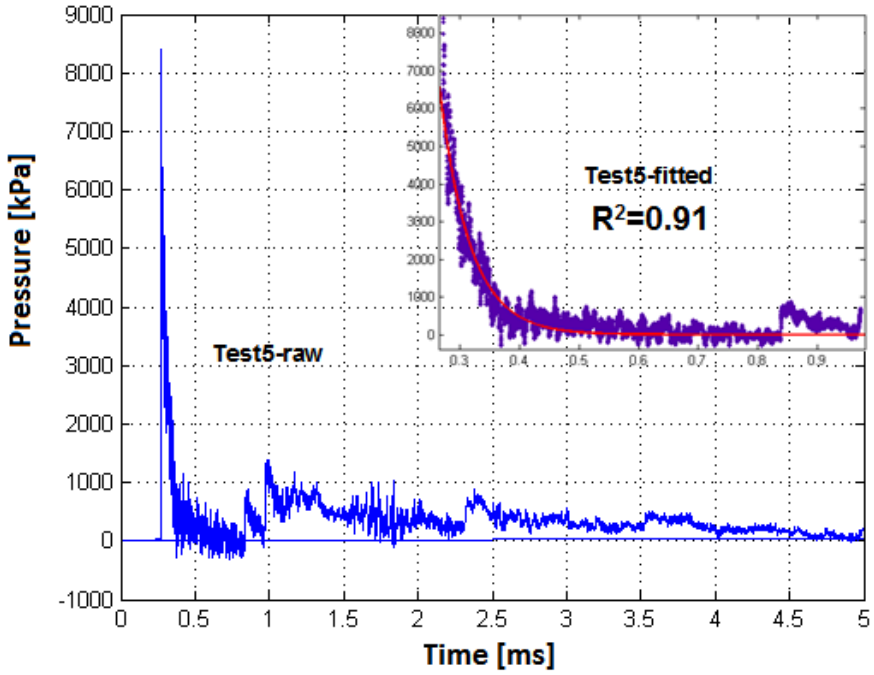

Figure D.11. Test 5 Data (150 g Charge Weight, 100% Venting Area)

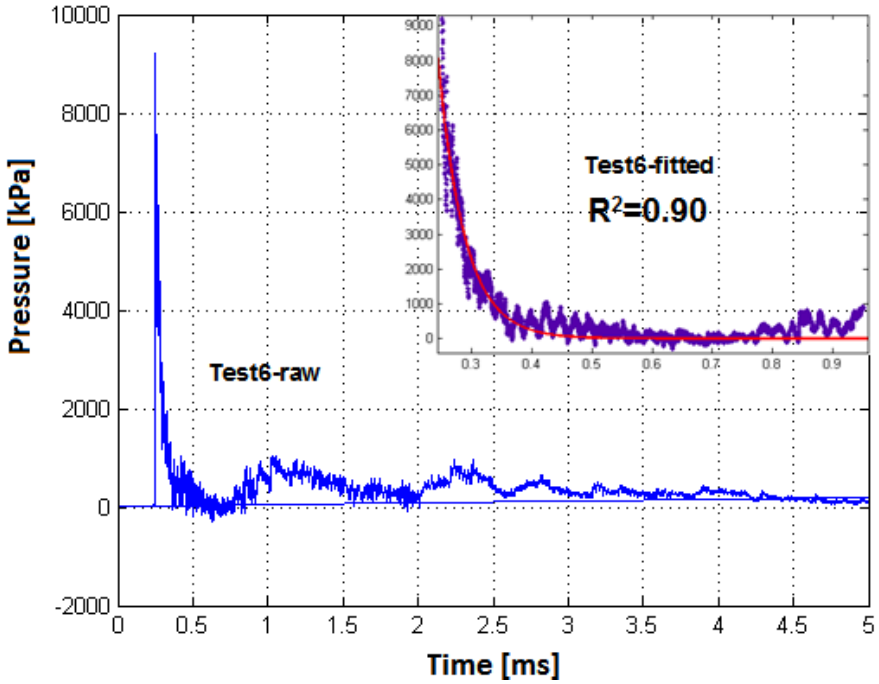

Figure D.12. Test 6 Data (150 g Charge Weight, 100% Venting Area)

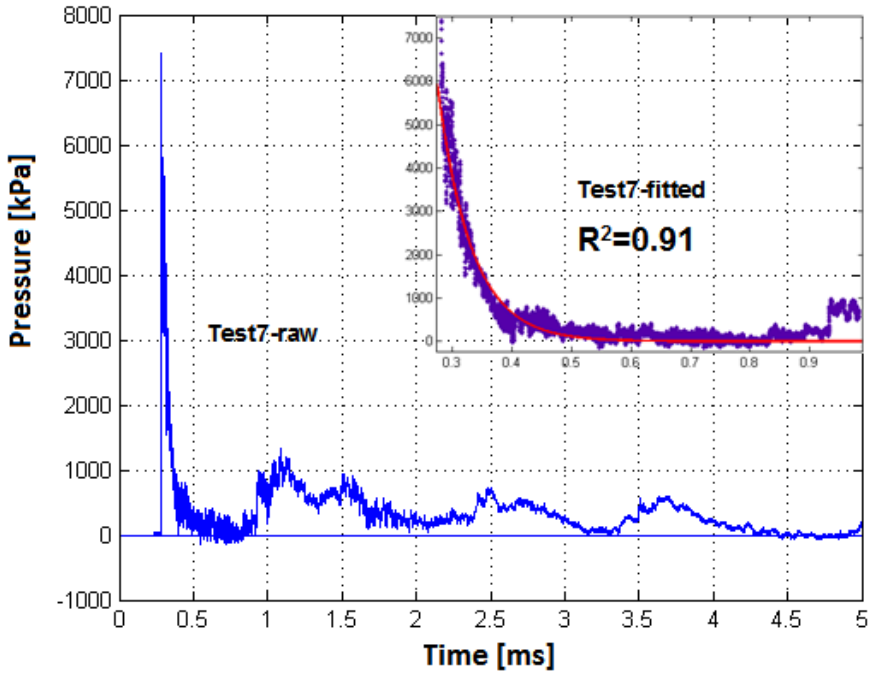

Figure D.13. Test 7 Data (150 g Charge Weight, 100% Venting Area)

APPENDIX – E

BLAST OVERPRESSURE TEST SETUP DETAIL

In this section, the details of the test setup are given. One may build the same setup by using the information below.

- Stiffener : 40 mm x 40 mm x 4 mm
- Steel Plate : 10 mm

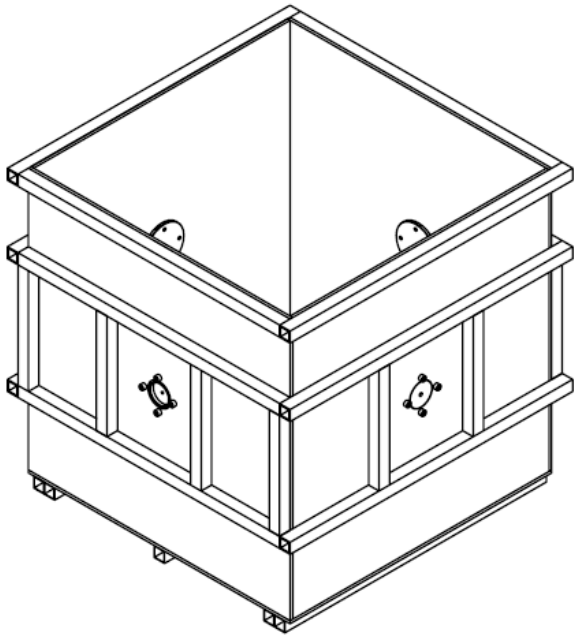

Figure E.1. Isometric View

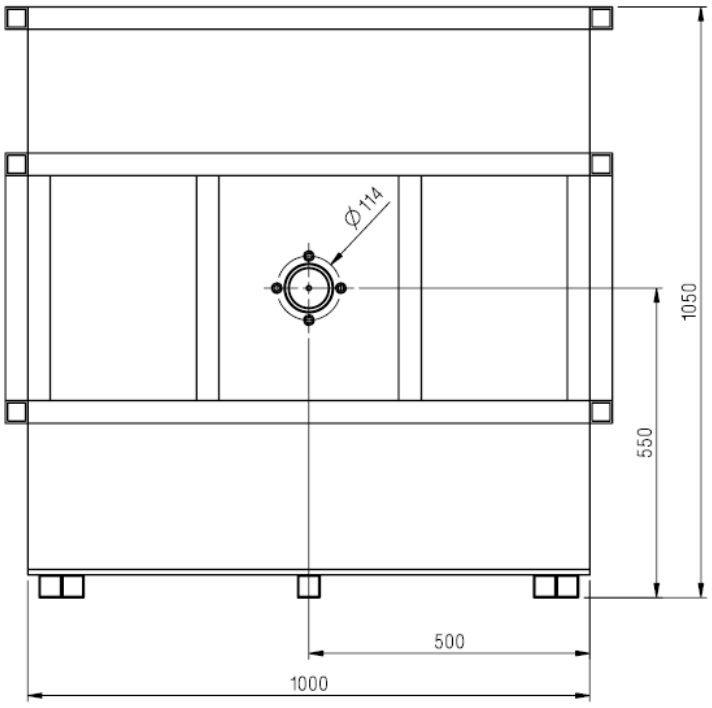

Figure E.2. Side View – 1

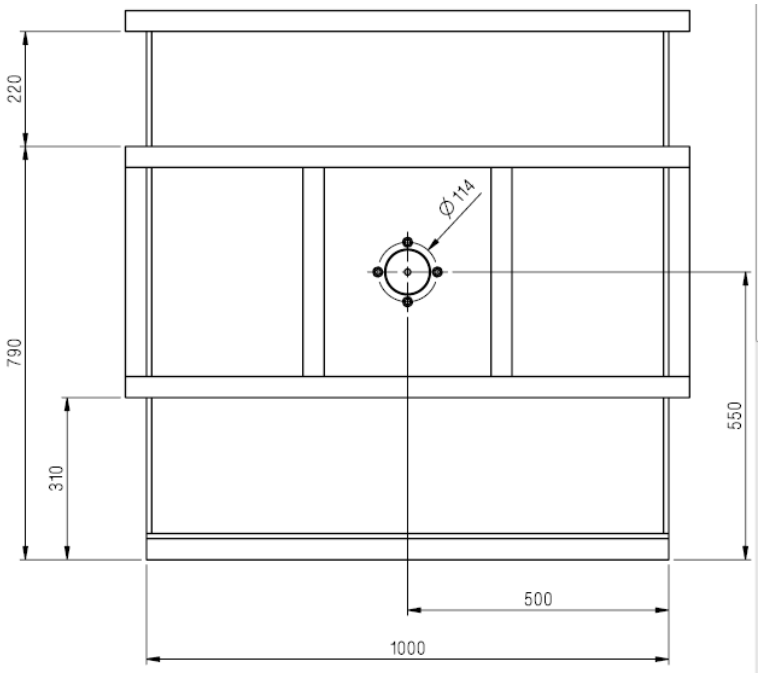

Figure E.3. Side View – 2

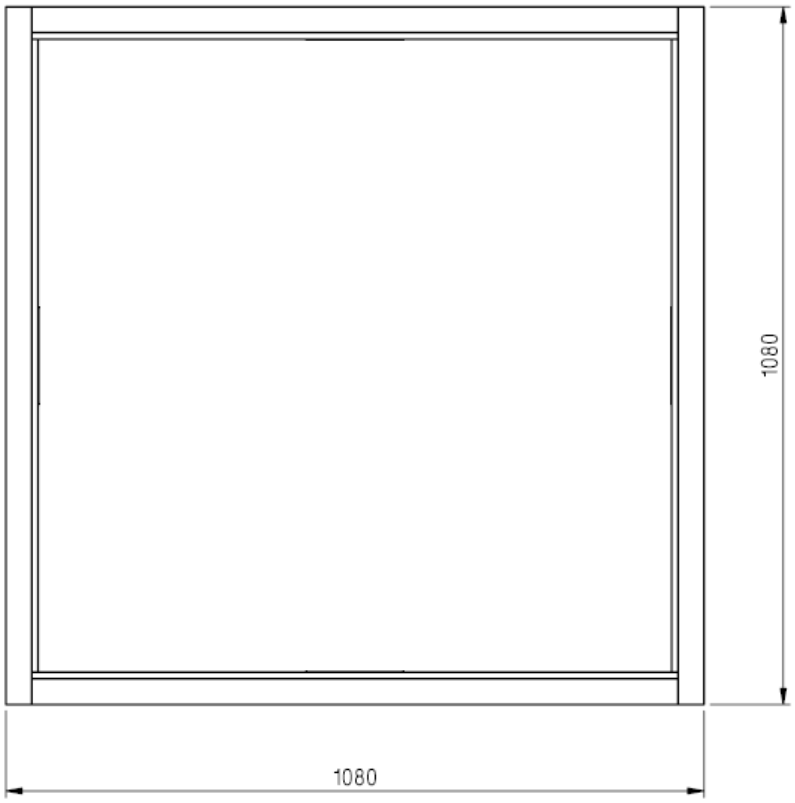

Figure E.4. Top View

APPENDIX – F

DATA FILTERING (MATLAB CODE)

```
clear all;
close all;
clc;

load('gram_elli.mat');

dummy = gram_elli(1:55999,:);

clear gram_elli;

Fs = 10*10^6;
dT = 0.2/1000;
f  = 1/dT;

[b,a]=butter(2,f*10/(0.5*Fs),'low');

count = 0;

for i = 1:2:7
count = count + 1;
t(:,count) = dummy(:,i);
end

count = 0;

for i = 2:2:8
count = count + 1;
gram_elli(:,count) = dummy(:,i);
gram_elli_f(:,count) = (filter(b,a,dummy(:,i)));
end

for i = 1:4
impulse_elli(i) = trapz(t(:,i),gram_elli(:,i));
```

```
impulse_elli_f(i) = trapz(t(:,i),gram_elli_f(:,i));
end


for i = 1:4
figure;
plot(t(:,i),gram_elli(:,i),'color','k');
hold on;
plot(t(:,i),gram_elli_f(:,i),'color','r');
end

clear dummy;
```